UNIVERSITY OF SOUTHAMPTON

FACULTY OF ENGINEERING, SCIENCE & MATHEMATICS

School of Engineering Science

Assessment of adhesively bonded connections for marine applications

by

Elouan Jarry

Doctor of Philosophy

June 2005

Abstract

This work concerns the study of adhesive bonding as a technique to join metallic ship structures. The thesis proposes a study of joints with thick adherends and adhesive bond for marine structures, based on a global-to-local approach considering both strength-based and fracture-based criteria. The objectives are to characterise a semi rigid class of adhesive through a local approach, assess selected structural joint designs potentially used in ship building and compare the two different approaches of assessment. It is divided in four parts, namely: a local strength approach, a local fracture-based approach, the assessment of the strength of structural joints and the assessment of defect tolerance criterion. The local strength approach deals with the assessment of an adhesive system (adhesive - primer - surface preparation) and selected adherends for different ageing conditions. At this stage, the particular focus is to characterise the change of behaviour due to increasing adhesive bond thickness through both experimental and finite element models. It is outlined that the shear strength of the joints decreases in a linear manner with the adhesive bondline thickness and a failure mechanism of the joint is proposed thanks to experimental results and finite element analysis. The local fracture-based approach deals with the assessment of fracture toughness of Double Cantilever Beam (DCB) adhesive joints. This analysis is carried out using analytical and numerical models which incorporate experimental data from the DCB tests. The adhesive system exhibits a high fracture toughness and the study underlines the influence of the bondline thickness on the fracture toughness of the joint while it is shown that accelerated ageing process lowers it. The structural joint assessment focuses on the joint behaviour in a tensile mode and aims to explain the mode of failure of two different types of joints of different adherend materials and different adherend thicknesses. The experiments and the numerical analysis helped to locate stress concentration areas and showed that failure occurs mainly due to tensile stress. To predict failure of these complex joints, a practical conservative criterion is used, based on both experimental and finite element results from the local joint analysis. Eventually, an assessment of the defect tolerance of the structural joints is carried out using finite element techniques and toughness data. The analysis considers the behaviour of structural joints with inserted cracks of different lengths for a nominal load level and the behaviour of the joint with a nominal crack length and different load levels. The fracture criterion shows good correlation with the strength based criterion.

Contents

List of Figures

List of Tables

Acknowledgements

First and foremost, I would like to thank Professor Ajit Shenoi who gave me the opportunity to carry out this work and provided patient and valuable guidance during these years. I would like to thank John Cantrill from VT Halmatic for manufacturing the specimens tested during this research. Part of the work has been carried out within the scope of the BONDSHIP project from which financial support is gratefully acknowledge. I also would like to thank colleagues and technicians from the School of Engineering Science and the Ship Science department with whom my relationship has been as friendly as scientifically fruitful throughout this work.

This work could not have been achieved without numerous people who, in a way or an other, have supported me. I would like to thank my parents and sisters who, even far away, encouraged me and provided a great deal of support. Elina, Sandra, Andrew, Colm and Ollie, playing music with you "Yokels" has helped me to overcome some difficult times. Renes, Cécile, Elena, Dominique, Frédérique, Sandrine, Fabien, et les autres... merci pour votre soutien et vos encouragements à Southampton ou ailleurs.

Very special thoughts go to the friendly people of 1 Mayfield Road: Marie, Fabrice and Thelonious who have shared my doubts and my hopes during two years even in the saddest time of their life: your optimism and strength have helped me a lot. Thelonious, your "joie de vivre" has been most appreciated during this time. Petit ange Jamadeen, you have watched over my shoulder the last weeks of this work and I will not forget it.

List of symbols

Latin symbols

A	insert film length for the debonding area of the DCB specimens
a	width of the butt strap specimen
a	crack length for the DCB specimens
a_0	Initial crack length
b	length of the strap of the butt strap specimens
B	width of the DCB specimens
C	compliance
C_0	initial compliance
C_m	machine compliance
C_{cor}	compliance correction due to indentation and machine stiffness
C_s	compliance of specimen
C_{sy}	System compliance
c	length of the main plates (Steel and Aluminium) of the butt strap joint
d_1	length of the overlap between the steel plate and the aluminium strap in the butt strap joint
d_2	length of the overlap between the aluminium plate and the aluminium strap in the butt strap joint
dA	change in the crack area for a uniform width B
dC	change in compliance
dU	energy change
E_a	Young's modulus of the adhesive
E_f	flexural modulus of specimen determined from test data
E_s	Young's modulus of the substrate in the DCB specimens
F	large displacement correction factor
G	fracture energy
G_{Ic}	Critical mode I energy release rate (fracture toughness)
h	height of adherends in DCB speimens when substrates are similar
h_1	height of the aluminium adherends in the DCB specimens
h_2	height of the steel adherends in the DCB specimens
I	second moment of inertia
J	contour integral use to calculate the fracture energy at the tip of a crack
K	Stress field intensity factor
K_I	mode I stress field intensity factor
K_{Ic}	critical mode I stress intensity factor

L	length of the DCB specimens
m	constant used in the DCB data post-processing
N	load block correction factor
n	slope of the plot of log(C) vs log(a) in the DCB data post-processing
P	force or load used in the DCB data post-processing
P_{max}	maximum value of force
r	radial coordinate in the polar coordinate system
s	arc of length along the integration line Γ
$\mathbf{T}$	stress vector
t_a	adhesive bondline thickness of the joints
t_{Al}	thickness of the main aluminium plate in the butt strap specimen
t_{steel}	thickness of the main steel plate in the butt strap specimen
t_{strap}	thickness of the aluminium strap in the butt strap specimen
U	energy
U_d	dissipated energy
U_{ext}	external work
U_k	kinetic energy
U_s	strain energy
$\mathbf{u}$	displacement vector
u_x	displacement along x-axis used in the finite element model
u_y	displacement along y-axis used in the finite element model
W	strain energy density
x	cartesian coordinate
y	cartesian coordinate

Greek symbols

δ	vertical displacement of the DCB specimen during testing
δ_{cor}	corrected value of displacement
δ_{max}	maximum vertical displacement
δ_{offset}	off-set displacement
Δ	crack length correction factor
ΔG	change in energy release rate
σ	stress
σ_x	axial stress
σ_y	normal stress
σ_{11}	axial stress
σ_{22}	normal stress
Γ	arbitrary path surrounding the crack tip
τ_{12}	shear stress
θ	circumferential coordinate in the polar coordinate system
ν	Poisson ratio

List of abbreviations

BSI	British Standard Institution
CBT	Corrected Beam Theory
ECM	Experimental Compliance Method
SBT	Simple Beam Theory
SEQV	Equivalent stress (commonly named Von Mises stress)
SX	Direct tensile stress (in the x-direction)
SY	Normal stress (in the y-direction)
SXY	Shear stress
S1	Maximum principal stress

Chapter 1

Introduction

Traditionally the shipbuilding industry uses welding, riveting and bolting as the primary process for joining the different structural parts of a ship. In the case of welding, it is well known that this process results in induced stresses during the fabrication stage which in turn lead to distortion in the shape of structural components and indeed, the ship itself. Considerable effort has thus to be expended to rectify these weld-induced distortions leading to increased production costs. One additional problem in the case of aluminium is the significant reduction in the fatigue load capacity in case of welded structures (Kecsmar & Shenoi 2004). When using bolts or rivets, the major issues are the stress concentrations induced by the singularity caused by the hole and galvanic corrosion if different materials are joined. As a consequence, either the structural topology has to be rearranged to cope with increased stress levels or the scantlings of the structure have to be enhanced. In either case, there is an increase in the weight of the structure. Since structural weight too needs to be minimised, especially in high speed, high performance ships, there is a need to investigate alternative joining techniques for aluminium structures: adhesive bonding is one of them.

1.1 The bonding technology

1.1.1 Comparison between fastening techniques

There are 3 major types of joint that can be encountered: welded joints, riveted joints and bolted joints. There are two topics of comparison that can be made, namely from a structural point of view and from a manufacturing or labour point of view (Semerdjiev 1970). These comparisons are summarised in Table 1.1.

In some situations (not to say most of them) the traditional and well established

techniques will not be overtaken by the adhesive technology as they would be more appropriate. The reason is because these techniques enable the structure to be loaded in either tension, compression, shear or a combination of these different modes with less harm than with adhesive.

1.1.2 A new fastening technique ?

The adhesive bonding technology has been used as a fastening technique for thousands of years. However, it has been used in structural engineering only for a few decades mainly because structural adhesives are made of chemical products like polymers the technology of which was not available before that time. It has been developed and used extensively for more than sixty years in the aeronautics and the aerospace industry. In ship research, adhesive has been considered to repair fasten structural parts of a ship since the late 1980' and early 1990' (Allan, Bird & Clarke 1986, Hashim, Winkle & Cowling 1990, Winkle, Cowling, Hashim & Smith 1991).

With laser welding, it probably represents one of the last development in the fastening technology after the traditional methods that are riveting, welding or bolting. However, like any technology and especially new ones, this one has assets and drawbacks: they are listed in Table 1.2.

1.2 Layout of the thesis

This study starts with a review of adhesive bonding used as a structural fastening technique in industry. This chapter presents the latest development concerning the methods to assess bonded joints: either undamaged or damaged. It also presents the specific research done in adhesive bonding for the marine industry. Based on this review, weaknesses in this domain are underlined and the motivations for the present work are detailed.

Part of this study was based on works carried out during an industrial project (Bondship 2003), the background of which is presented in Chapter 3 followed by the methodology adopted during this work. These chapters are followed by two chapters regarding a local approach of basic joint designs focusing respectively on the strength and fracture mechanics aspects of adhesive joints. Typical considerations include the influence of the adhesive thickness and adherend materials on the strength of joints and the crack propagation along the adhesive bond. Chapter 7 is

dedicated to the study of the strength behaviour of more complex structural joints designs that are used in a high speed craft and are first presented in Chapter 4. The fracture behaviour of these joints is the topic of Chapter 8 where their tolerance to damage is investigated: it includes the analysis of joints with different crack lengths at different load levels. Chapter 9 will focus on a discussion about the integration and the relevance of the two approaches in the design of a bonded lightweight superstructure for a high speed craft.

A final chapter concludes on this study and proposed new directions of research to enhance the knowledge in adhesive bonding for marine structures.

Tables

	Structure		Labour	
	Advantages	Disadvantages	Advantages	Disadvantages
Welding	Strong joints & rich database	Join only similar materials & distortion problems	Technique well established	Tedious labour & heavy equipment
Riveting and bolting	Join different materials & strong joints	Join thick material only. stress concentration & drill structure	Well established technique	Tools manipulation & repetitive tasks
Adhesion	Join thin and different materials. uniform stress	Lack of data base	Straightforward application technique	Need of clean environment and labour protection

Table 1.1: Comparison of different fastening techniques

Advantages	Disadvantages
Join plates of different materials: metal to metal joints, composite to composite or metal to composite joints are among the numerous possibilities	Limitation in the load bearing capacities
Join relatively thin plates & high strength to weight ratio	Limitation in the thermo-mechanical properties
The stress distribution is almost uniform in the joint	Limitation in their use in hostile environments like water
Good performance in fatigue are achieved	Possible chemical hazards associated with its use during its application and fire safety has to be carefully looked at as it is a flammable product
Good noise and vibration damping and insulation capacities	Application to be done in a relatively clean environment
From a manufacturing point of view. the application procedure is relatively straight forward	Lack of long term data
Better tolerance to geometrical inaccuracy	Guide lines only emerging

Table 1.2: Advantages and disadvantages of adhesive bonding

Chapter 2

Literature Review

2.1 Introduction

When choosing to use adhesive technology to build a structure, the designer needs to have a basic knowledge of bonded joints that are going to be used. This knowledge encompasses the mode of failure, the static and dynamic behaviours and the behaviour in degraded environmental conditions and will be gained thanks to experimental as well as mathematical modelling. The modelling of adhesive joints have been the subject of research since adhesive joints have been considered in the industry to fasten structural elements. It include in particular the assessment of the stress field in the bond, the fracture mechanics of adhesive joints and modelling of the long term behaviour via the assessment of the damage due to environmental degradation. These tools are essential in the understanding to design safe and durable bonded structures. The following sections present the latest developments in the modelling of joint in the field of stress analysis, fracture mechanics and environmental degradation.

2.2 Assessing adequacy of perfect joints

The knowledge of the stress distribution in an adhesive bond is of primary importance for the designer to mininise stress concentration and assess safety factors. Hence, lap joint theories have been a matter of investigation for now almost 70 years and numerous authors have proposed analytical solutions to compute the stress in a bonded joint. These theories have been developed progressively with successive approximations depending on the types of joints and their configurations but also depending on the power of the numerical tools available. The following intends to summarise the major methods derived to date showing their limitations and the major assumptions that characterise them.

2.2.1 Analytical modelling

The first works carried out about adhesive as a structural fastening device are attributed to (Volkersen 1938). This very first analysis took into account the fact that the upper and lower substrates were not totally rigid and deform themselves elastically when loaded. Figure 2.1.

The second major contribution in the analytical study of adhesively bonded lap joints is due to the work of (Goland & Reissner 1944). The main improvement in their work, compared to the one of Volkersen, is that they first considered the bending of the bonded plate due to load eccentricity. From this assumption, they have identified what is called the bending moment factor k. This factor represents physically the rate of transfer of the bending moment to the edge of the joint. Figure 2.2. Their study is described as valid for two limited cases, namely:

- When the adhesive layer is so thin that the flexibility of the joint is neglected. This is the case of bonded wooden and plastic plates.
- When the flexibility of the joint is mainly due to the adhesive layer. This is the case of adhesively bonded metal plates.

Whereas the previous theories assumed constant shear and normal stress through the adhesive thickness, work done by (Volkersen 1965) introduced this variation in the equations describing the mechanical behaviour of the joint. He showed that a basic theory considering constant σ_y through the adhesive layer underestimates the peel stress by almost 50% . He noticed that shear and normal stress concentration decreases with increasing adhesive thickness suggesting design of joints with thicker adhesive layer to the detriment of joint strength. He also suggested that failure in single and double lap joints is due to peel and not shear stress.

The major following work on adhesive bonding was due to (Hart-Smith 1973). Several issues were investigated concerning not only elastic-plastic adhesive but also failure modes, influence of adherend stiffness imbalance and thermal effects. The analysis presented in the paper was an elastic-plastic analysis taking into account adhesive plasticity and including adhesive material and geometrical properties in the calculation of the bending factor.

Hart-Smith identified three types of failure mode, namely:

- One due to load eccentricity coming from direct load stress and bending stress: failure is identified in the adherend outside the joint.
- Adhesive failure due to shear stress: this mode is potentially extremely rare, confirming suggestion from (Volkersen 1965).
- Two failure modes associated with peel: either adherend is made with metal: in this case failure occurs in the adhesive, or adherend is made of filamentary composite adherend and in that case peel strength in the inter laminar fibre is much less than of the structural adhesive, therefore failure occurs in the adherend.

Two other effects were investigated that are thermal effects and stiffness imbalance. The author showed that if materials of different thermal expansion coefficients are used as adherends, this difference influences the transfer of load therefore bending moment and associated coefficient k are changed. Also, he stressed that a balanced joint made with the weakest of the adherends involved in the imbalance one, is stronger than the imbalance joint. This imbalance also increases stress concentration. Eventually, if there is no stiffness imbalance but thermal mismatch between adherends, this will increase the bending moment in the adherend of lower coefficient of thermal expansion. Generally speaking, stiffness imbalance or thermal coefficient imbalance will reduce the joint strength. Some restrictions concerning the work of Goland & Reissner were pointed out especially that their theory (Goland & Reissner 1944) is strictly speaking only valid for light loads and small overlap of joints. However, (Tsai & Morton 1994, Cooper 1979) confirmed that the theory of Goland & Reissner is sufficiently accurate to enable a qualitative assessment of the influence of geometrical and material parameters.

Analytical solutions have not been able to model the zero shear stress that should occur at the edge of the joint. Indeed, equations of solid mechanics stipulate that at the free surface of a solid shear stress is nil. The analysis done by Allman (Allman 1977) not only enabled to model this elementary boundary condition at the edge of the joint but was also valid for a wide range of elastic substrate materials. His method used the basic equations of solid mechanics like the previous ones (Cornell 1953, Goland & Reissner 1944, Hart-Smith 1973) but for the convenience of the calculation, a stress function was introduced based on strain energy consideration. Once the solution was derived, a qualitative analysis was shown to compare the new method with the classical one from Goland & Reissner for different lap joint designs. It was found that stress concentration is reduce from 15 to 30% compared

to classical theory Goland & Reissner: this is due to the possibility of modelling zero shear stress at the edge of joints.

The following closed form analysis are all improvements of Goland & Reissner's with additional refinements concerning adherends: orthotropic adherends were included in the models of (Renton & Vinson 1977), and (Delale, Erdogan & Aydinoglu 1981). Results of the first one were in good agreement with photo-elastic analysis and results of the second were confirmed by finite element models. (Ojalvo & Eidinoff 1978) outlined the importance that variation of shear through the thickness can have in the outcomes of analysis. Their study included also bond thickness variation and showed that difference between classical theories and the new theory occurs only at the edge of joints where stresses are the highest.

As it has been seen, the previous analysises focused only on some specific joint designs like orthotropic or isotropic adherends, single lap joints or sometimes non-identical adherends. (Bigwood & Crocombe 1989) tackled this problem and set up a method that considers that any suitable bonded structure can be reduced to an adherend-adhesive sandwich where complex loading can be applied. Although the method does not model a zero shear stress at the edge of joints, it has been successfully validated with finite element analysis. However, like (Hart-Smith 1973), it was highlighted that adherend mismatch introduces errors in the results.

Eventually, some authors like (Carpenter 1991) and (Tsai & Morton 1994) evaluated the accuracy of several analytical theories, compared them to each other and investigated the influence of the different assumptions made in the various methods. (Carpenter 1991) showed that shear and peel stresses are generally insensitive to the assumptions except in the case where neglecting shear deformations in the adherend causes the stress to vary by up to 30%. The author also showed that inconsistencies highlighted in (Goland & Reissner 1944) are balanced by the absence of shear deformations in the adherend. (Tsai & Morton 1994) compared some available analytical solutions to a finite element model including geometric non linearities to account for large deformations due to bending moment. They concluded that the model by (Hart-Smith 1973) is appropriate to assess edge moment in the case of short overlaps and varied adhesive thicknesses whereas the proposed modified Goland & Reissner's model is suitable for long overlaps in the definition they give for this parameter.

2.2.2 Numerical modelling

Since the early 1970' it has been noted an increase in the use of finite element method to assess the stress in adhesive bonded structures. Since it is considered as a powerful and accurate tool for structural design, it has been progressively used to validate analytical solutions and experimental modelling. The interest of numerical model compared to closed form analysis is that it is possible to easily analyse stress in more complex structure and the influence of different parameters such boundary conditions or material properties that an analytical method cannot do.

Finite element techniques to assess stresses in lap joints were first reported by (Wooley & Carver 1971). The analysis was based on a linear displacement function with two elements through the thickness of the adhesive layer. The analysis was done for a range of elastic modulus ratios from 0.1 to 1000 and adherend length to adherend thickness ratios. Although simulations were done considering plane stress analysis, comparison was made with results from Goland & Reissner's theory and good agreement were found according to stress concentration.

An early use of finite element tool was also proposed by (Adams & Peppiatt 1974). Their work focused on stress concentration at the end of the joint and a parametric study was carried out concerning end effects with the presence of spew fillet at the edge. Comparison between joint with and without fillet was done and it was shown a reduction in maximum stress up to 70% in the case of shear and 80% in the case of peel stress. Also, the influence of the fillet size on the stress distribution was observed: a 70% reduction in maximum shear stress was obtained at the end of the adhesive layer and maximum stress occurs in the adhesive at the adherend corner. Eventually, it was shown that the existence of a chamfer due to etching of adherend reduces maximum stress in this area to up to 40%.

(Harris & Adams 1984) used a non-linear finite element technique to predict the mode of failure and failure load of single lap joints with a series of different adherends and adhesives. The results were compared with experimental and analytical results. The finite element analysis used was able to account for the large displacement rotations that occur in a single lap joint under load, and elasto-plastic behaviour of both the adhesive and the adherends was considered. A failure criterion based on the uniaxial tensile properties of the adhesive was used: depending on the type of adhesive used, the authors found that a maximum stress criterion can be appropriate, whereas a maximum strain criterion can be employed for other cases.

(Reddy & Roy 1988) investigated the influence of three different types of boundary conditions in the stress distribution in the adhesive layer. Their model, validated with classical analytical theories, showed the importance of these conditions as they can significantly alter the stress distribution in a lap joint. They also outlined the influence of the mesh in the stress distribution: it was found that a non-uniform mesh implies less scatter in the results than a uniform one.

The use of a local failure criteria is subjected to numerous possibilities: maximum shear or peel stress or principal stress or modified Von Mises citerion among others. Hence, (Crocombe 1989) used finite element analysis to predict failure in bonded joints and proposed a failure criterion based on global yielding (as opposed to local failure criterion like peak stress) that describes more the onset of failure rather than the global rupture. This global yielding applies "when a path of adhesive along the overlap region reaches a state in which it can no longer sustain significant increase of applied load".

(Bigwood & Crocombe 1990) used finite element method to validate an analysis taking into account non-linear material behaviour of the adhesive. Further validation was carried out in comparing results of different elastic plastic models and close agreement were found between them for the shear and transverse stresses. Moreover, based on the study in (Crocombe 1989) adhesive thickness effects were investigated. It was shown that unlike elastic analysis that predicts increase of strength with increase of adhesive thickness, yielding progresses more rapidly in thick joints therefore leading to the expected loss of strength.

In order to assess different lap joint theories, (Carpenter 1991) presented a special adhesive element that allowed to control parameters for different assumptions. Results using this element converged with the corresponding closed form analysis having the same set of assumptions. However, it was shown that increasing the number of elements in the adhesive thickness leads to an increase in the stress magnitude confirming the equations of elasticity that predict stress singularity at a bi-material interface. The author therefore concluded that stress predicted by either finite element or closed form analysis are convenient artificial values.

(Tsai & Morton 1994) outlined that geometric non-linearities are due to the eccentricity of the load path implying large rotation deformations. They used a finite

element method to assess the k-factor (ie joint edge moment) and compared the stress distribution in the adhesive layer with selected closed form solutions. Close agreement was found within a 10 % margin between classical solutions and the non-linear model for both shear and normal stresses. An interesting feature was that normalised longitudinal, peel and shear stresses decreased with increasing load. This is caused by the reduction of edge moment due to the eccentricity and large deflection effects. The numerical study also emphasised a zone of uncertainty confirming suggestions done by (Ojalvo & Eidinoff 1978).

In the shipbuilding industry, joints used are thicker and an increase of adherend or adhesive thickness modifies the stress distribution in both the substrate and the adhesive bond. (Bezine, Roy & Vinet 1996) used finite element modelling to investigate stress in composites adherends. Their analysis showed that the stress concentration leads to delamination but that stress distribution is insensitive to overlap length. They also showed that the stress concentration can decrease by 50% when using tapered joints.

Thanks to finite element analysis, two studies by (Tsai, Morton & Matthews 1995) and (Li, Lee-Sullivan & Thring 1999) outlined that longitudinal stress in the adhesive is not negligible. With a 2-D geometrical non-linear analysis, (Li et al. 1999) showed that maximum stress occurs in a single lap joint in an area close to the adhesive-adherend interface at corner ends. This suggests a critical locations for adhesive failure initiation that are at opposite ends of joint overlap and confirm a failure theory proposed by (Ojalvo & Eidinoff 1978). The investigations carried out by (Tsai et al. 1995) concern composites lap joints and showed that large deformations in adherend near the overlap must be taken into account in the analysis.

Eventually, finite element analysis was used by (Li & Lee-Sullivan 2001) to compare the influence of stress state assumptions and the boundary conditions in the stress distribution of lap joints. It was concluded that the distribution is more sensitive to the boundary conditions than to the stress state. However, it was noticed that these boundary condition effects decrease together with the load.

2.2.3 Environmental degradation

One of the major challenges faced when using structural adhesive bonding in industry is the understanding of degradation due to environmental attacks. This degradation is due to a complex combination of damage of both the adherends and

the adhesive itself as well as their interfacial zone leading to uncertainty about the durability of adhesive joints. The durability of an adhesive joint depends not only on the time of exposure and type of environmental attacks (such as for example water and temperature) but also on the type of surface preparation of the adherend. Extensive research has been carried out on these different facets of durability aspects of adhesive joints.

Environmental degradation of adhesive joints can be caused by many different factors listed by (Kinloch 1990) though water is generally considered as the main one causing joint degradation. Different modes of access are identified (Adams, Comyn & Wake 1997) as: ingression from and along the interface, ingression by micro-cracks in the adhesive, absorption by the adhesive, absorption from the adherend (rare). This leads to different weakening processes: swelling, causing internal stress in the adhesive bond, damage at the interface between adherend and adhesive or degradation of the bulk adhesive properties.

(Lee, Kwon & Cho 1998) have investigated the strength of bulk adhesive and compared it to the strength of an adhesive tubular joint with respect to the level of absorbed moisture. They found that adhesive joints are stronger than bulk adhesive because of swelling effects. They also pointed out, like many others (Venables 1982, Bowditch 1996), that surface treatments increase strength retention under hygrothermal environment.

Similarly, (Zanni-Deffarges & Shanahan 1995) have compared the behaviour of bulk adhesive and adhesive joints using a gravimetric technique. They showed that the elastic modulus of the bulk adhesive decreased while water diffused into the adhesive. They also developed a model that predicts diffusion in adhesive joints taking into account changes in the overall elastic behaviour of the bulk adhesive. Discrepancies between experimental and numerical results led them to suggest capillarity diffusion at the interface between adhesive and adherend accelerating water ingress.

(Crocombe 1997) assessed the response of bonded lap joint in a degraded environment such as water within a numerical framework including a mechanical-diffusion analysis to determine the spatial variation of moisture in the adhesive. He studied the effects of the adhesive fillet and its influence was shown to be significant over a long period of time. Also, after translating material data from thick adherend shear test into tensile properties from the open literature, he showed that degradation of

the bulk adhesive Young's modulus could be degraded by 80 % after 8 weeks at 50°C and 95% relative humidity. The analysis led him to predict failure of the joint; he suggested a failure initiation in the middle of the overlap as the bondline is shown to be more brittle there than at the edge in a wet environment.

(Armstrong 1997) studied the influence of long term ageing on adhesive joints in distilled water at room temperature. Different adhesives and different surface treatments were tested through a wedge test programme over a five year period. He suggested that the durability of adhesive joints depends more on the durability of the oxide layer developed at the interface of the joint than on the durability of the bulk adhesive.

Bulk adhesive as well as interfacial degradation aspects were discussed by (Bowditch 1996). He particularly studied the effects of temperature, time and external load on immersed lap joints. He outlined that at high temperature, surface preparation is not a key aspect in the strength of the joint as failure is cohesive, unlike at low temperature where failure becomes interfacial. He also concluded that weakening effects due to interfacial attack can be balanced by strengthening effects due to relief of internal stress by water.

As previously noticed, surface pretreatment is of great importance to retain the strength of adhesive joints over a long period of time. In this respect, (Brockmann 1986) showed that an adhesive joint is a three dimensional multi-material system in which all the materials influence each other. This influence is emphasised in the case of ageing process. (Jones, Pitcher, Pool & Stone 1986) have studied the performance of four different pre-treatments on five different titanium alloys through a wedge test programme. They demonstrated the importance of micro-mechanical interlocking in the durability of adhesive joints.

(Beevers 1999) has studied the effects of stress in the adhesive on the environmental ageing process and reviewed durability test methods with stress applied to the joint. He emphasised that the analysis and interpretation of durability test data are subject to a good understanding of the mechanisms involved in the degradation process with a particular importance in the derivation of life prediction models. In this respect, the author studied the uncertainties due to extrapolation of durability test data by means of acceleration factors. The method is validated with an application case using historical data obtained from an analysis of old bonded structures.

The difference of degradation due to distilled water, salt water or salt spray environment has long been determined. However, contradictory results were found. McMillan (cited by (Adams et al. 1997)) showed that joints exposed to salt spray water for three months were more damaged than joints exposed to semitropical environment for three years. But Albericci (cited by (Armstrong 1997)) showed that distilled water did more damage on epoxy, acrylic and polyurethane paint coatings than salt water. (Holton, Spinks & Isle 1992) did a comparison of unloaded and loaded joint behaviour in still water, 0.5 % salt water and 5 % salt water. They concluded that low salt concentration was more damaging to the joints than distilled water or high salt concentration water.

Recently, (Hart-Smith 1999) has emphasized that tests used nowadays do not say anything about durability of adhesives but help to assess the quality of the surface preparation (ie before bonding) in the case of metal to metal adhesive bonding. As a result he also advocates the need of similar durability test as the one developed by Boeing for metals (ASTM 1998). In a shipbuilding environment, the wedge test can be used to assess the adhesive system including the adhesive, the surface preparation and the surface coating applied on the adherends. Earlier, (Wilson, Sheasby & Maddison 1997) had already emphasized that more than one durability test method should be implemented to achieve the best bond in term of strength and durability. through three different test methods they demonstrated the importance of combining the data in the selection of the best combination of adhesive and surface treatment.

Another attempt to develop a durability test method was made by (Knox & Cowling 2000*b*) who considered accelerated ageing as a means to assess long term performance of surface pre-treatments. The specimens consisted of steel plates with a thick film of adhesive to be tested. The test consisted of ageing the specimens at 100% relative humidity (r.h) and testing them by stripping the adhesive and recording the load required to remove it. The tests were shown to be successful in rapidly detecting changes in strength at the interface of and adherend/adhesive/primer system. Further, they investigated the performances of adhesive joints with thick steel adherends in a degraded environment (Knox & Cowling 2000*a*). More specifically, they showed the beneficial influence of spew fillet in the strength of aged lap joints and found that water affects both the bulk adhesive and the interfacial region with the adherend.

2.3 Assessing adequacy of damaged joints

2.3.1 Introduction

Many types of defects can be found in the adhesive joints due to voids, foreign matters, non-sticky areas, weakly bonded regions or mechanical and chemical attacks. Hence, a combination of these in a high stressed region can lead to crack propagation. Therefore fracture mechanics analysis is a practical tool to predict how a defect will propagate within the joint in such conditions. This approach used to analyse adhesive joint behaviour should be considered as a complementary method to the stress - strain analysis.

More generally, it can be said that fracture mechanics help to answer a series of questions:

- What is the remaining strength for a corresponding crack size?
- What is the critical crack size for a given service load?
- How long does it take for a crack to grow from an initial size to a critical one?
- What is the tolerable flaw size at the beginning of the structure's life?
- Concerning non-destructive testing, how often should the damage structure be inspected?

As the stress - strain approach is used to assess the strength of an ideal bonded structure (ie non damaged), the fracture mechanics helps to characterise the toughness of the adhesive itself and understand the mechanism of crack propagation. Generally speaking, this characterisation relates 3 fundamental parameters that are applied load, crack size and fracture energy (Griffith 1920, Ripling, Mostovoy & Corten 1970, Kinloch 1990).

As shown by Figure 2.3 there are three different modes of fracture that can be considered, namely: tensile opening mode or mode I, in plane shear mode or mode II and out of plane shear mode or mode III. In most structures, the predominant and most damaging mode is the mode I but it is usually a combination of two or three modes that will effectively be observed when the crack propagates.

2.3.2 Analytical modelling

The first reported analytical model is due to Griffith (Griffith 1920) and was originally applied to glass materials. The author stated that a crack will grow when sufficient energy is released. In other words, crack will grow when all the work done by the applied external forces and the elastic energy stored in the material is converted in elastic surface energy.

Unlike Griffith who considered an energy approach, (Irwin 1957) considered a stress-strain approach to crack propagation. He demonstrated that the stress field around a brittle crack can be described with two parameters: the applied stress normal to the crack and an invariant parameter (invariant with respect to the material) called the stress intensity factor.

The approach of fracture mechanics applied to adhesive bonding was also divided into two: an energy approach and a stress strain approach; the equations associated with these concepts are presented in Appendix A.

An elastic stress-strain approach was considered by (Erdogan 1963) and (England 1965). It was found that the stress surrounding a crack tip of dissimilar materials is proportional to $\frac{1}{r^{1/2}}$ too, where r is the radial distance from the singularity. Also it was shown that the stress presented an oscillating behaviour at the crack tip that is not physically possible.

On the other hand, the energy approach which is more experimental-based and was developed by (Ripling, Mostovoy & Patrick 1963, Ripling et al. 1970) based on Griffith principles. The aim is to obtain a description of the adhesive with a resistance curve (R-curve) plotting the fracture energy G_c vs crack length Δa, Figure 2.4. They chose to use this concept rather than a stress field description of the crack tip because adhesive materials are heterogeneous systems and defined G_{Ic} as a being a material constant. (Rice 1968) proposed a method based on a path independent integral to calculate the deformation at the tip of a cracked linear or non-linear elastic material.

The definition of an adhesive bond can encompass both adhesion of metallic or composite sheets and matrix of composite materials. Hence, a series of studies have been carried out concerning delamination of polymer composites and have been applied to adhesive bonding afterwards. (Hashemi, Kinloch & Williams 1989) and (Hashemi, Kinloch & Williams 1990) showed that a series of correction were needed

in the calculation of fracture toughness of composite specimens. This is due to:

- Deflection and rotation of the crack root,
- Large displacement observed during testing of the specimen,
- Stiffening effects if end blocks are used.

Deflection and rotation of the crack tip are not taken into account in beam theory analysis that considers them to be zero. Therefore the authors proposed a correction factor proportional to the height of the composite ply and taking into account elastic properties of the material. Large deformations of the specimen are due the combination of slender beam and high toughness of the material but also to the presence of end blocks that tilts causing the specimen to distort. The stiffening effects imply to correct the measured vertical displacement. The correction factors take into account both large deformation and end-blocks effects. Further investigations have been carried out concerning different testing procedure and are going to be discussed later in this chapter.

(Blackman, Dear, Kinloch & Osiyemi 1991) outlined the attention to pay when choosing a method to analyse experimental data from Double Cantilever Beam specimens and reviewed the different approaches that can be used, derived from simple beam theory. However, all the four methods described in the Letter were based on an original formula and result on a combination of different parameters. Also, proof of the useful character of the correction factors described by (Hashemi et al. 1989), (Hashemi et al. 1990) were shown experimentally.

2.3.3 Numerical modelling

(Trantina 1972) was the first author to report numerical analysis of cracked adhesive joint through finite element analysis. Fracture toughness and stress intensity factor were assessed via compliance method and displacement method respectively. The author also investigated the influence of adhesive thickness in the stress distribution around the crack tip. He found that fracture energy G_I decreases with increasing adhesive thickness. Also remarkably, for very thin adhesive thickness, fracture energy of adherend-adhesive system becomes similar to the fracture energy of the adherend alone. The analysis allowed to show the equivalence between fracture energy G and stress intensity factor K in the case of fracture in bonded sheets.

(Wang, Mandell & McGarry 1978) numerically investigated the influence of adhesive thickness on the stress field surrounding a crack tip. Effect of adhesive thickness on the stress intensity factor was found negligible for various adhesive to adherend modulus ratios and it was outlined that the stress singularity is limited close to the crack tip. Effect of adhesive thickness were shown more apparent with stress distribution exhibiting small divergence around it. Further conclusions were drawn concerning the influence of modulus ratios: it was found that the singularity is reduced between the case of monolithic system and the case of an adhesive adherend system. Also, they showed that the trend of stress at the crack tip decreases with increasing adherend to adhesive ratios: the stress intensity factor decreases with increasing stiffness of adherends.

(Ouezdou & Chudnovsky 1988) investigated the adherend adhesive interaction and proposed a model that took into account the adhesive layer in a Double Cantilever Beam. They outlined that the adhesive layer notably affects the strain energy release rate. The latter is increased with increasing adhesive layer and as the adhesive rigidity decreases for a given geometry. The authors also noticed that even if adhesive and adherends stiffness are of the same order of magnitude, the adhesive layer still contributes to the fracture toughness.

Following the work from (Fernlund & Spelt 1991), (Fernlund, Papini, McCammond & Spelt 1994) used finite element analyses to validate the concept of the J-integral approach combined with large deformation beam theory, to obtain a closed-form expression of the fracture energy taking into account applied loads in cracked adhesive sandwich. Their assumptions were fairly restrictive for the application of the expression: the adhesive layer was assumed to have minor effects on the deformation of the joint and the cantilever was assumed perfectly built-in implying no rotation of the beam root. However, their results correlated with non-linear finite element analysis and experimental data within less than a 10% margin. The interesting feature of this method was that it is not necessary to have the knowledge of stresses in the adhesive layer but just applied loads providing a more general approach as presented by Bigwood & Crocombe (Bigwood & Crocombe 1989).

(Hamoush & Ahmad 1989) developed a failure criterion to estimate the interface separation load for adhesive joints with dissimilar materials based on the evaluation of the J-integral. Their method was a combination of analytical, numerical and experimental analysis as the finite element analysis was used to compute the strain

energy release rate based on the input loads from experiments. They concluded that the critical energy release rate can be used as a material property and as a failure criterion for interfacial crack between two different materials because it is independent of adhesive thickness, initial crack length and type of applied load. While the critical energy release rate G_c remained constant with the latter parameters, it was outlined that the mode I and mode II components of G_c are not.

(Pradhan, Iyengar & Kishore 1995) used finite element analysis in order to assess the strain energy release rate of various adhesive joint geometries. Their model was not based on the J-integral evaluation but on a crack closure representation and only required knowledge of nodal forces and displacements. Single-edge notch tensile specimen, four point bending of a cracked lap shear specimen and a cracked double lap joint with two different boundary conditions were considered. Also, they considered different locations of the crack at the interface and different growth directions. Their investigations led to the conclusion that crack growth and crack location are sensitive to boundary conditions but critical crack length is independent of rigidity of constitutive materials and independent of whether or not a pre-crack is made; this was the same conclusion made by (Fernlund et al. 1994). Concerning adhesive thickness influence, low adherend to adhesive thickness ratio implies fast and unstable crack growth and low failure load. They therefore highlighted the importance of having low adherend to adhesive elastic modulus ratios, low overlap ratios and high thickness ratios in order to get strong double lap joints. This last point confirmed conclusions made by (Ouezdou & Chudnovsky 1988).

2.3.4 Influence of geometry

Although Ripling & Mostovoy assumed that the fracture energy was a material constant, it was shown by several authors that the adhesive thickness and the adherends materials can influence the fracture toughness value of adhesive joints.

Previously cited, (Wang et al. 1978) initiated investigations on the influence of adherend materials on the stress field surrounding the crack tip. (Bell & Kinloch 1997) experimentally and showed that the adhesive fracture energy may depend on the type of adherends used even when cohesive failure occurs. This dependence was numerically shown to arise from the elastic modulus of the substrate that influence the stress profile ahead of the crack. In their case, the higher the stiffness of the adherend, the higher the G_{Ic} value.

(Yan. Mai. Yuan. Ye & Sun 2001a) conducted experimental and finite element analysis on DCB specimens. They showed that critical energy release rate G_c and critical J-integral J_c depends on the adherend stiffness. The values were lower in the case of stiffer adherend (steel compared to aluminium adherend) while the J-integral approach was less sensitive to the change of adherend material properties but gives more conservative results. The stress approach was in agreement with the results found by (Wang et al. 1978) but the results from the fracture approach were different to the results given by (Bell & Kinloch 1997. Blackman. Kinloch & Paraschi 2001).

(Blackman. Kinloch. Paraschi & Teo 2003) have used the main three analytical models based on the energy approach described in Appendix A to measure the mode I fracture energy of adhesive joints. They considered both DCB and TDCB specimens with three different set of adherends and assess the influence of each analytical models and the adherends. They showed that the G_{Ic} values were independent of the joint geometry but dependent upon the substrate materials used due to the curring process and the glass transition temperature of the different materials.

(Kinloch & Shaw 1981) were one of the first authors to investigate the fracture behviour of joints with thick adhesive. They considered TDCB joints with steel adherends and increasing adhesive thickness (0.1 mm to 3 mm) and assessed the fracture energy G_{Ic} for a range of adhesive thicknesses. temperatures and rate of loading. They found that the fracture toughness reach a maximum value for a specific bond thickness but remain than the fracture energy from the bulk adhesive. They explained this phenomenon via the shape of the plastic zone developed at the crack tip. ie. in terms of constraints.

(Daghyani. Ye & Mai 1995) used compact tension (CT) specimens made with aluminium and rubber-toughened resin to assess a relationship between the fracture energy and the bond thickness. considering elastic-plastic model of the adhesive. Hence they used the J-integral approach to obtain the fracture energy. They found that J_c was highly dependent on the adhesive bond and increases with the thickness towards the fracture toughness of the bulk adhesive. They identified brittle fracture for thin between 0.04 mm and 0.5 mm and tough fracture mechanisms for bond thickness beyond 1 mm.

(Yan et al. 2001a) also considered the effects of adhesive thickness on the fracture toughness of DCB joints. The analysis was carried out with aluminium substrate

and elastic-plastic analysis for adhesive between 0.4 and 1.8 mm. Like the previous authors, they show the complex behaviour of the fracture toughness of the joints with respect to adhesive thickness. They showed that for a same load level, the opening stress ahead of the crack was higher in the case of smaller bond thickness.

(Yan, Mai & Ye 2001b) proposed a model to explain the dependence of the joint fracture with bond thickness. According to their study, this dependence is due to a competition between two fracture mechanisms. Linear increase of toughness with thin adhesive bonds is explained by the high constrained from the adherends while for thick bonds, it decreases due to the blunting of the crack tip with increasing load.

2.4 Actual marine applications

Before adhesive joints were considered to connect structural elements in ships, works were carried out in the 1980's on the possibility to use adhesive for crack repair. The interest is that it is cost effective and can be used in a straightforward manner compared to welding. (Allan et al. 1986) have investigated the possibility to bond high Young's modulus patches (steel and carbon fibre) to cracked aluminium ship structures. Fatigue test were carried out on different configurations of patches with different adherends and adhesives. The method was proved to be useful with highlight of need of good surface preparation. Steel patch was shown to have a better fatigue life than carbon fibre one and concerning patch design, it was suggested that tapering the adhesive is more efficient than tapering the plate itself. (Grabovac, Bartholomeusz & Baker 1993, Grabovac 2003) have used carbon fibre composite materials as a reinforcement of an aluminium superstructure prone to fatigue induced cracking. They showed that the reinforcement was still in place and that no further crack propagation occurred in a 7-year period.

Adhesive bonding has been investigated shipbuilding and offshore applications for more than a decade. Early studies were made by University of Glasgow to investigate adhesive bonding as an alternative to welding for the attachment of structural stiffening. (Hashim et al. 1990) have tested different possibilities of steel stiffeners bonded to flat plates. They concluded that adhesives have the potential to be an alternative to welding for some structural connections in shipbuilding although it should not be a simple substitution. The adhesive bonding process can be implemented in shipyards. However, the authors outlined lack of data concerning joint

behaviour such as corrosion effects, creep behaviour of joints, fatigue life and crack propagation in adhesive bonds.

(Winkle et al. 1991) further developed investigation concerning adhesive bonding in marine environment. Temperature and creep effects were studied, fatigue strength and marine environmental degradation were assessed. Furthermore, their focus turned to bonding of sandwich structures and dissimilar materials. Their conclusions were that adhesive offers the possibility to join a large variety of materials used in the marine industry. They outlined again the lack of long term performance and a concern with respect to strength at high temperature. Concerning a more detailed analysis of bonded joints, they showed that strength not only depend on adhesive properties but more on the stiffness of adherends. They therefore suggested that care should be taken in extrapolating data from small-scale analysis to large-scale one. They emphasized the importance of finite element analysis of simple joint to quantify the stress level in larger structures.

(Judd, Dodkins & Maddison 1996) carried out an extensive analysis of an adhesively bonded aluminium structure for a 56-metre vessel. Analysis included joint design, adhesive selection process, test programme, construction and facilities and the implication in terms of weight and costs. They concluded that adhesive bonding would offer a subsequent weight reduction and eliminate any distortion in the structure. However, they emphasized the need to carry out more extensive durability studies concerning adhesive joints and reckoned the possibility to further optimise the scantling and building processes. Like (Winkle et al. 1991), they highlighted the limitations of analytical tools to evaluate stress in bonded joints and pointed out the interest of finite element analysis to analyse different joint configurations.

(Hashim 1999) presented an experimental and numerical programme carried out at the University of Glasgow on thick steel adhesive joints for shipbuilding. For adhesive selection procedure, tests such as shear strength and cleavage tests were considered to be useful to compare different products. Environmental degradation was studied and it was shown that loss of joint strength was about 10% per year in marine environment. It was also pointed out that it is difficult to correlate results obtained in laboratory conditions and those obtained in a real environment during a relevant period of time. For the use of analytical or numerical modelling methods, it was suggested to use beam theory with a suitable correcting factor to assess stress and deflection of longitudinal elements adhesively bonded. Closed-form and finite

element analysis were considered to be reliable design tools to assess local stress in simple and complex bonded structures respectively.

(Hashim & Knox 1999) carried out an extensive work on the design of joints with thick adherend and epoxy adhesive. They considered two design concepts: double butt strap joint with composite adherends and steel straps and shell-to-frame joints under tensile loading. They concluded that the strength of the joints depended on the geometry of the substrate (thickness and design) and identified critical zones prone to stress concentration at the interface of the adhesive and the composite. (Hashim & Knox 2004a) also investigated the behaviour of other joint design with thick adherend. They presented three case studies where they investigated the influence of joint tapering, the use of thick composite adherends and the behaviour of joints at high temperature. From this study, they concluded that joint design can be more important than the materials used. They also validated the creep resistance of bonded stiffened panels under fire conditions.

Recently, the BONDSHIP programme (Weitzenböck, McGeorge & Osnes 2004a, Roland, Manzone, Kujala, Brede & Weitzenböck 2004) aimed to promote adhesive bonding in European shipyards in order to reduce production and operating costs in shipbuilding. More specifically, work was carried out on adhesive modelling (Wang, Mieth & Capeletti 2004) and the design and construction of an aluminium superstructure that is reported by (Cantrill, Kapadia & Pugh 2004).

2.5 Summary – Motivations

The previous sections were dedicated to the presentation of the state of the art concerning the assessment of adhesive joints for structural applications. This encompassed the evaluation of stress distribution within the adhesive bond of perfect joints and the assessment of damaged joint assemblies via a fracture mechanics approach. From this analysis, few comments can be done concerning certain issues:

- An extensive work has been carried out in the past decades on linear and non-linear analytical solutions to assess stress and strain distribution in adhesive bond. Nonetheless, except in the work by (Bigwood & Crocombe 1989), none of them allows complex loading or load applied on complex joints. This can only be done using numerical analysis such as finite element.

- Because the use of adhesive technology was mainly limited to the aeronautics

industry, that considers thin sheets, few studies have been carried out on the behaviour of bonded joints with thick adherends.

- Most of the adhesives involved in the researches presented above exhibit rigid material properties with Young's modulus between 1 and 5 GPa. Indeed, hardly any adhesive with semi-rigid and non-linear material properties have been considered to date.

- Some research has been carried out on the influence of adhesive layer on the strength of adhesive joints but for a limited range of thickness: up to 2 mm. This is due mostly to the fact that adhesive technology has been identified with aeronautics industry that achieves a high level of tolerance and quality assurance that the shipbuilding industry is not capable of without considerable expenses. Also as in the case of thick adherends, high adhesive thickness implies a bending moment harmful for the joint.

- Strictly speaking, analytical methods to assess stress/strain distribution would be no longer valid in the case of large adhesive thickness. It is therefore necessary to understand the mechanism of failure and the behaviour of joints with high thickness with an other tool other than closed-form solution.

- The studies carried out on the influence of adherend materials on the fracture toughness of adhesive joints only consider adherend with same stiffness and results available are usually contradictory.

- Few works have involved the study of complex joint designs whereas an extensive work have been undertaken on simple lap joints with various materials and under various conditions.

- Many researchers have outlined the lack of long term data either under dynamic loads or environmental degradation. This, implying a lack of general guidelines or design rules, explains the low enthusiasm of designers to use such a technology as a structural fastening method.

- Generally speaking, very few works have been published regarding the analysis of large adhesively bonded structures in a marine environment considering a combination of methods such as stress/strain approach and a fracture mechanics approach.

The following Chapter will highlight the current weaknesses that will be addressed in this study and will explain how the research will be developed in order to fill the actual lack of knowledge in this domain.

Figures

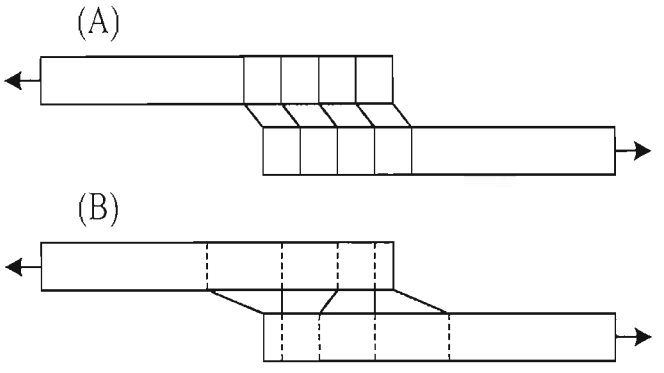

Figure 2.1: Different concept of stress analysis in adhesive bond: (A) simple analysis. (B) Volkersen's analysis

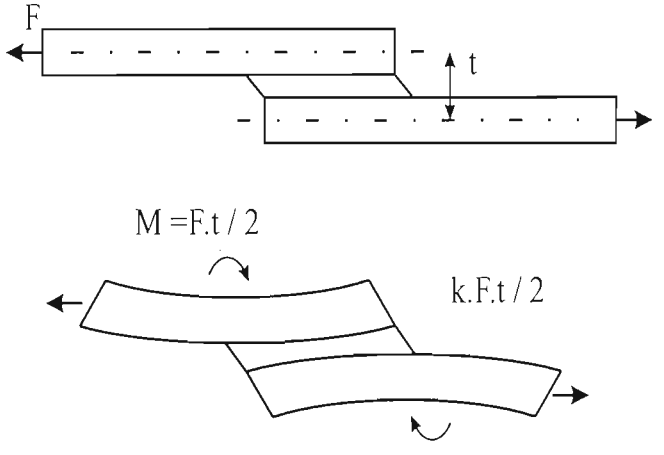

Figure 2.2: Goland & Reissner's k factor concept

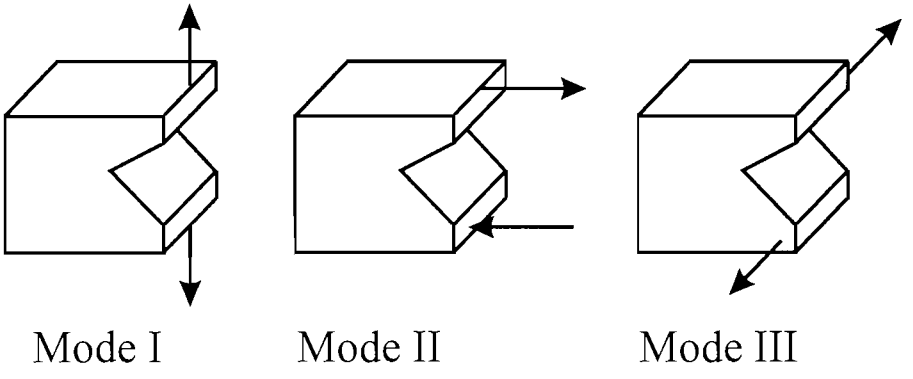

Figure 2.3: Fracture modes

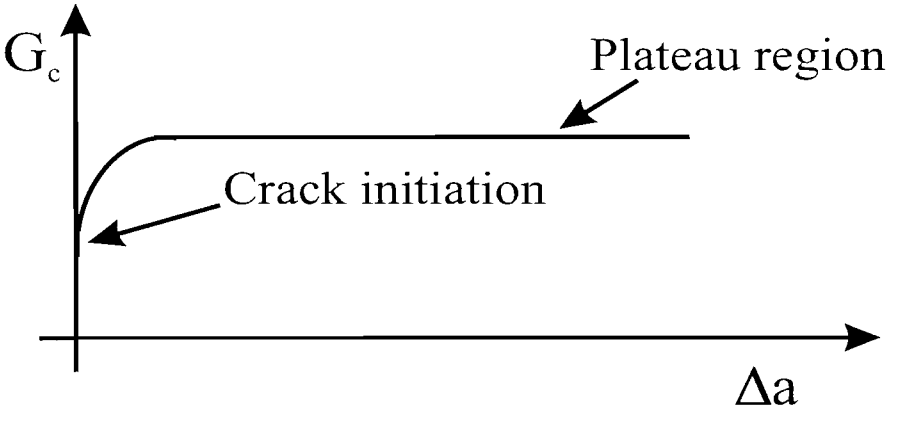

Figure 2.4: Fracture modes

Chapter 3

Background

3.1 Introduction

In order to consider the possibility of using the adhesive bonding technology in a marine context, it was necessary to choose a structure to validate this concept. From a production point of view, the structure had to be large enough to get relevant data and results in terms of tolerance and costs that could be extrapolated or compared to future works. Hence, from an analysis point of view it would lead to realistic stress levels.

3.2 Case study

The case study envisaged here for this analysis is the superstructure of a 34-m ship proposed by VT Halmatic (UK), partner with the University of Southampton of the BONDSHIP project (Bondship 2003). This project, funded by the European Union during the period 2000-2003 aimed at promoting the use of adhesive bonding as a structural fastening technique in the European shipyards.

The superstructure comprises of four principal units and a mast as shown in Figures 3.1 to 3.2. Each unit consists of aluminium extruded box sections. The individual units are assembled as grid work and then brought together to form the unit-to-unit adhesively bonded butt strap connections. The whole assembly is then adhesively bonded on the deck of the ship made of steel. This adhesion technique enables an easier and faster assembly process involving less heavy tools (Cantrill et al. 2004). All the specimens tested and studied thereafter were chosen, designed and manufactured by VT Halmatic.

3.3 Adherend materials

The material used in the framework of the superstructure are the following:

- Mild steel,
- Aluminium alloy 5083 series 6082 extruded box section,
- Aluminium alloy 5083 series plates.

On one hand, mild steel is used in the primary structure of the ship and in this respect represents the deck on which the superstructure is put on. On the other hand, aluminium alloys are used for structures above the deck of the ship as they present a higher strength to weight ratio than steel. The reason for these materials to be chosen was because they represent typical materials used in marine industry and specifically in the superstructure mentioned in the previous section. Aluminium alloys 5xxx series have a high corrosion resistance and aluminium alloy 6xxx series present good weldability and corrosion resistance that make them suitable for ship-building (Polmear 1995).

Mechanical characteristics of these adherend materials are given in Table 3.1.

3.4 Adhesive system

The adhesive system represents not only the adhesive material itself but also the associated surface preparation and primer if used.

As mentioned in the literature review in Chapter 2, there are different types of adhesives, classified according to their mechanical behaviour: rigid, semi-rigid and flexible adhesives. In the case of the superstructure, considering a rigid adhesive would lead to a structure to stiff, whereas a flexible adhesive would not be strong enough to sustain the applied loads. Therefore, the intermediate solution of the semi-rigid adhesive was adopted as it met the requirement mentioned above.

The selected adhesive is a Plexus product named MA 550. It is a two-part methacrylate adhesive designed for structural bonding of thermoplastic, metal and composite assemblies. Notice from the manufacturer indicates excellent fatigue endurance, outstanding impact resistance and a service temperature range from -55^{o}C to $+120^{o}$C that corresponds to the basic specifications for a marine environment. Tests carried

out by Centre Technique d'Arcueil on the bulk adhesive gave the results presented in Figure 3.3 and Table 3.1 summarises its mechanical properties. Although this adhesive is considered as a rigid adhesive with a Young's modulus of 309 MPa, it can be seen that linear portion of the mechanical behaviour is fairly restricted either in tensile and shear behaviour.

In order to ensure a stronger interlocking between the adhesive and the adherends, a surface preparation was carried out based on manufacturer requirement for non-coated substrates (Cantrill et al. 2004). The aluminium and steel surfaces were initially ground using an 80 grit disc. The surface was then cleaned and degreased using an acetone wipe. A PC120 primer from Plexus was applied straight after to increase the long-term strength of the bond after been exposed to the marine environment. It was left to dry for five minutes before bonding. The adhesive was applied by two different methods: a pneumatic gun and a Mix-Pro dispenser. The Plexus MA550 adhesive had an open time of 45 minutes and a cure time between 1 $\frac{1}{4}$ and 1$\frac{1}{2}$ hours at 23°C, however these times were considerably extended due to a relatively cold working environment.

3.5 Butt strap joints

For the butt strap, the adhesive was liberally applied on both surfaces for the samples with the 1 and 3mm adhesive gap. Strips of wood were clamped along one of the base plates in order to locate the upper plate. The 1mm gap was set using 1mm thick washers spaced approximately 100m apart. Three stacked washers were used to set the 3mm gap.

The 5 and 10mm thick bond lines were sealed around the edges using tacky tape and the adhesive was injected through a series of holes, as shown in Figure 3.4. Each hole was sealed off once the surrounding area of the cavity was full.

3.6 Double Cantilever Beam specimens

For the DCB specimens, a 51mm debond area was formed at one end of the plates using PTFE tape with adhesive backing a 1mm thick bond-line was formed using 1mm thick washers at the corner of each plate Figure 3.5. The adhesive was liberally applied on the plate. During the curing procedure a 25kg weight was applied to close the joint in the middle of the plate. All surfaces were cleaned and prepared using

the technique described above in Section 3.4.

3.7 Structural joints

As mentioned in Section 3.2, stiffeners are designed as extruded aluminium box sections. Two different designs were investigated, namely:

- Deck-to-superstructure joints, Figure 3.6: they represent the connection of the superstructure assembled in units that is bonded to the deck of the ship.
- Unit-to-unit joints, Figure 3.7: they represent the connection between each unit as defined in Section 3.2. The extruded aluminium box sections are bonded as butt strap connections.

The reason behind the choice made by the shipyard of such frame design was that it would lead to less complex welding of joints during the fabrication phase. The steel-to-aluminium joints were manufactured in 500mm lengths and cut into 80 mm lengths for testing. The surface preparation and bonding application were followed as described in Section 3.4, with the aluminium box section being clamped against the side plate and steel box section during the curing process. The aluminium strap was attached after the main joint had been manufactured. The joint design specified that a nominal 3 mm adhesive thickness was required between all bonding surfaces. This thickness was achieved using polyethylene tile spacers, which happened to be 3 mm thick. The manufacturing procedure for the aluminium-to-almuinium connection was the same as for the steel to aluminium connection, Figure 3.8, but were made in 1150 mm lengths.

3.8 Summary

This chapter has presented all the elements necessary to the understanding of the present study such as the adherend materials, adhesive system and different joint designs that will be referred to in the following chapters. Based on this data, the next chapter is going to expose the methodology adopted to investigate adhesive bonding in a marine environment.

Tables

	Adhesive	Al 5083	Al 6082	Steel
E (MPa)	309 ± 42	71000	69500	200000
$R_{p0.2}$ (MPa)	-	145	310	205
R_m (MPa)	14	300	340	600

Table 3.1: Mechanical characteristics of adherend and adhesive materials used in structural joints. E: Young's modulus, $R_{p0.2}$: yield strength, R_m: ultimate strength

Figures

Figure 3.1: Patrol craft and ship superstructure.

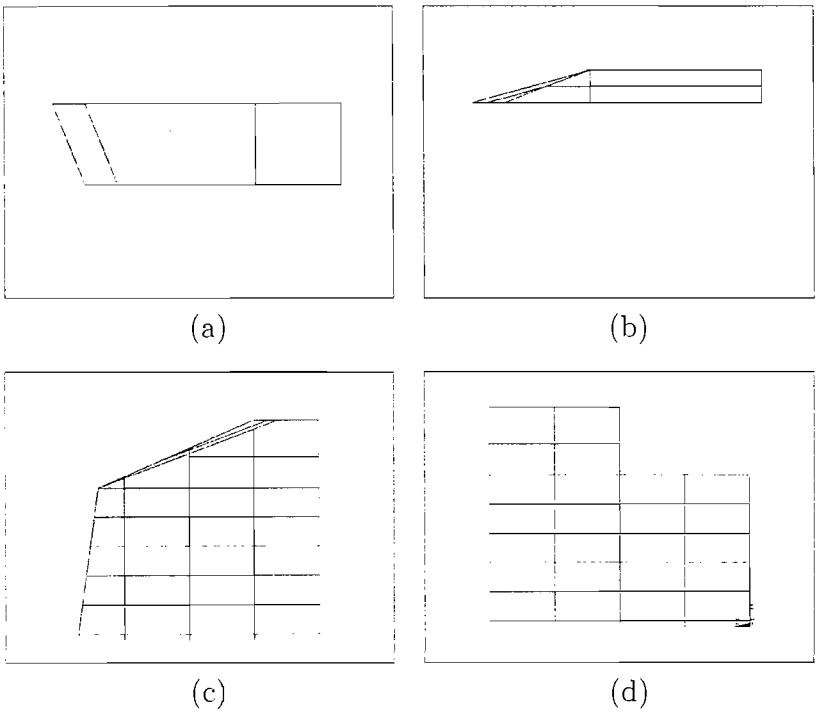

Figure 3.2: Model of the superstructure units prior assembly: (a) Unit 3, (b) Unit 4, (c) Unit 1, (d) Unit 2.

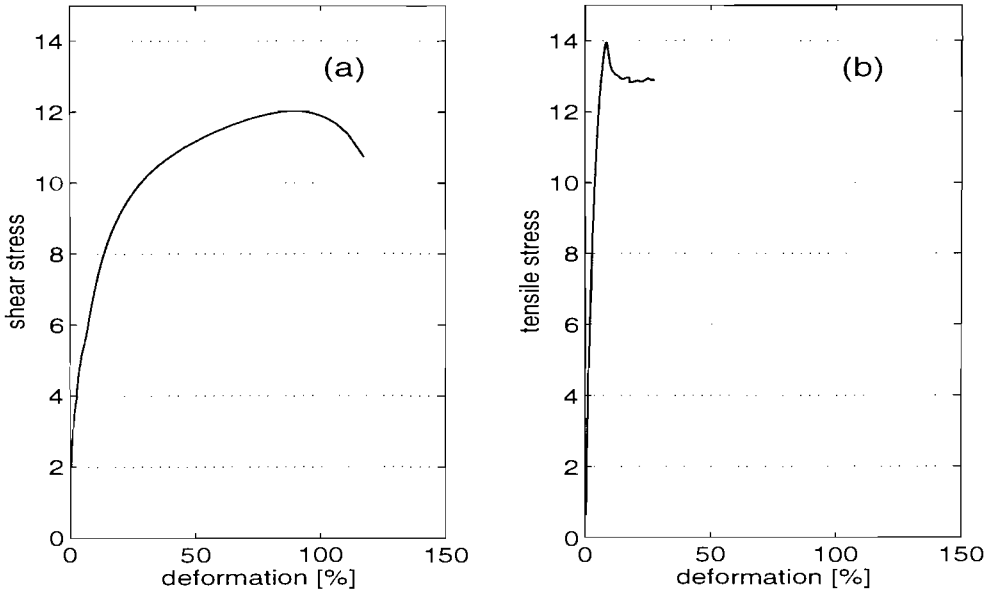

Figure 3.3: Adhesive mechanical properties; (a) shear properties, (b) tensile properties.

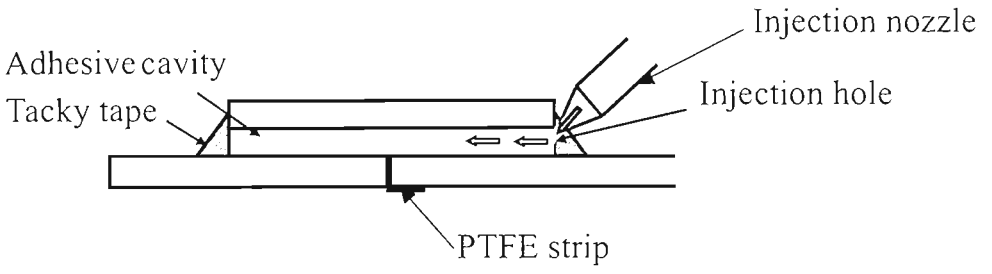

Figure 3.4: Injection of adhesive for the butt strap joint with 5 and 10 mm adhesive bond

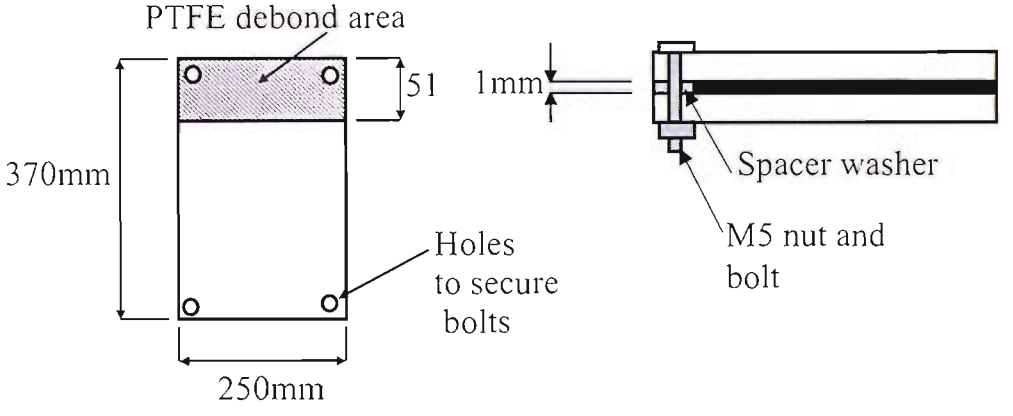

Figure 3.5: Plate for the double cantilever beam specimens

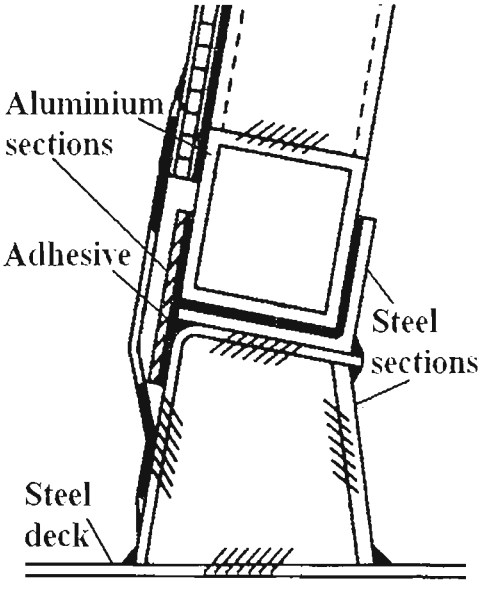

Figure 3.6: Deck to superstructure structural joint

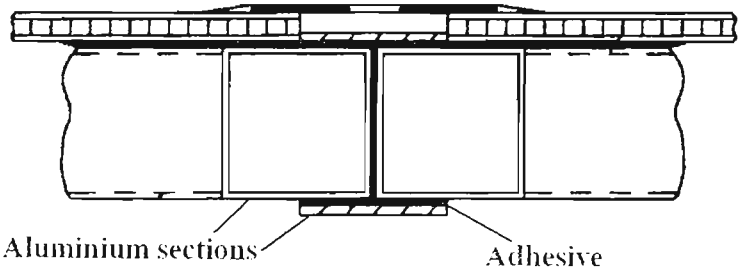

Figure 3.7: Unit-to-unit structural joint

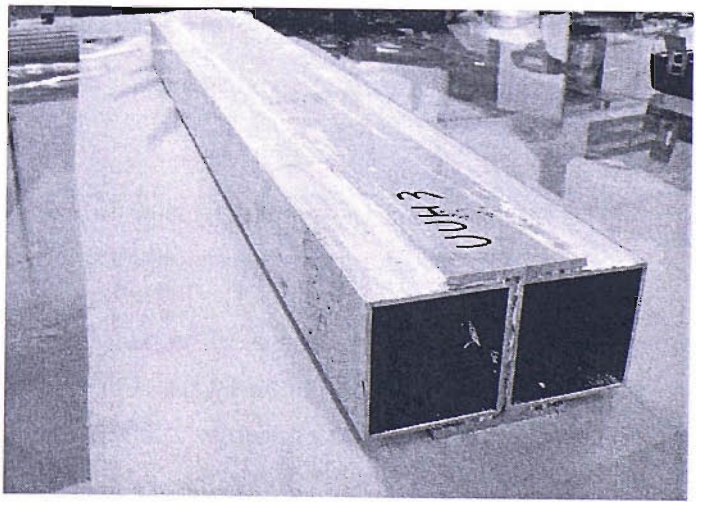

Figure 3.8: Aluminium-to-aluminium connection beam to be cut into 5 specimens

Chapter 4

Methodology

4.1 Introduction

As pointed out in the literature review, there is a lack of understanding concerning the use of adhesive bonding for large structures with thick adherends and relatively thick adhesive (more than 1 mm), especially in a shipbuilding environment. Specifically, knowledge needs to be enhanced in the following areas:

- The influence of adhesive thickness variations at large scale (typically 1 to 10 mm) and the influence of environmental degradation on the strength of joints.
- The influence of different metallic adherends of relatively high thickness, (typically 3 to 6 mm) in the strength of joints.
- The mechanical behaviour of large structural adhesive joints typically used in shipbuilding.
- The integration of both a fracture criterion and a strength criterion for the assessment of basic and structural joints.

The present study seeks to address each of these aspects and to give some insight into the behaviour of adhesively bonded joints to be used in a marine environment. The reason to cover such different aspects lies in the approach adopted to consider adhesive bonding in a global structure. The next sections describes the layout of the study and outline the key aspects that are going to be developed in the following study.

4.2 Overall description

The goal of this research is to advance knowledge towards a basic methodology for the designer who wants to include adhesive bonding as a structural fastening technique in the design of a ship. Figure 4.1 illustrates the the overall approach on which the present study is based.

The approach can be divided into three parts. The first part is more concerned about decision making and design process than actual investigation, dealing with structural and joint design and selection of adhesive. The second part deals with the strength analysis of joints and the third, with energy-based analysis of the joints. However, overall, the philosophy that will guide this research is based on a "global to local" approach but this step by step approach does not prevent these steps to be interrelated as it will be shown during this study.

At an early stage, the design data available are the global structural design, the materials to be used and the load specifications. The structure is based upon a conventional all welded superstructure of a 34m Customs & Excise Cutter by Vosper Thornycroft. It consists of modular aluminium units bonded to each other and a steel base plate. Each unit comprised a welded aluminium 6000 series framework to which an aluminium honeycomb 5000 series cladding was bonded to form the walls and flooring, (Cantrill et al. 2004). The load specifications are derived from the High Speed Craft code from the DNV rules (DNV 2001).

Structural joint synthesis was carried out by Vosper Thornycroft: it implies in particular the specification of the joint requirement and its functions. In this case, adhesive bonding was chosen to transmit loads between units: load transmission was mainly through compressive and shear stresses at the ship to superstructure joint for both the baseline and honeycomb clad versions. The "range of feasible designs" stage in Figure 4.1 implied the choice of one design from a range of possibilities such as T, I, top hat and box sections. This choice is dictated by factors such as cost of the joint during production, its structural function, environmental conditions and maintenance capability during in-service conditions. In this case, the aluminium framework consisted of extruded box sections, the joint between units was based on a double butt strap joint design while the joint between the steel base and the whole framework was also based on similar butt strap joint design, Figures 3.6 and 3.7.

Then two questions must be answered that will strongly determine the future study. The first is "Is the joint design a complex one?". If the answer is NO, then a simple design leads to a simple stress-strain analysis with closed form solutions e.g. (Goland & Reissner 1944, Bigwood & Crocombe 1989) and a limited experimental program. On the other hand if the answer to the question YES, then a programme involving finite element analysis and testing at small scale, should be considered. The results from the experimental programme could be extrapolated for the original design. In the present case, the joint designs are relatively simple but are included in a rather complex structure, hence an FE analysis and an experimental programme were considered. Then, from the complex design, a simpler one should be identified as the generic joint design: here the designs being based on double butt strap joints, it is chosen to use the single butt strap joint as a generic joint design, Figure 4.3. This enables the strength assessment of the adhesive system, combining all the adherend materials found in the structural joints. For the energy based assessment, double cantilever beams offered a convenient mechanism to assess the mode I fracture toughness of the adhesive. This design was chosen for its simplicity and because mode I fracture was considered more likely to occur in the joints: it is the most damaging mode for the structure.

The use of closed form solutions for the stress analysis is usually limited by the geometry of the joint but also by restricting assumptions relating to adherend materials, adhesive layer thickness and the stress distribution through the thickness of the adhesive. In this respect, they only provide an indication of the level of stress in the adhesive bond as most of them fail to account for zero shear stress at the edges of the joint. However, this type of analysis is relatively easy to set up and can be sufficient for preliminary sizing and dimensioning.

The second question to be answered is "Does the structure have load bearing capabilities?". It is related to the complexity of the joint. It is an important step as this will determine the type of adhesive that has to be used, based on basic manufacturer specifications. If the joint is designed for aesthetic purpose and carries little load, then a flexible adhesive could prove to be sufficient. On the other hand, if the joint is designed to carry a significant load, then a rigid adhesive needs to be considered. The main characteristics of the rigid adhesives are a high material stiffness and relatively low strain to failure (typically 2-5%). Flexible adhesives, on the other hand, tend to be more compliant and non-linear in their stress-strain

behaviour. Ideally, a comprehensive screening test programme needs to be carried out to select the most suitable adhesive system for the structure, but this was not in the scope of this study. In this case study, an alternative solution to rigid and flexible adhesives was adopted, choosing a semi-rigid adhesive to achieve a compromise between gap filling capabilities, strength and cost. It was also necessary to select an adhesive that would fall into the tolerance margins without too much loss of strength.

Once these choices have been made the assessment of the adhesive behaviour is carried out. This includes the assessment of the bulk properties of the adhesive material such as the Young's and shear moduli as well as the ultimate strength to failure and the stress-strain behaviour. Figure 3.3 shows the tensile and shear behaviours of the adhesive used in this study and Table 3.1 summarises its mechanical properties as well as the properties of the adherends used.

4.3 Field of investigation

All the data presented previously gives all the necessary input to carry out a study on generic and structural joints: these steps, described in the bottom part of Figure 4.1 are briefly presented in the following and will be developed in Chapters 5 to 8.

The load response of the global model concerns the assessment of the load resisting capacity of the superstructure defined in the very first step of the chart. The requirements of the structure are its ability to withstand a certain level of hydrostatic and hydrodynamic external loading defined by regulatory bodies (DNV 2001). This should identify load transfer mechanisms and the inherent high loaded regions that need further detailed studies.

The structural joint models deal with the load transfer and failure mechanisms at generic connections identified in the global model to be critical in terms of stress. The load input and boundary conditions for this assessment are obtained from the global model. The nature of the analysis type is derived from the assessment of the joint detail.

The local joint model deals with the analysis of the joint detail. Typical considerations at this level include topological dimensioning, material choices, analysis types and failure mode. This analysis is essential in underpinning the scantling choice and production process specification in terms of adherend surface preparation and

adhesive application.

Then the frame of the actual research is divided as follows and developed thereafter:

- Basic joint behaviour and assessment of adhesive system from both a strength and fracture mechanics approach,
- Assessment of environmental degradation on the local joint design,
- Structural element: behaviour of perfect joints and assessment of the stress state in the adhesive bond.
- Structural element: behaviour of damaged joints.

From the design of a superstructure, structural joint designs are defined (see (Cantrill et al. 2004) and Figures 3.6 and 3.7). The original design, Figure 3.6, was simplified to obtain a more basic experimental joint model, Figure 4.2. The butt strap joint, Figure 4.3, will constitute the basic joint design on which a parametric study will be carried out for the strength based assessment of local element, Chapter 5. To assess the adhesive system from a fracture mechanics approach, Chapter 6, local elements are defined as Double Cantilever Beam specimens (DCB) made with the different substrates presented earlier in Section 3.3. This first part will provide a database concerning the adhesive system and a series of input for the assessment of non-damaged and damaged structural elements: mode of failure of the joints, mechanical behaviour and stress-strain assessment, critical fracture energy of the adhesive and joint sensitivity to adherend and adhesive thickness.

The assessment of a structural joint can be subdivided into two parts. The first part concerns the assessment and prediction of the strength of perfect joints through experimental and numerical analysis, Chapter 7. The second part is dedicated to the assessment of the tolerance to damage of structural elements via a numerical analysis, Chapter 8.

A general analysis will provide data on the behaviour of large bonded structures in marine environment for future users. This will provide a better knowledge of adhesive technology in general and on semi-rigid adhesive joints in particular. It will also serve to improve confidence for the design of ship structural components with bonded joints.

Figures

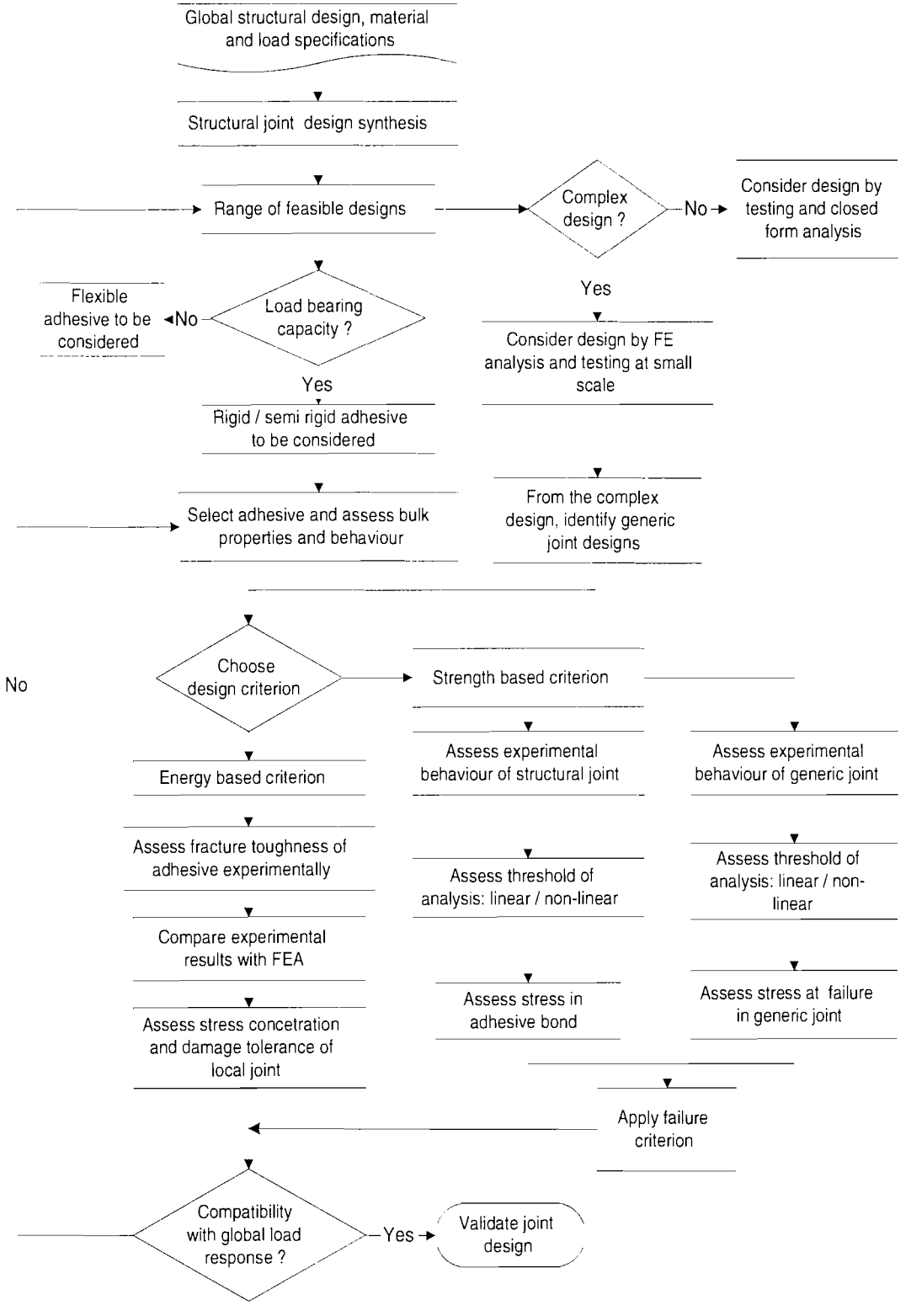

Figure 4.1: Flow chart presenting the general methodology adopted for the thesis

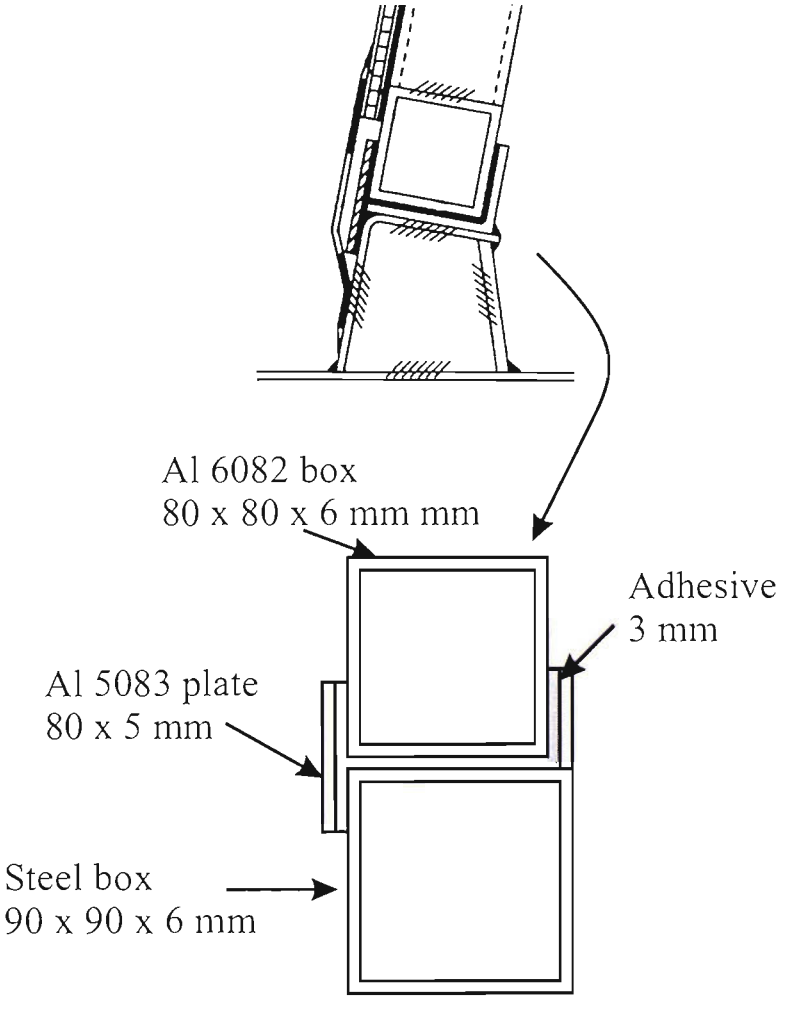

Figure 4.2: From the original structural design to the test model. not to scale

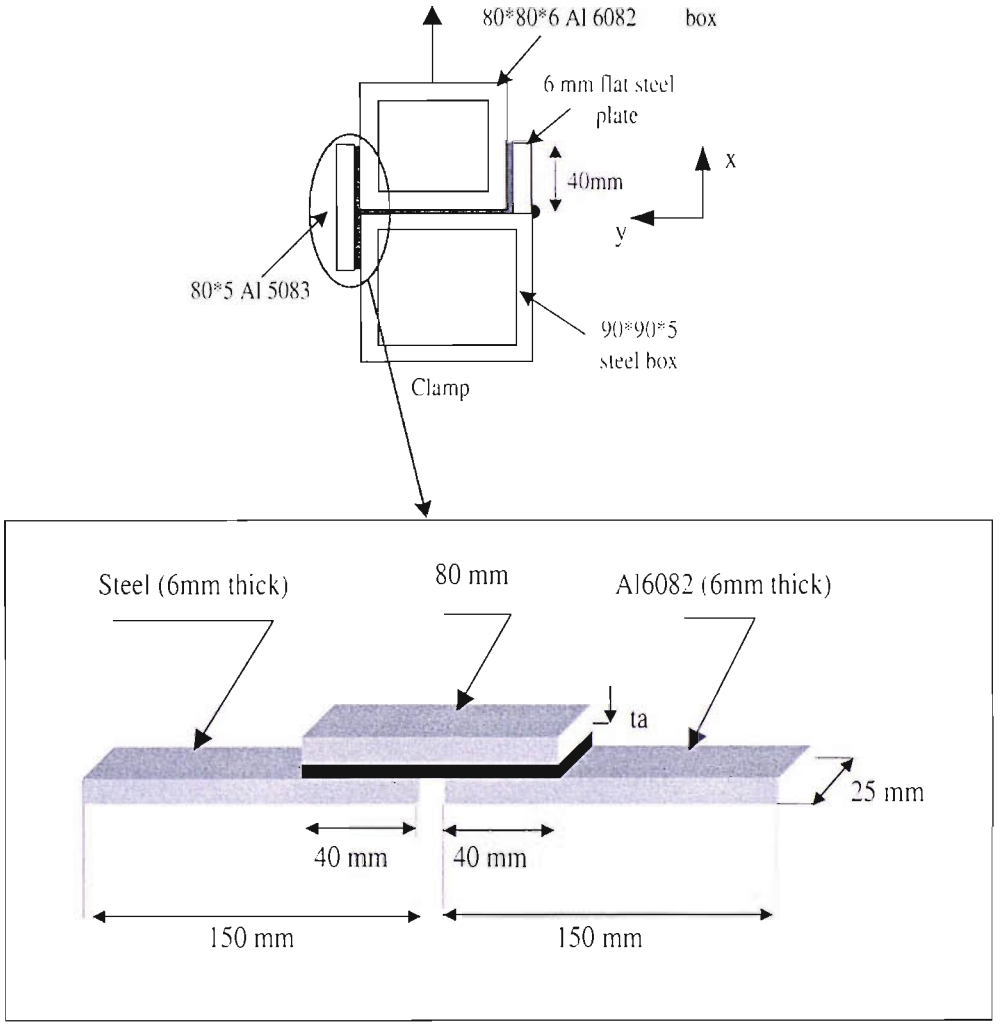

Figure 4.3: Butt strap geometrical and material specifications

Chapter 5

Strength-based assessment of adhesive system

5.1 Introduction

The previous chapters defined the context of the study and the philosophy that will guide it. In order to justify the use of the materials presented earlier (Chapter 4, section 3.3) it is necessary to assess their combination as an adhesive joint in terms of ultimate strength in different conditions.

During the preliminary design of a structure the criteria are stress-based because the structure is assumed to be perfect and defect-free. It is therefore regarded as being a continuum, lending itself to stress-based calculations. The calculations at this stage can involve relatively simple closed-form solutions derived from analytical modeling as seen in references (Goland & Reissner 1944, Hart-Smith 1973) among others. However, the more complex the geometry, the more difficult it is for the designer to use these solutions, therefore other tools such as finite element analysis must be used.

An important aspect for the integrity of an adhesively bonded structure is the influence of adhesive bond thickness on the strength of the structure. Environments such as shipyards, tooling and experience are not yet sufficient to meet the low tolerances seen in aeronautics. This sometimes leads to the manufacture of joints with thicker adhesive bonds than originally specified, as reported by (Cantrill et al. 2004) and studies concerning these effects at such a scale are rare (Colak 2001). The design of structural joints presented in Chapter 4 is based upon a double butt strap joint design as shown in Figures 3.6 and 3.7. From that design, a more generic design can be extracted, Figure 4.3. Although this joint design is not strictly subjected to the same type of load, shipyard experience showed that it was at this location where

large deviations from the nominal adhesive thickness could occur. It is therefore of interest to qualify and quantify the losses of material properties associated with these adhesive variations.

Also, one of the major challenges faced when using structural adhesive bonding in industry is the understanding of degradation due to environmental attacks. This degradation is due to a complex combination of damage of both the adherends and the adhesive itself as well as their interfacial zone that leads to uncertainty about the durability of adhesive joints.

In order to enhance the durability of adhesive bonds, some chemical treatments for adherends are available and are used extensively in the aeronautics industry. However, other industries, such as shipbuilding, cannot afford such high quality surface preparation and the process, in this case, has still to remain basic (Cantrill et al. 2004). Another important aspect for the integrity of an adhesively bonded structure made in a hostile environment such as shipyard, is the influence of adhesive bond thickness on the strength of joints.

The present chapter therefore aims to investigate the influence of large scale variations of adhesive thickness as well as environmental degradation on the strength of simple butt strap joints joining steel and aluminium alloys adherends through an experimental programme.

5.2 Experimental programme

The objective of the experimental programme is to characterise the strength and the mechanical behaviour of single butt strap joints and investigate the influence of different varying bondline thicknesses and hygrothermal ageing on the joint behaviour and mode of failure. This type of experiment has been carried out by various researchers (Adams et al. 1997) on lap shear joints with similar metallic adherends such as aluminium, steel, titanium or composite. However, very little data is available on different joint geometries and on bonding different metallic adherends.

5.2.1 Materials

The joints considered are butt strap joints as presented in Figure 4.3. The butt strap joint consists of an aluminium plate (alloy Al 6082) and a steel (grade A) plate joined together with an aluminium strap (alloy 5083). These materials were

chosen because they represent marine grade products that can be used in shipbuilding (Cantrill et al. 2004). Mechanical properties of these materials are presented in Table 3.1.

The selected adhesive is a Plexus product named MA 550. It is a two-part methacrylate adhesive designed for structural bonding of thermoplastic, metal and composite assemblies. Tests carried out by Centre Technique d'Arcueil (CTA) (Brede 2002) on the bulk adhesive gave the results presented in Figure 3.3. The adhesive has an average Young's modulus of 309 MPa and an ultimate strength of 12 MPa in dry conditions at 20°C.

To manufacture the specimens, an aluminium plate (alloy Al 6082, 500 mm × 150 mm) and a steel plate (500 mm × 150 mm), as main substrates, were bonded with an aluminium plate (alloy 5083, 500 mm × 80 mm). The following surface preparation was carried out prior bonding, based on manufacturer's recommendations for non-coated substrates:

- Aluminium and steel surfaces were ground,
- Surfaces were acetone wiped to clean and degreased them,
- Finally a primer PC 120 product from Plexus was applied straight after and left dried at least 5 min prior bonding.

Four adhesive bond thicknesses were considered: 1 mm, 3 mm, 5 mm and 10 mm to account for low tolerance that may be encountered in practice. The test specimens were then cut in strips of 25 mm in order to get similar specifications as in the standard test on lap shear joint (BSI 2002*b*). In the following, the 1-, 3-, 5- and 10-mm adhesive joints will be referred to as joints A, B, C and D respectively. The geometrical particulars for the joints are given in Table 5.1.

The choice of such coupon test design was dictated by ship design considerations for the integration of structural adhesive joints in the manufacture of a prototype of a superstructure for a patrol craft (Cantrill et al. 2004).

5.2.2 Ageing environment

In order to investigate the effects of water on the joint behaviour, an accelerated ageing test programme was carried out. Two ageing conditions were considered in accordance with the British Standard BS EN 29 142:1993 (BSI 1993):

- Specimens were immersed in a bath of distilled water for 3 weeks at 40^o C.
- Specimens were immersed in a bath of distilled water for 6 weeks at 40^o C.

The standard is relatively open in the sense that it leaves the possibility to use different level of environmental degradation (relative humidity and temperature). The conditions mentioned above were chosen because distilled water was thought to be more damaging for the adhesive bond than salt water (Albericci, cited by (Armstrong 1997)) but also for practical reasons as the level of the solution's salinity is tedious to keep steady (Earl 2001). The given temperature was chosen because it accelerates the absorption mechanisms while keeping the environment below the glass transition temperature T_g of the adhesive (Kinloch 1990, Earl 2001): T_g for the adhesive used was 120^oC. Also, it should be noticed that the joints were put in the bath so as to be horizontally immersed, the width of the joint being in an horizontal plane. This latter point is of importance as some studies (Knox & Cowling $2000a$) have shown that the orientation of the joint during accelerated ageing can affect its durability.

5.2.3 Test set up

Specimens were tested in an Instron universal-testing machine, equipped with a 100 kN load cell and controlled by an Instron 8800 controller, Figure 5.2. Tests were carried out up to failure of the specimen at ambient laboratory conditions 1 hour after being taken out from the environmental chamber and wiped. The rate of loading, constant during the experiment, is taken at 1.0 mm/min.

Specimens were clamped with 40 mm of the main substrates between the grips of the rig. No tabs were used, because unlike in lap shear joints the main bonded plates (Al 6082 and steel) are not eccentric.

During the test, displacement of the cross head and corresponding load were recorded up to failure of the specimen. Crosshead displacement was considered adequate with extensometer usage being unnecessary because: (a) the thickness of the specimens was too large (6 mm of main adherend + adhesive thickness + 5 mm strap adherend) and (b) although it was possible to predict from basic principles that the overlap between aluminium adherends should fail first, some samples started to fail between steel and aluminium making it impossible to set up an extensometer on the specimens.

5.3 Test results

The results are subdivided in three categories: unaged specimens, 3 week aged specimens and 6 week aged specimens. In each category, ultimate and residual strengths were observed and mode of failure was considered through the visual analysis of the interfacial failure of the joints.

5.3.1 General observations

From Figure 5.3 and Table 5.2, it was observed that joints A exhibit a higher ultimate load than the other joints with thicker adhesive bonds. The ultimate load decreases (from 10 kN to 7 kN) as the joint becomes more compliant with increasing adhesive thickness. Although the ultimate load carried by joints A to C is similar, the stiffness is clearly decreasing with increasing adhesive thickness. However, as can be noticed from Figure 5.4, loss of stiffness due to ageing is not as remarkable as the loss due to increase of adhesive thickness. It should be noticed that the degraded characteristics observed for joints B compared to the other joints are due to a poor manufacture. Indeed, prior to testing, voids were observed in the bondline as shown Figure 5.6.

During the tests, it was observed that failure of the joints was brittle for small adhesive thickness (ie 1 mm) and was getting more progressive as the bond thickness increased. In terms of failure modes, it was mainly cohesive within the adhesive for thin adhesive bond whereas for increasing thicknesses more and more interfacial failures zones were detected. Also, it was observed that with increasing adhesive thickness, as the failure was much more ductile than for a thin adhesive layer, cracks could be seen not only initiating at the edge of the specimen but also at the midspan of the joints. It should also be noticed that due to a poor bondline, joint B exhibited poor mechanical characteristics due to the presence of voids in all the failed specimens.

5.3.2 Unaged specimens

5.3.2.1 Load deflection curves

The load deflection curves for joints A and C (see Table 5.1 for nomenclature) are shown to be very consistent in terms of behaviour and ultimate load, Figure 5.3. On the other hand, joints B and D presented less consistency in both behaviour and strength.

A linear portion of the curve can be easily identified for joints A and B whereas for joints C and D, the linear portion of the joint behaviour is much more restricted.

5.3.2.2 General behaviour

It was noticed that although failure occurred mostly longitudinally along the interface with either the lower or upper metallic adherend, it also initiated, during the loading process, transversly from the middle of the overlap length as shown in Figure 5.5. The crack propagated as if the adhesive was ripped, sometimes symmetrically or only in one side of the bond towards the opposite interface due to the bending of the specimens. This phenomenon, that weakened the joint and accelerated its failure suggests a stress concentration at the centre of the overlap length where steel and aluminium adherends edges face each other.

For joints B to D, permanent deformation was observed in the aluminium strap as shown by Figure 5.5 (b) and (c). This permanent deformation was less apparent for joints A Figure 5.5 (a).

5.3.2.3 Failure modes

Concerning the modes of failure of the specimens:

- In the case of joints A, despite voids in some adhesive bonds, all failures occurred consistently cohesively within the adhesive: Figure 5.7 (a). It was noticed that one of the five specimens failed between the steel and aluminium adherends whereas the others failed between the aluminium substrates. However this singular case resulted from a weak bond caused by the presence of a washer included as a spacer within the adhesive bond. This mode of failure between aluminium adherends occurs because aluminium is less rigid than steel, hence causing failure between the weakest adherends.

- In the case of joints B, failure was difficult to assess because of a poor adhesive bond implying "large" zones where adhesion did not occur. Indeed, this latter was dotted with voids spread transversally within the joint as seen in Figures 5.6 and 5.7 (b). Over 6 specimens tested, 5 failed between the two aluminium adherends one failed between aluminium strap and steel adherend.

- For joints C specimens, failure occurred cohesively within the adhesive for all the specimens: Figure 5.7 (c). However, the failure occurred very close to the

adherend, usually less than a millimetre from the adherend-adhesive interface. Also, failure occurred both longitudinally and transversally through the thickness of the adhesive see Figure 5.5. Cracks initiated at the longitudinal free surface either purely transversally or diagonally towards the aluminium strap and starting to propagate along the adhesive-aluminium interface. However, failure occurred usually before it could really propagate all along this interface.

- Joints D presented 50 % cohesive failure. Very smooth failure zones were observed compared to rough areas observed for the previous series of joints: Figure 5.7 (c). As for joints of class B, transverse failure through the thickness of the adhesive was observed. Figure 5.5 (c).

5.3.3 3-week aged specimens

5.3.3.1 Load deflection curves

As for the unaged specimens, the load deflection curves of specimens A and B present a linear portion followed by short non-linear zone leading rapidly to failure, see Figure 5.8. The joints C and D exhibit a non linear behaviour during all the quasi static loading process. In terms of ultimate load, as shown by the low standard deviation in Table 5.2, the results are still very consistent except for the joints B.

5.3.3.2 Failure modes

Specimens were tested an hour after being removed from the bath and dried with a rag. A layer of rust was observed on the metallic parts indicating corrosion of the immersed steel.

- Joints A show a similar pattern of cohesive failure as the unaged specimens, Figure 5.9 (a), suggesting a similar load transfer when the joint is loaded. No presence of water was found within the adhesive bond; however one of the specimens presented part of adhesive failure at the edge of the joint suggesting damage from water. The spew fillet observed at each edge of the joints seemed to have prevented water from penetrating the adhesive bond, thus strengthening the joint. Four joint failures were of type III between the aluminium strap and the inner aluminium adherend and one failure was of type II between the steel adherend and the aluminium strap as presented in Figure 5.10 and defined by (Adams et al. 1997) p 63.

- Failure mode of joints B was difficult to assess because of a poor application of the adhesive, implying a poor adhesion. Figure 5.9(b). Large voids in the

bond allowed water to damage the interface between adhesive and adherend: a combination of corrosion and water itself that seemed to have dissolved the primer inducing premature failure of the joint. It was noticed that for the joint that failed mainly adhesively between the adhesive-primer system and the steel, no spew fillet was observed at the edge.

- All specimens of class C presented a small spew fillet at the edge of the adhesive bond and all failures occurred between the aluminium strap and the steel adherend Figure 5.9 (b). One specimen failed almost completely adhesively. When failure occurred cohesively, the pattern was close to the interface, similar to a joint with 1 mm adhesive thickness: the adhesive acted as a sandwich core between 2 metallic substrates. Also, as in the case of the unaged joints, failure occurred both longitudinally and transversly through the thickness of the adhesive.

- Failure of the class D specimens occurred mainly adhesively (between 40 and 90 % of the bonding area exhibited adhesive failure), Figure 5.9 (c). Where cohesive failure was observed, it was close to the interface with one or the other adherend. This is possibly due to a poor surface preparation on the steel adherend because the surface of the steel did not appear to be very well ground and sometimes hardly any primer was observed on either steel or adhesive. Failure was also observed to initiate transversly through the thickness of the adhesive.

5.3.4 6-week aged specimens

5.3.4.1 Load deflection curves

Figure 5.11 presents the load deflection curve of the batch of specimens tested after 6 weeks of ageing. As in the previous cases, the joints presented a good consistency in their behaviour, although joints A showed a higher scatter concerning the ultimate load.

5.3.4.2 Failure modes

Similarly as for the 3-week aged joints, a layer of rust was observed on the metallic parts consequently to the corrosion of the steel adherend under water.

- Joints A showed a similar mode of failure as presented in Figure 5.12 (a). Presence of the fillet seemed to have prevented damage due to water except in one case where adhesive failure occurred: the presence of a spacer and absence

of a spew fillet probably allowed the water to corrode the steel interface in this case, thus weakening the joint. Failure was of type II and III as previously defined.

- For joints B, two of the specimens presented a cohesive mode of failure together with a relatively good strength. Failure in the fillet was of type II for both samples. However, other samples were of poor quality due to water ingress through voids in the bondline. Failure occurred between the aluminium strap and aluminium inner adherend in four out of five cases. Figure 5.12(b). This is explained because the bondline was probably poorer between the aluminium adherends than between the aluminium strap and the steel adherend, implying premature failure in this zone rather than in a zone where corrosion has not yet occurred.

- The joints C were shown again to have cohesive failure close to adherend as in the case of a thin adhesive layer Figure 5.12 (b). Transverse cracks initiated through the thickness of the joint as previously noticed. Influence of a small spew fillet was not remarkable as alteration of the interface at the edges of joints was observed: dark line as circled on Figure 5.12.

- Joints D presented a similar locus of failure to the 3 week aged series with mainly adhesive failure. Figure 5.12 (c). This was due to a poor surface preparation of the steel adherend and permanent deformation of the aluminium strap. In some of the specimens, failure initiated both between the steel adherend and the aluminium strap on the one hand and the aluminium inner adherend and the strap on the other. This phenomenon was emphasised by the presence of gap in the middle of the over lap of the joint that appeared during the application and curing process because of the particularly large thickness of the adhesive layer: Figure 5.13. Failure through the thickness of the adhesive was also observed as previously noticed for other specimens.

5.4 Numerical modelling

Observations from the experimental programme showed a series of aspects that needs further consideration. Among these critical points are the influence of adhesive thickness in the failure mechanism of the joints, the influence of geometrical non-linearities and the influence of material non-linearities. Indeed, it was shown, Figure 5.5 (b) and (c) that significant permanent deformation occurred in the adherend while adhesive thickness increased. Also, the shear and tensile properties presented

subsequent non-linear behaviour. Therefore a finite element analysis was carried out to investigate the influence of these parameters.

5.4.1 Finite element model and boundary conditions

The model considered is a butt strap with 2-D 8-Node structural solid elements from ANSYS package as presented Figure 5.15. The element is defined by eight nodes having two degrees of freedom at each node: translations in the nodal x- (u_x) and y- u_y directions. The adhesive is assumed to be isotropic and the analysis done in a plane strain condition.

The geometry and the finite element models were the same in the three cases. The first case considers the adhesive to have linear material properties, the second case includes geometric non-linearities and the third one considered the adhesive to have non-linear material properties. In the non-linear case, the numerical analysis was performed using a multi-linear elastic method: this method describes a conservative response in which unloading follows the same stress-strain path as loading (ie with no hysteresis effects) particularly suitable to model non-linear elastic materials.

The boundary conditions match as closely as possible the conditions encountered during the tests and are described as follow: the degree of freedom u_x and u_y of the first four columns of nodes on the left main plate (steel) are blocked to represent the clamp. The last four columns of nodes on the right main plate (Aluminium) are constrained in the u_y direction only and constrained to move together in the u_x direction.

5.4.2 Convergence analysis

Before any analysis of the adhesive stress should be carried out, a sensitivity analysis to the mesh density has to be done in order to show convergence of the model towards a single solution. Two criteria were chosen to check the convergence of the results. The first one is stress based, as the main focus of the analysis is the stress in the adhesive bond of the joint. The second one is based on the stiffness of the model. The reason for having a second criterion is to cross check the first result as the stress analysis showed that a singularity occurs at the horizontal free surface portion of the bond line, making difficult a sensitivity analysis based on stress values.

The stress-based convergence criterion was check on joint A (1 mm adhesive thick-

ness): the normal and shear stresses along a line of an arbitrary 4 mm close to the gap of the joint (Figure 5.16) was computed for an increasing number of nodes, hence number of degree of freedom. Figure 5.17 shows the evolution of both stresses: it can be seen that beyond 9000 nodes in the model the results converge for both the peel and shear stresses. As joint A has the thinest bond of the four joints the singularity at the gap is most pronounced of the four joints, hence it is assumed that a convergence is met for the following joint B, C and D.

For the cross check with the stiffness values, the sensitivity analysis was carried out in two steps: in first instance, an analysis was made varying the mesh density through the thickness of the adhesive and a second analysis was made varying the mesh density along the overlap of the joint. Tables 5.3 to 5.6 summarise the variation of stiffness due to the mesh density of the adhesive bond. It can be seen that the stiffness is insensitive to an increase of elements along the overlap whereas it is slightly sensitive to a mesh variation through the thickness of the adhesive.

5.4.3 Load displacement behaviour

First of all, to assess the range of validity of the three methods used, the load-displacement results of the three models were compared to the experimental load-displacement curves for joints A to D, Figure 5.18.

5.4.3.1 Linear model

For joint A the linear model fits with the experimental curve up to 7 kN. For joints B to D, the linear portion is more and more restricted yielding to a poor agreement between the linear model and the experimental results.

5.4.3.2 Geometric non-linearities

Table 5.7 presents the different stiffnesses of the butt strap joints modeled with linear material properties and including geometric non-linearities. It can be seen that except for joint C, including geometric non-linearities results in stiffer models than those with purely linear adhesive properties. The stiffness is higher because taking into account geometric non linearities will make the displacement smaller for a given load and then will give stiffer results as shown by (Narasimhan, Shenoi & Jeong 2004) in the case of single lap joints.

5.4.3.3 Material non-linearities

For this model, load was gradually applied to each model up to 8.1 kN with 30 load increments. Each load increment was subdivided into a sufficient number of sub-steps in order to obtain convergence of the results. Corresponding displacement of a node picked at the nodal force position was recorded.

Results are presented in Figure 5.18. Each experimental curve presented here is representative of the corresponding batch of samples tested.

It is observed that in the case of joints A and B, the numerical model and the experimental data are in good agreement, the joint B results matching very closely with the experiment. For joints C and D, it is observed that numerical and experimental results do not match as closely as for thinner adhesive layer. Results agree up to 4 kN in the case of joint C and up to less than 2 kN in the case of joint D. However, these results although being less accurate than the previous ones, give consistently stiffer results compared to the experiments.

5.4.4 Stress in adhesive bond

5.4.4.1 Linear model

Adherend and adhesive materials present linear mechanical properties and each series of joint was modelled according to their average geometrical dimensions Table 5.1. However, the experiments showed that significant deformation occurred during the test due to the asymmetry of the joint. This strongly suggested the need to include the effects of geometric non-linearities in the model. Also, as most of the specimens exhibited failure close to the bottom interface, the stress was taken as close as possible to this interface of the joint. Figures 5.19 and 5.20 show the peel and shear stress at a distance $\frac{t_a}{10}$ away from the bottom adherends (steel and aluminium) for different adhesive thicknesses at a load level of 8 kN. This load level was chosen sufficiently away from the portion of linear behaviour of the joint in order to show the difference between purely linear model and the model including geometric non-linearities.

The shear stress profile is typically one found in single and double lap shear joint studies (Adams et al. 1997) and (Goland & Reissner 1944). The butt strap joint can be seen as a combination of two single laps. The shear is constant along the adhesive bond and peak stress values occur at the edges. In this case, a high shear gradient

is observed in the middle of the overlap due to a geometrical singularity. The peel stress profile is slightly dissimilar to the one in lap shear joints: there is still a compressive zone around the edge of the main adherends (steel and aluminium) but not at the edge of the strap. It is is noticeable that the magnitude of the peak of peel stress is far beyond the ultimate tensile strength of the adhesive itself, however this peak is due to the material discontinuity observed in this region. This phenomenon is then corrected when the effects of geometric non-linearities are included. A lower and more realistic peel stress level is observed close to the gap, whereas the trend and magnitude remain unaffected elsewhere. Also, hardly any change is observed in the shear stress profile.

5.4.4.2 Material non-linearities

The stress profile in the adhesive layer is presented in Figures 5.19 to 5.22 for normal and shear stress. The graphs present the stress at the middle of the adhesive layer and at a distance $\frac{d}{10}$ from the bottom adherends.

The peel stress generally decreases with increasing adhesive thickness: a peak of stress is observed at 22 MPa for 1 mm adhesive thickness and 12.7 MPa for 10 mm. Hardly any difference is observed between the stress profile at the bottom interface and the one at the middle of the adhesive layer except a peak that occurs at the edges of the joint in the case of the bottom adhesive layer. This peak is noticed to be higher than the one at the gap position in the case of the 10 mm adhesive thickness joint. A slight imbalance is observed that is more accentuated for relatively small adhesive thicknesses (1 and 3 mm). A drop in the stress is also noticeable at the middle of the overlap where a free surface occurred at the gap between the main steel plate and the main aluminium plate.

For the shear stress, the profile is noticeably different depending on whether it is calculated near the bottom interface or at the middle of the adhesive. However, the level of stress remains of same order of magnitude between 1 and 10 mm of adhesive around 7 MPa. The profile is similar for the bottom interface and middle adhesive layer in the case of 1 mm adhesive thickness with a high gradient in the gap area. This gradient remains when adhesive thickness increases, when the interface close to the bottom interface is considered but is smoothened in the middle of the adhesive and drops towards the gap.

5.5 Discussion

5.5.1 Influence of adhesive thickness

From Figure 5.14 (a), it is observed that the shear strength decreases almost linearly with adhesive thickness (a 99 % correlation being found). This is justified because of the poor adhesive bond observed for these joints that biased the results. Loss of strength is compared to the strongest joint which is the unaged butt strap with 1-mm adhesive thickness (Joints A table 5.1). The loss of strength for the unaged specimens B and C are 12.1 % and 32.0 % respectively. A similar study was carried out by (Colak 2001) who observed the effects of both adhesive thickness variations and epoxy composition on the strength of steel rods bonded into a precast concrete panel. He concluded that the adhesive shear strength was dependent on the adhesive formulation: while with a certain adhesive composition X, the shear strength would remain unaffected by the adhesive thickness, another composition Y would present more complex variations.

The bond thickness also influences the general behaviour of the butt strap joints. For the joints from B to D, permanent deformation was observed in the aluminium strap as shown by Figures 5.5. This indicates that in addition to initial bending, significant peel occurs during the test. Small initial bending stress was due to geometrical adherend imbalance and the distortion induced by the welding in steel adherend as joints B to D had to have an additional plate welded to the steel adherend because it was originally to short. Even without these discrepancies, plasticity would have occurred in the strap: the series of butt strap specimens with 1 mm adhesive thickness that meet the correct specification without any adherend imbalance exhibits a small curvature of the strap showing start of plasticity. As shown by (Adams et al. 1997) for the case of a double lap and double strap joints, the joint does not experience any net bending moment because the loads are not eccentric. However it experiences internal bending between the strap and the inner adherends, acting as local single lap shear, leading to a tension-compression phenomenon within the adhesive bond. This phenomenon is emphasized in the case studied because of the asymmetry of the butt strap joint as the centre of inertia of the joint is not on the same line as the applied loads and its distance to that line increases with increasing adhesive thickness.

Figure 5.14 (b) shows the variations of joint stiffness with respect to adhesive thickness. The figure shows a sharp decrease in stiffness at the first increment of thickness

(from 1 mm to 5 mm) then it still decreases but less sharply from 5 mm to 10 mm.

The peel stress magnitude in the adhesive layer of the butt strap decreases with increasing adhesive thickness. Physically, when the adhesive layer is increased, the low modulus of the adhesive material predominates inducing a higher flexibility of the joint and thus lower normal stresses in the adhesive bond. This effect is used in the design of peel-stress relief at the edge of adhesive joints as mentioned by Hart-Smith in (Pocius & Dillard 2002). However, this predominance of the adhesive materials has the converse effect of decreasing the shear strength of the joints as shown by the Figure 5.14 (a). Indeed, as the adhesive is sufficiently thick, it could be treated as an "adherend" material causing substantial adherend mismatch, shear strength reduction and premature failure of the joint (Hart-Smith 1973).

Also, as presented earlier, experimental results have shown that transverse cracking clearly occurred in the adhesive bond, Figure 5.5. These cracks are due to the presence of a gap between the bottom adherends of the joints thus presenting an adhesive free surface. When the joint is loaded, the strap bends because of the eccentricity of the load path, causing the horizontal adhesive free surface to be torn apart. For the thicker adhesive bonds (joints B and C), the crack has some room to propagate during the test. This sometimes led to failure at the strap interface, Figure 5.5 (c). This is also true for joints A but is less apparent, Figure 5.5 (a) because failure occurred cohesively before the crack reached the opposite interface with the strap.

The results in Figures 5.19 and 5.20 allow the deduction of the failure mechanisms. The figure suggests that failure initiating at the gap free surface is due to high peel stress associated with a high gradient of shear stress. Finite element analysis also showed (Figure 5.23) that the principal stress directions are horizontal at the free surface and at 45^o near the corner of the bottom adherends confirming the observations of the experimental results.

5.5.2 Influence of non-linearities

5.5.2.1 Influence of geometric non-linearities

Geometric non-linearities were considered because the asymmetry of the butt strap joint induced large rotations due to the internal bending moment. Taking these deformations into account in the model enable a reduction in the stress within the

adhesive bond and to have it at a more realistic level. It can be noticed that for joint A, the peel stress profiles are very similar because no large rotations of the joint were observed. Except close to the gap, the peel and shear stress profiles of both models are similar for joints A to C showing that the large rotation of the joint affect a fairly restricted zone. For joint D, the shapes of the peel stress profiles are slightly different, suggesting that large deformations start to affect a larger part of the joint.

Figure 5.19 emphasizes that including the geometrical non-linearities has some substential effects in the peak of normal stress whereas it does not affect the shear stress profile.

5.5.2.2 Influence of material non-linearities

The multi-linear elastic method used to model the material non-linearities proved to be adequate for adhesive joints up to 5 mm. Beyond this limit, the experimental and numerical models are slightly divergent. One of the cause would be the large rotation of the joint due to the very thick adhesive bond.

In terms of stress, by including the material non-linearities for the adhesive a more realistic stress level is achieved, as the effects of plastic deformation are taken into account. The stress profile is usually unchanged but peak values are leveled.

5.5.3 Influence of ageing

Figure 5.24 shows the influence of ageing on joint strength and stiffness. In term of performance with respect to time, the highest strength was shown for the type A joints. However, the type C joints (5 mm adhesive thickness), though shown to be slightly weaker than type A, did not present high decrease in strength with time. The loss of strength was of about 5 % for joint type C and 15 % for joint type A after 6 weeks. Also, Table 5.2 shows that, although the standard deviation of unaged specimens is consistent between each type of joints (0.47, 0.28 and 0.57 for type A, C and D), it is globally increasing with time (1.28, 0.43 and 0.27 respectively after 6 weeks). Indeed, after 6 weeks joints A present a higher scatter than type C and type D joints. Type C joints show an increase of strength between 3 weeks and 6 weeks. That may be atributed to a better average quality of bond within the specimens tested. Similar trends were observed by Brewis and coworkers (mentioned by (Adams et al. 1997) p 302).

Figure 5.24 summarises the evolution of stiffness of the joints with respect to ageing. Only a slight decrease is observed with increasing time. A similar trend was found by (Knox & Cowling 2000*a*) who noticed a plateau region up to 6 weeks and a drop of stiffness leading to an other plateau region up to 12 weeks. This decrease of tensile stiffness can be explained by the adhesive that plasticises after being aged.

In terms of failure mechanism, (Knox & Cowling 2000*a*) also noticed that failure of joints cannot only be due to water ingress in the adhesive and in the scope of this study, failure mode analysis suggests that failure occurred via interfacial degradation from water. Indeed, Figures 5.9 and 5.12 show some shaded areas at the edges of the joints corresponding to water ingress. Also, most of the failure (though not all) occurred at the interface with the steel adherend. Observations suggested that failure was not due to corrosion since the locus of failure (Figure 5.9 and 5.12) does not show the presence of corrosion within the bondline area. This phenomenon was originally explained by (Kinloch 1990) who showed that in some cases corrosion is a post-failure mechanism.

5.6 Conclusion

This Chapter has focused on two main issues concerning adhesive bonded single butt strap joints: the influence of the combination of water and temperature and large scale adhesive thickness variations on the strength and behaviour of the joints. From this study, the following conclusions can be drawn:

- Significant strength and stiffness reductions occur with increasing adhesive thickness (up to 40 % loss of strength and up to 80 % loss of stiffness between 1 mm and 10 mm adhesive thickness).
- The loss of strength is estimated to decrease linearly with respect to adhesive bond thickness but a more complex behaviour is observed with respect to time. Experimental results suggest interfacial degradation at the steel interface at the edges of the joint.
- The loss of joint stiffness is not significant after 6 weeks in a bath of still water but can also be modeled with a linear model with respect to time up to some extend. A more complex behaviour is observed with respect to adhesive thickness.

- In terms of failure mechanisms, the finite element analysis suggests that failure of unaged butt strap joints is due to a combination of high peel stress and a high gradient of shear due to the presence of an adhesive free surface.

Tables

Joint	t_a	a	b	c	d_1	d_2	t_{steel}	t_{Al}	t_{strap}
A	1	25	80	150	39.5	39.5	6	6	5
B	3	25	90	150	49	40	5	6	5
C	5	25	84	150	41	42	5	6	5
D	10	25	83	150	42	43	5	6	5

Table 5.1: Geometrical particular of joints. all dimensions in mm (nomenclature refers to Figure 5.1)

Adhesive thickness	Non aged	Aged 3 weeks	Aged 6 weeks
1 mm	9.79 ± 0.47	9.52 ± 0.93	8.33 ± 1.28
3 mm	5.40 ± 1.12	2.64 ± 1.31	4.76 ± 2.52
5 mm	9.83 ± 0.28	9.20 ± 0.63	9.31 ± 0.43
10 mm	6.88 ± 0.57	6.08 ± 0.31	6.39 ± 0.27

Table 5.2: Ultimate load of butt strap joints (values are in kN)

Number of elements through the thickness	Number of nodes	Model stiffness [kN/mm]	Number of elements along the overlap	Number of nodes	Model stiffness [kN/mm]
3	7058	19.81	20	3302	19.78
5	7374	19.81	40	5134	19.78
10	8094	19.80	60	6614	19.78
15	8834	19.80	80	8094	19.78
20	9574	19.79	100	9574	19.78

Table 5.3: Sensitivity of model stiffness to adhesive mesh density for joint A.

Number of elements through the thickness	Number of nodes	Model stiffness [kN/mm]	Number of elements along the overlap	Number of nodes	Model stiffness [kN/mm]
3	7058	12.94	20	3302	12.85
5	7374	12.89	40	5134	12.85
10	8094	12.85	60	6614	12.85
15	8834	12.82	80	8094	12.85
20	9574	12.80	100	9574	12.85

Table 5.4: Sensitivity of model stiffness to adhesive mesh density for joint B.

Number of elements through the thickness	Number of nodes	Model stiffness [kN/mm]	Number of elements along the overlap	Number of nodes	Model stiffness [kN/mm]
3	7058	9.94	10	3302	9.84
5	7374	9.88	20	5134	9.84
10	8094	9.84	30	6614	9.84
15	8834	9.82	40	8094	9.84
20	9574	9.81	50	9574	9.84

Table 5.5: Sensitivity of model stiffness to adhesive mesh density for joint C.

Number of elements through the thickness	Number of nodes	Model stiffness [kN/mm]	Number of elements along the overlap	Number of nodes	Model stiffness [kN/mm]
5	7374	7.48	20	5134	7.41
10	8094	7.41	40	6614	7.41
15	8834	7.38	60	8094	7.41
20	9574	7.35	80	9574	7.41
30	15774	7.33	100	11054	7.41

Table 5.6: Sensitivity of model stiffness to adhesive mesh density for joint D.

	Joint A	Joint B	Joint C	Joint D
Linear model	19.8	12.8	9.8	7.4
Model with geometric non-linearities	20.6	12.9	9.5	8.4

Table 5.7: Comparison of the stiffness of numerical models [kN/mm].

Figures

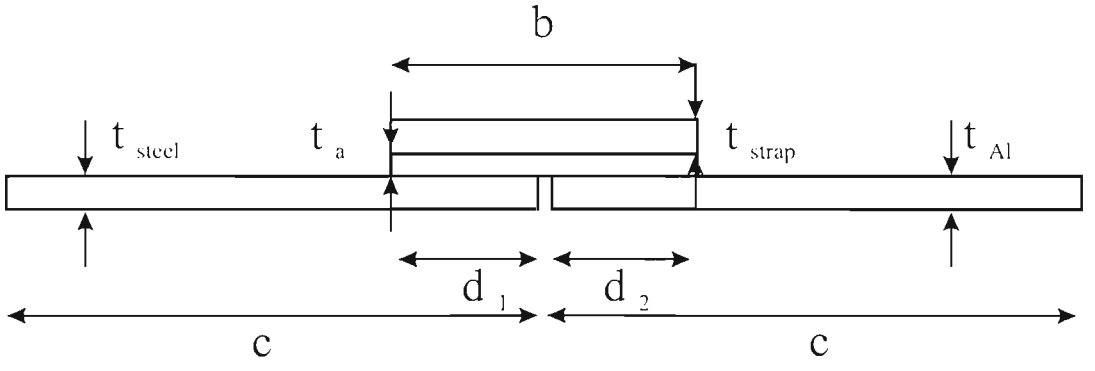

Figure 5.1: Butt strap geometrical and material specifications (not to scale)

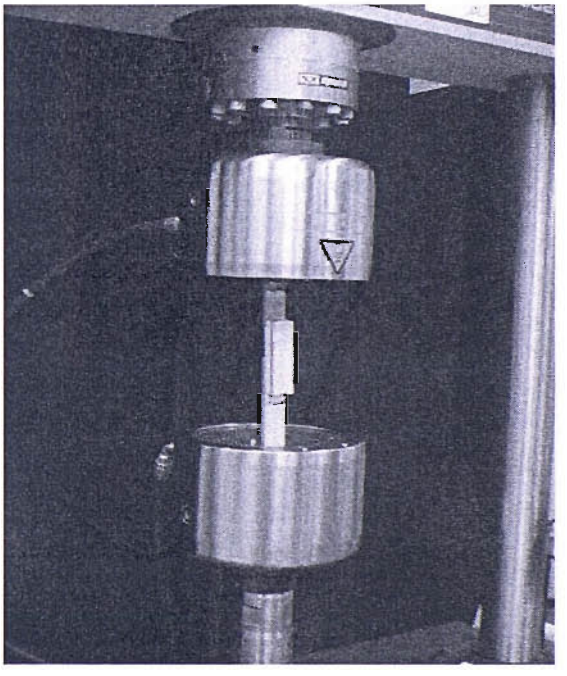

Figure 5.2: Butt strap test setup

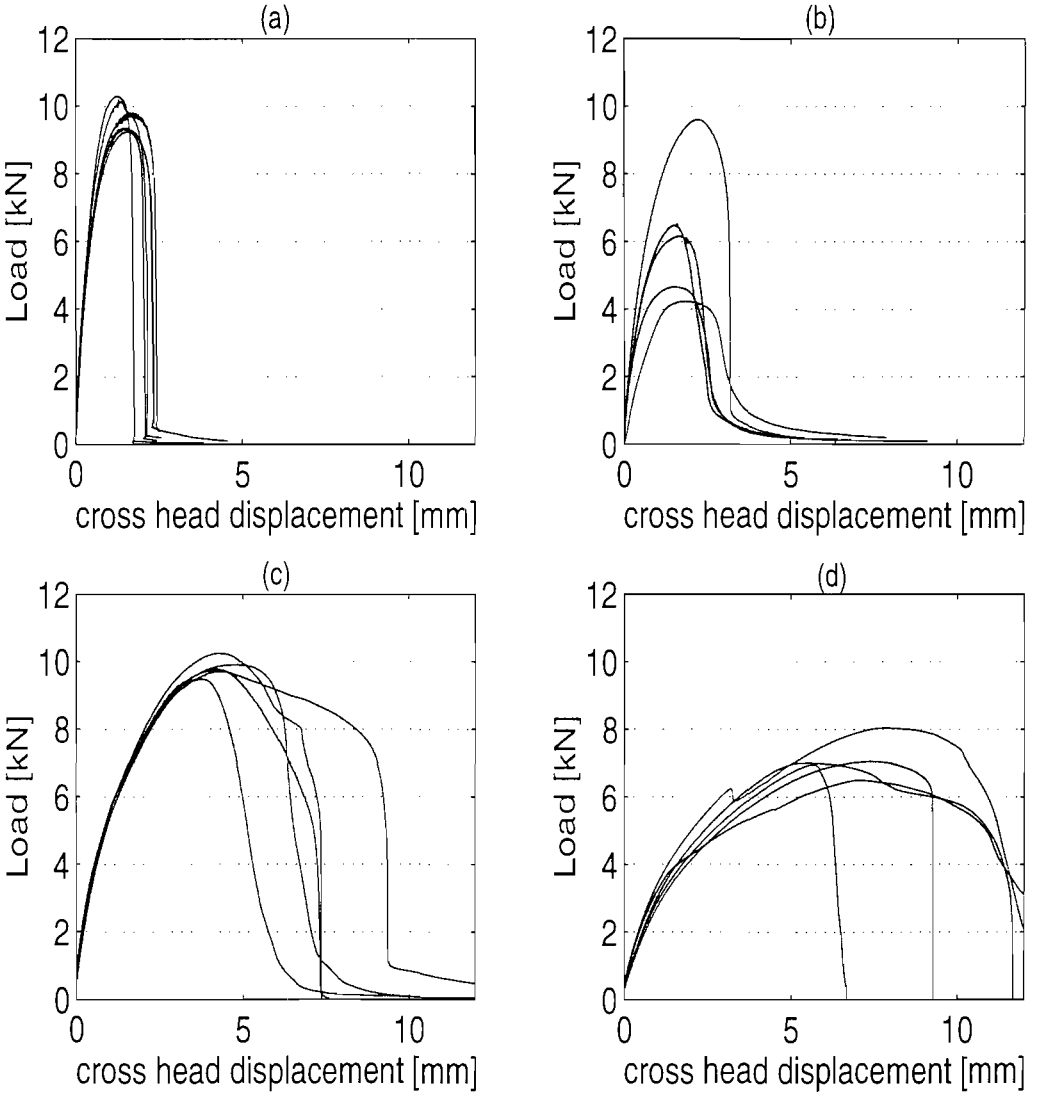

Figure 5.3: Typical experimental behaviour of unaged butt strap joints: (a) 1 mm (b) 3mm, (c) 5 mm, (d) 10 mm adhesive thickness

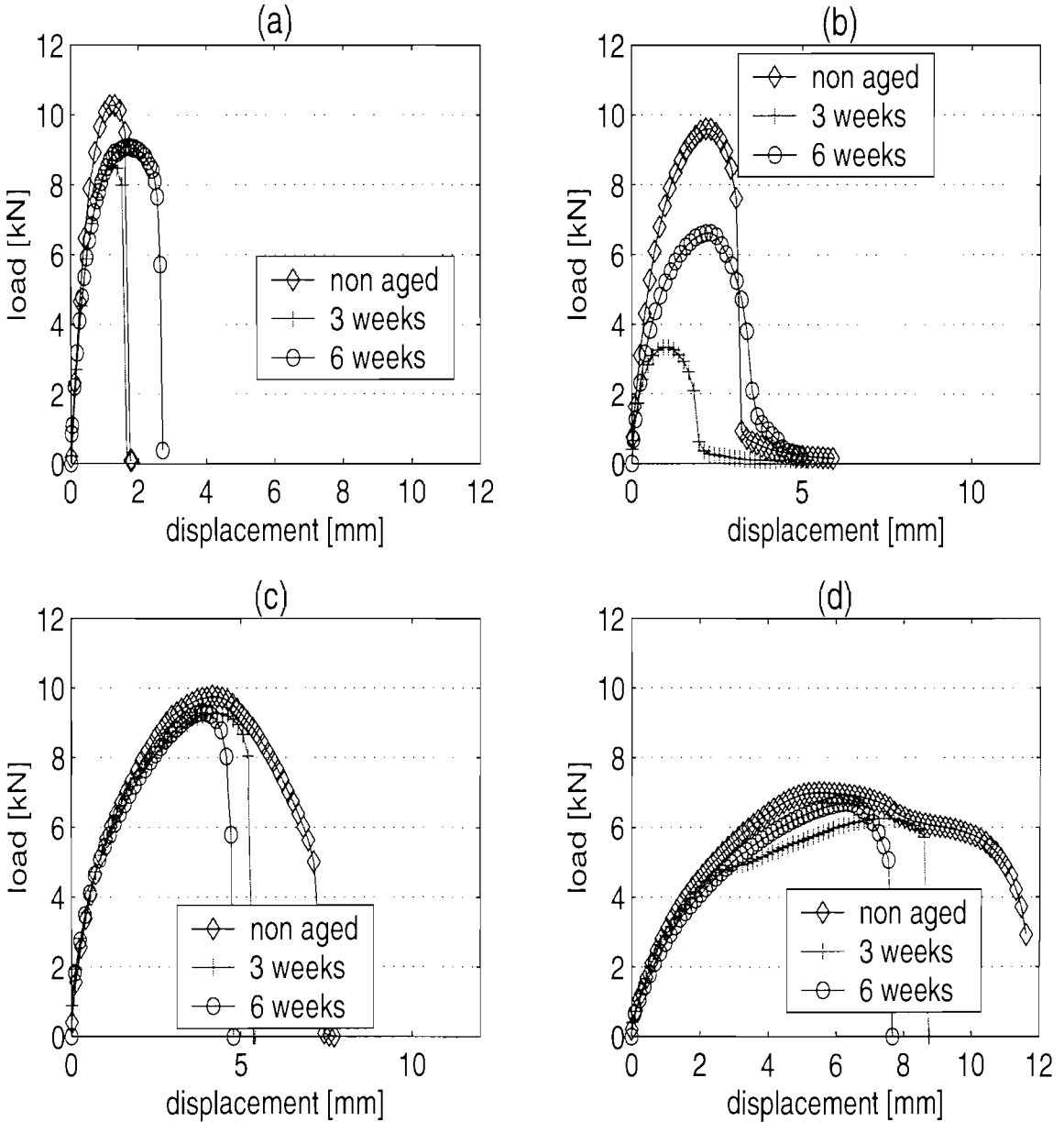

Figure 5.4: Influence of environmental degradation due to water on the stiffness of butt strap joints: (a) 1 mm adhesive thickness, (b) 3 mm adhesive thickness, (c) 5 mm adhesive thickness, (d) 10 mm adhesive thickness

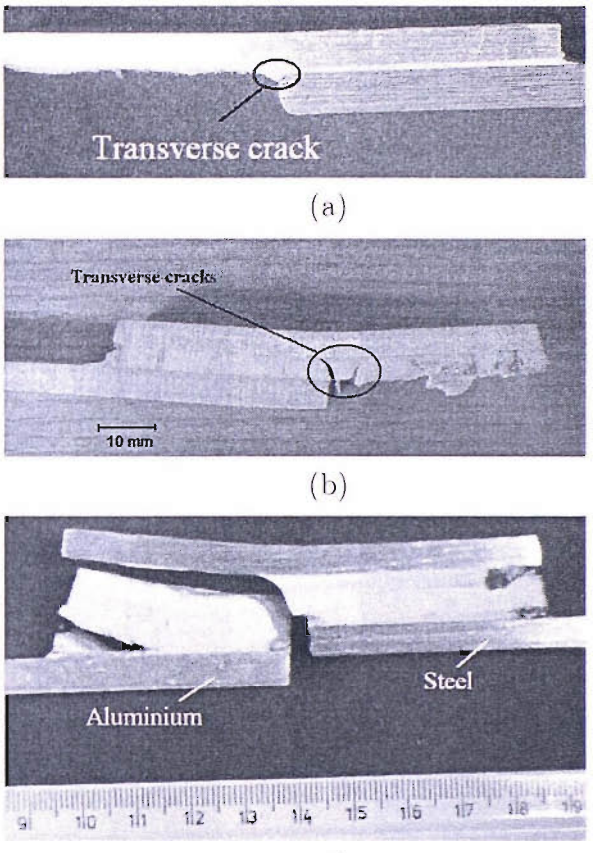

Figure 5.5: Transverse crack in the adhesive layer of butt strap joints and permanent deformation of the strap: (a) 1 mm. (b) 3 mm. (c) 10 mm

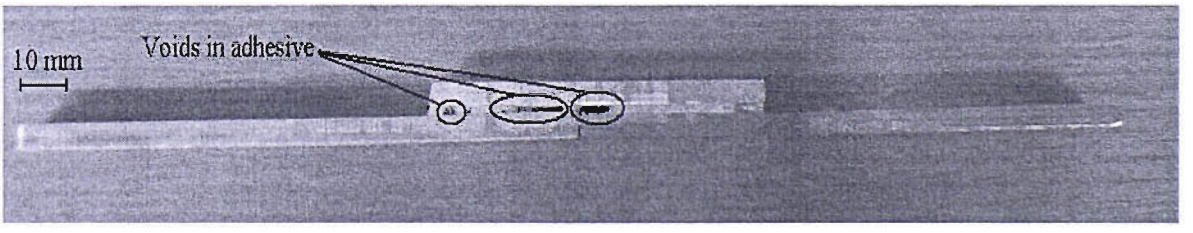

Figure 5.6: Voids in butt strap joints with 3-mm adhesive thickness

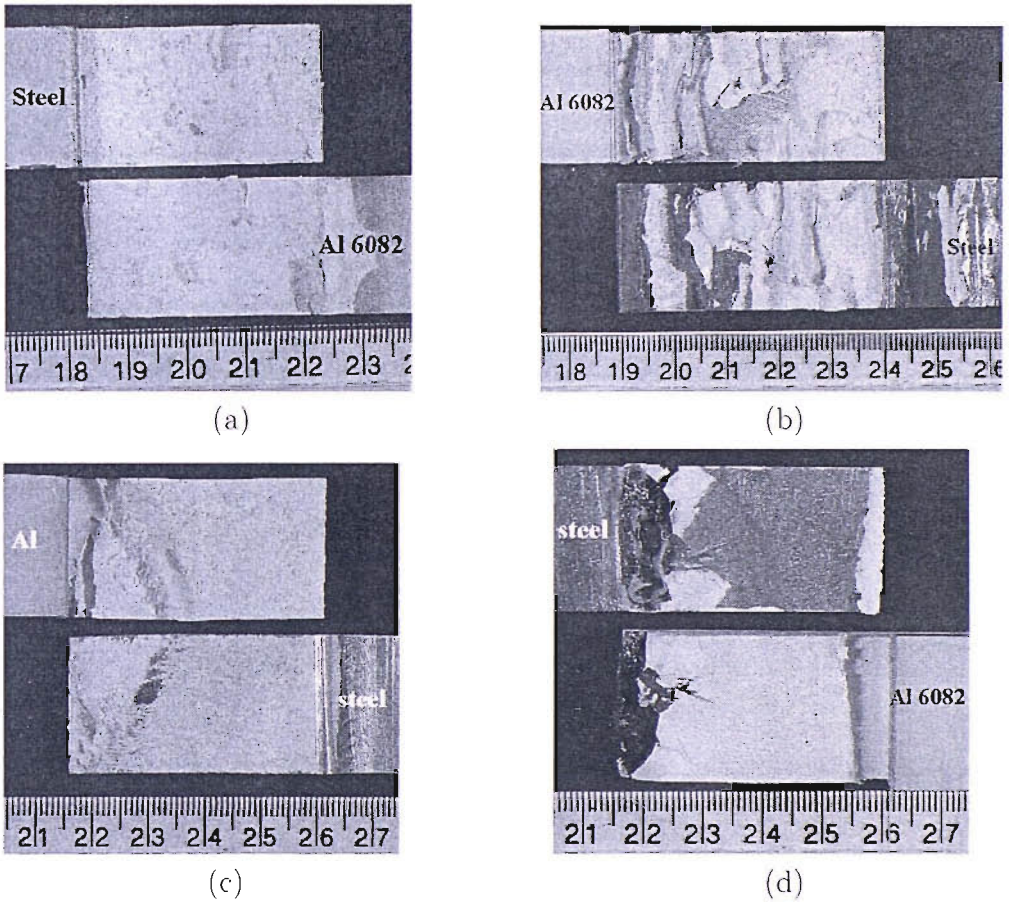

Figure 5.7: Adhesive failure mode of unaged butt strap joints: (a) 1 mm, (b) 3 mm, (c) 5 mm, (d) 10 mm adhesive thickness

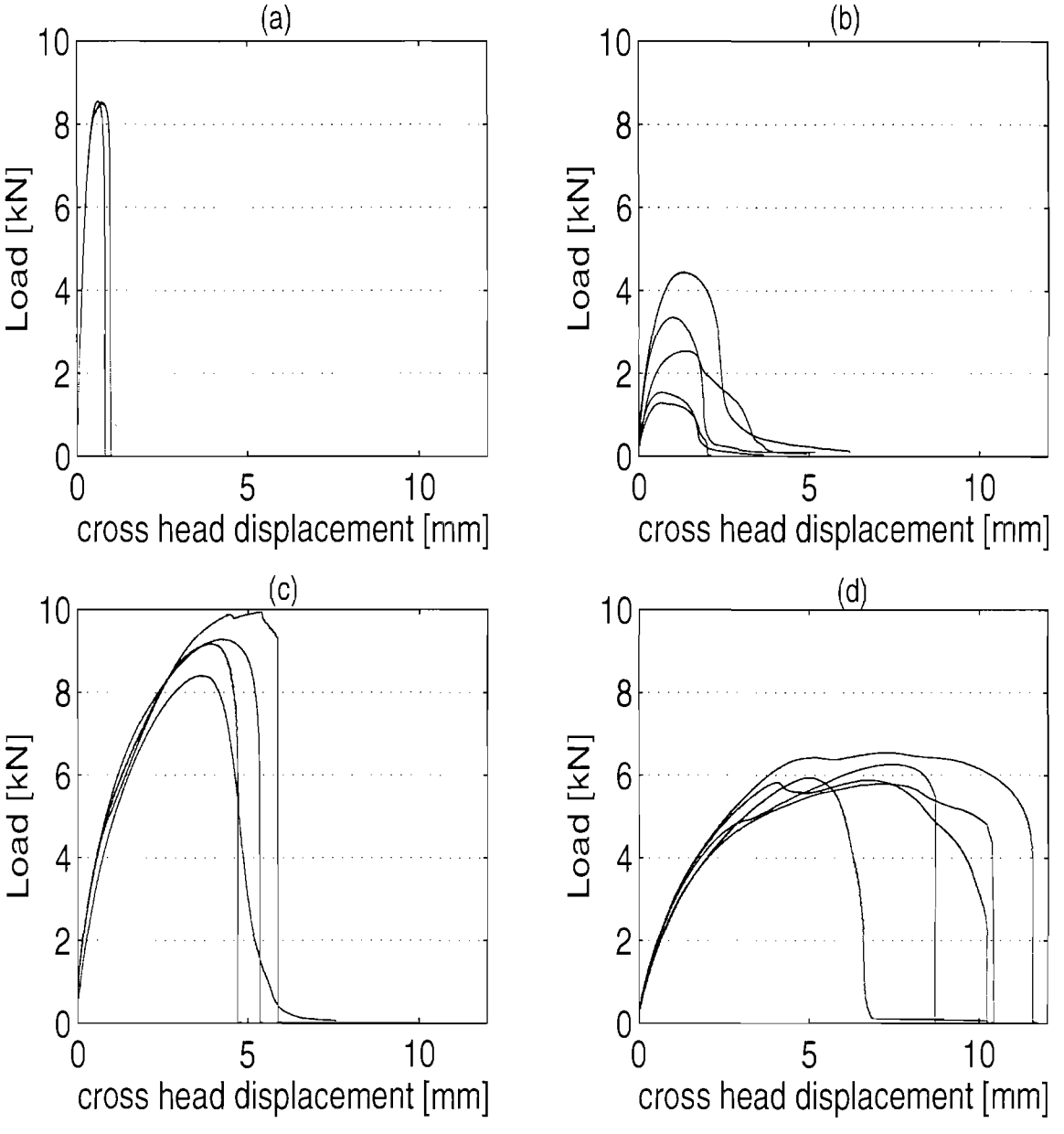

Figure 5.8: Typical experimental behaviour of 3 week aged butt strap joints: (a) 1 mm (b) 3mm, (c) 5 mm, (d) 10 mm adhesive thickness

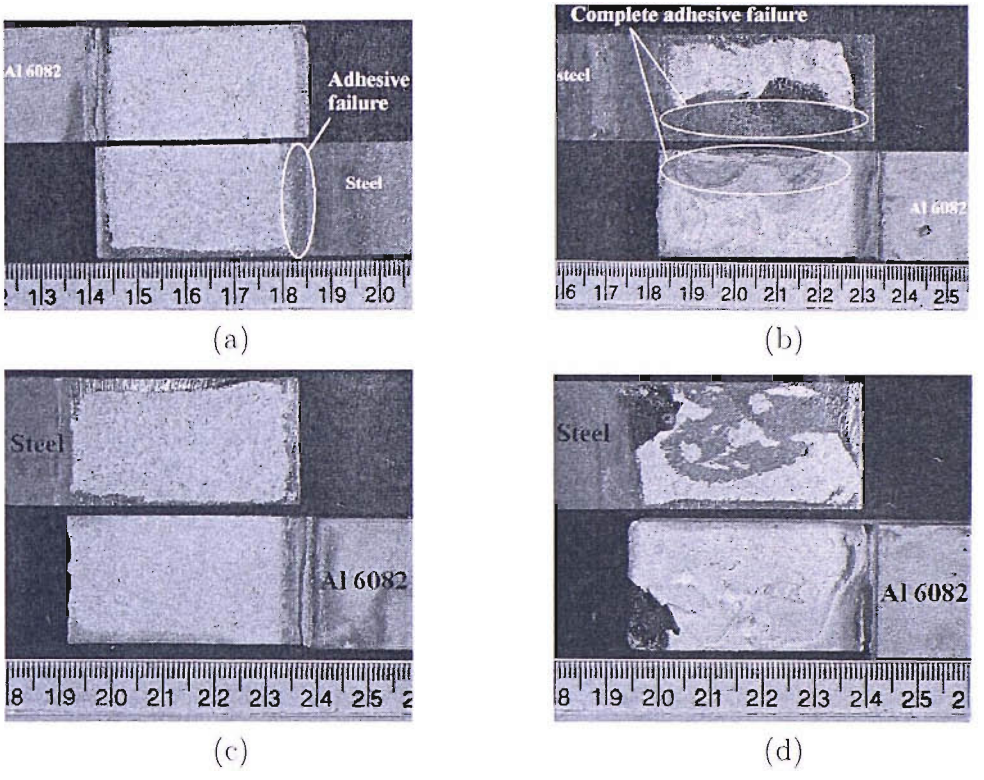

Figure 5.9: Adhesive failure mode of butt strap joints after 3 weeks ageing: (a) 1 mm (b) 3mm. (c) 5 mm. (d) 10 mm adhesive thickness

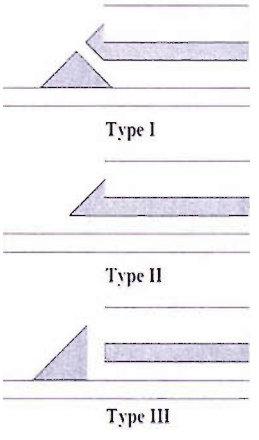

Figure 5.10: Pattern of failure in lap joints

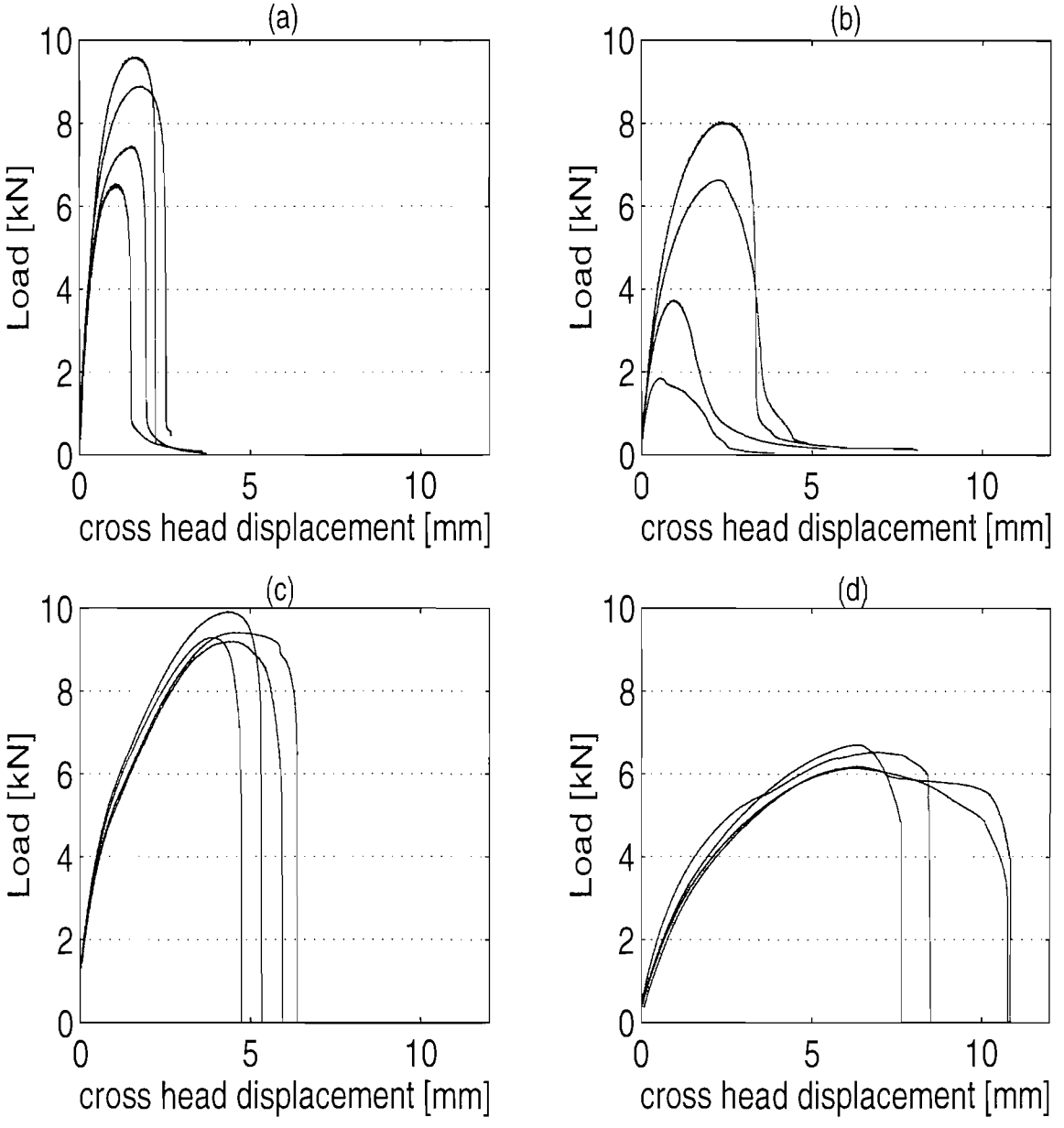

Figure 5.11: Typical experimental behaviour of 6 week aged butt strap joints: (a) 1 mm (b) 3mm, (c) 5 mm, (d) 10 mm adhesive thickness

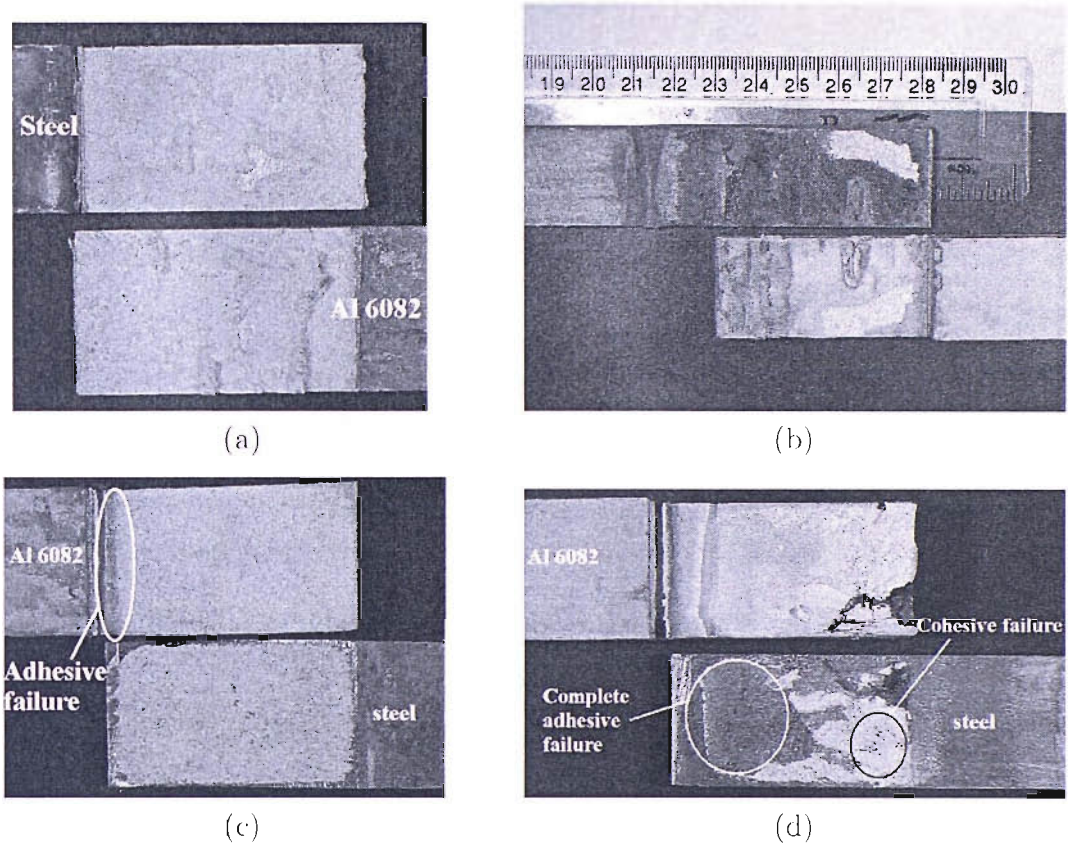

Figure 5.12: Adhesive failure mode of butt strap joints after 6 weeks ageing: (a) 1 mm (b) 3mm, (c) 5 mm, (d) 10 mm adhesive thickness

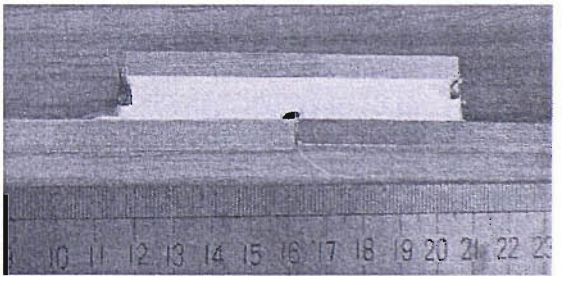

Figure 5.13: Central void in adhesive layer for 10 mm adhesive thickness butt strap joint

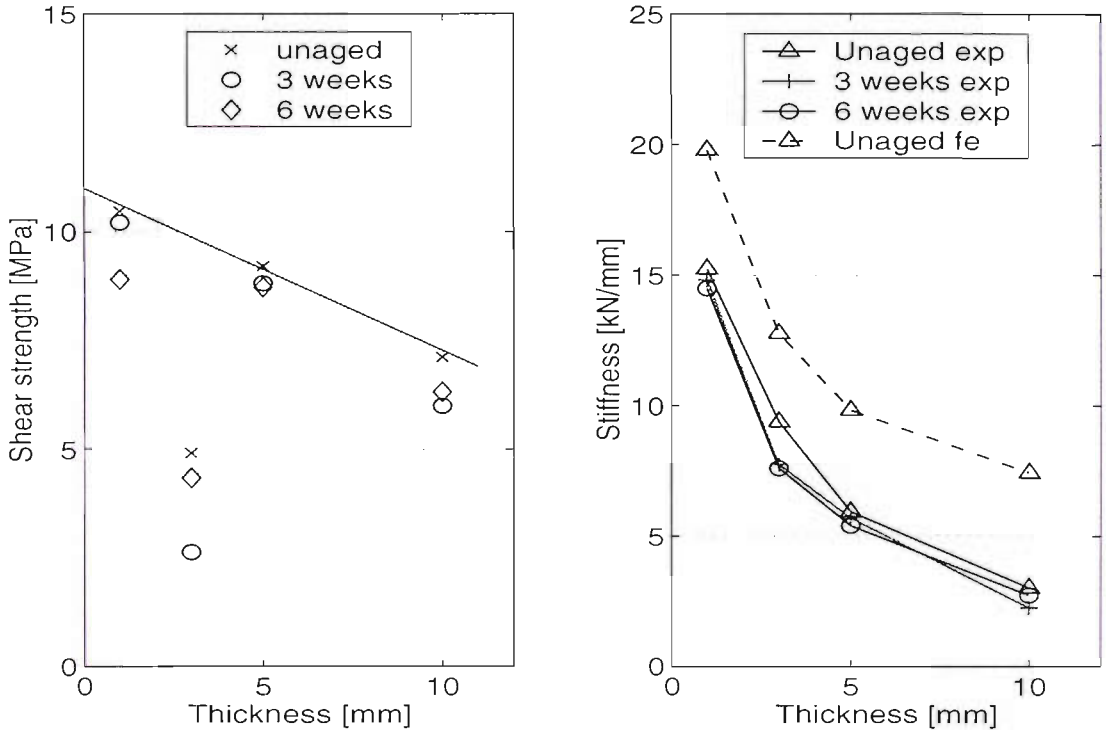

Figure 5.14: Influence of adhesive thickness on the strength (a) and stiffness (b) of butt strap joints. In figure (b) dash line are numerical results, straight lines are experimental results

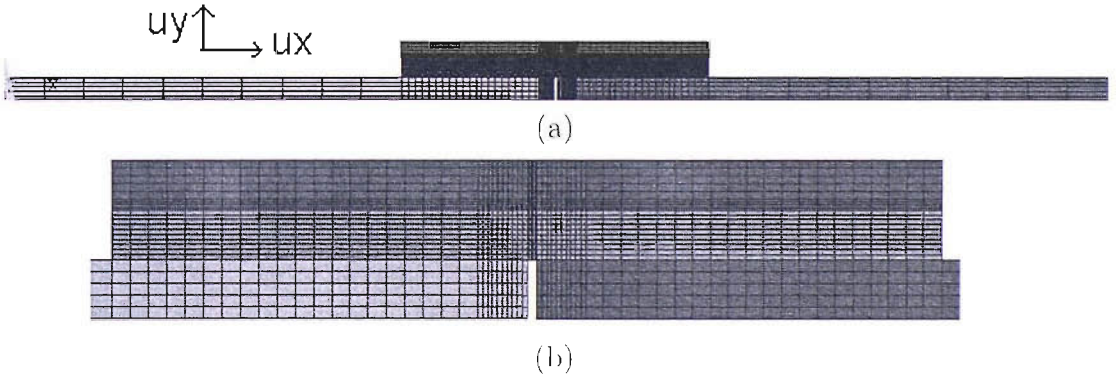

Figure 5.15: Finite element model of butt strap joint: (a) Global view (b) Adhesive bond mesh

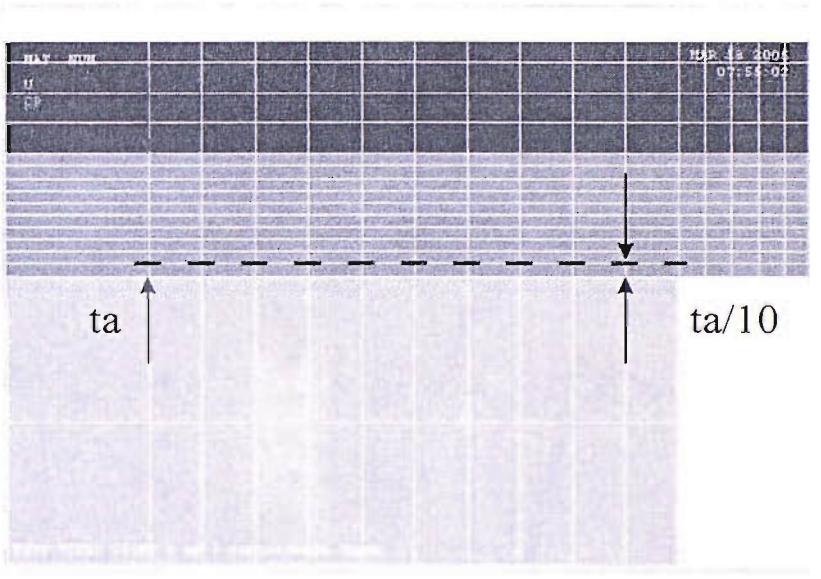

Figure 5.16: Line of node used to check the convergence of the numerical results. t_a is the adhesive bond thickness

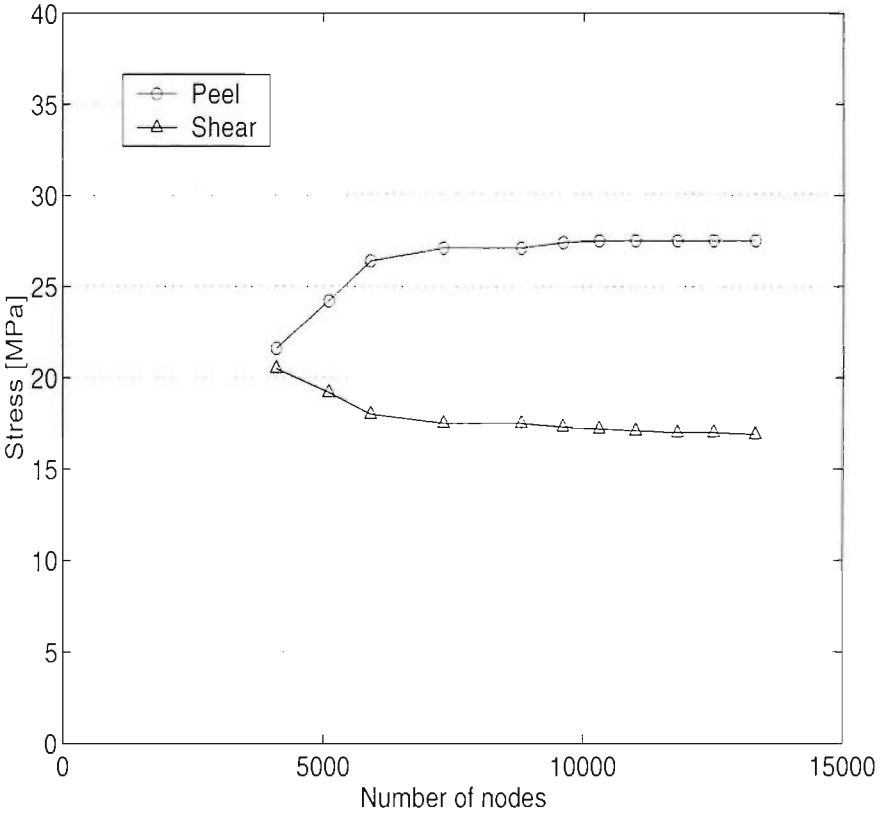

Figure 5.17: Convergence check of the stress values in the adhesive bond

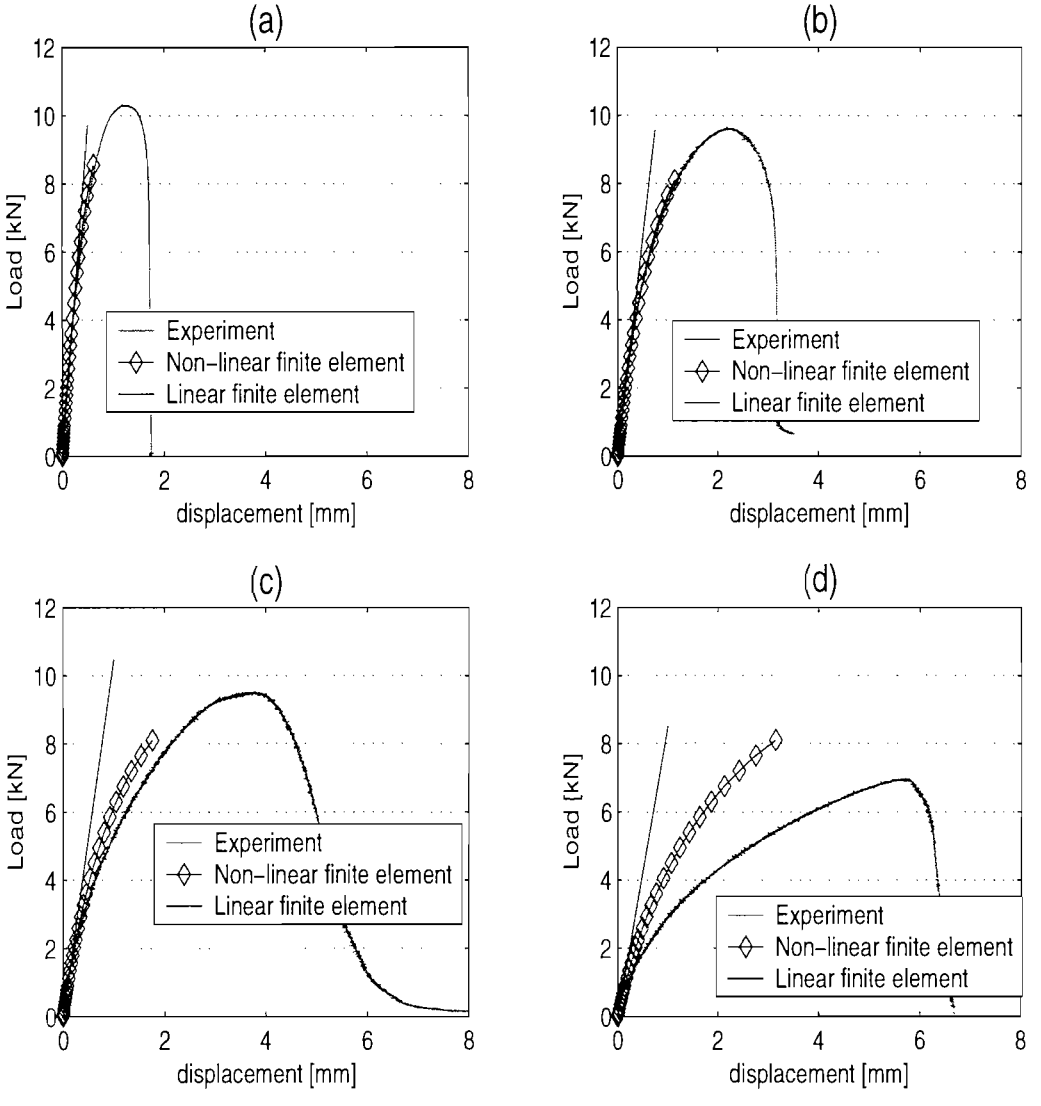

Figure 5.18: Comparison of experimental, linear and non-linear finite element load displacement curves

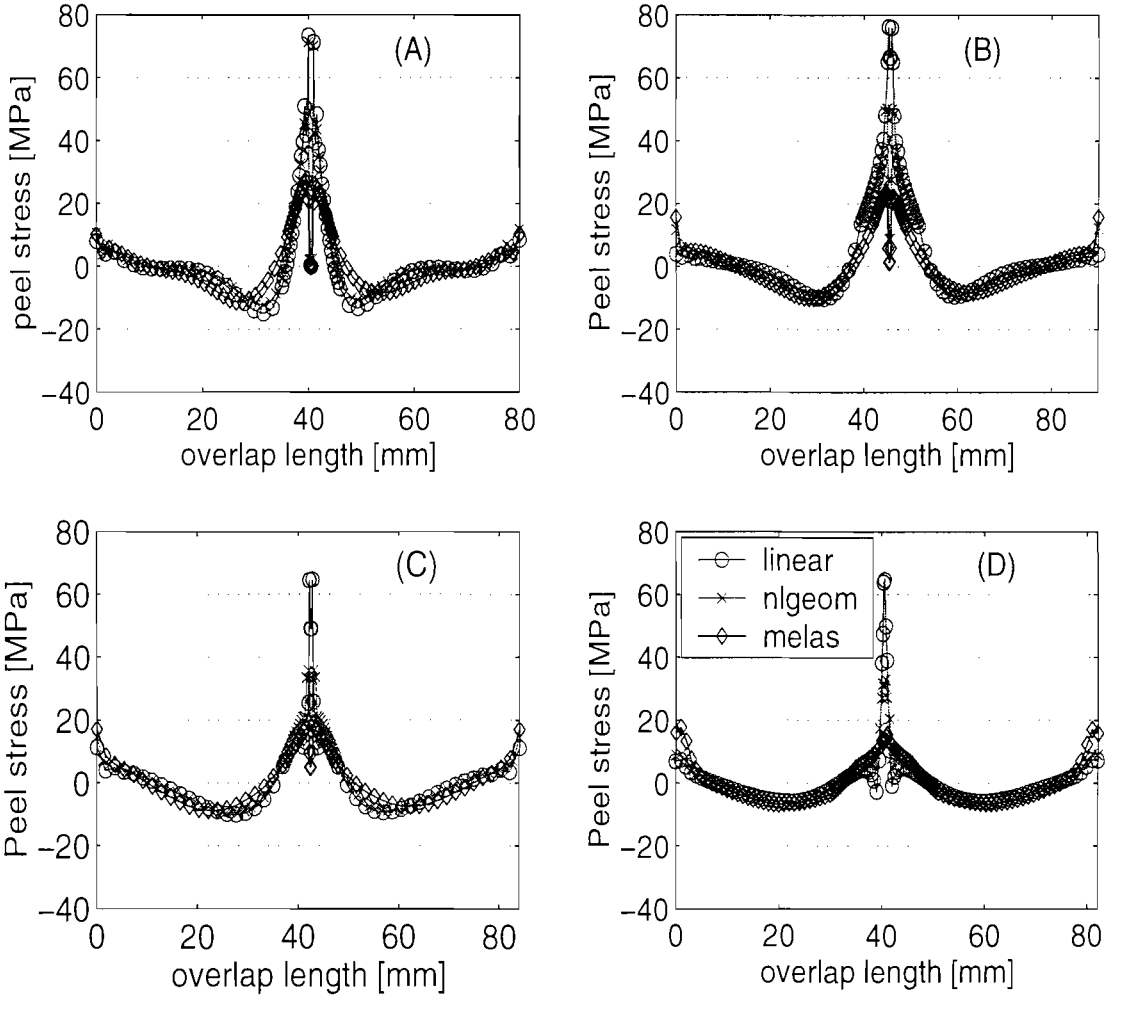

Figure 5.19: Normal stress in butt strap adhesive layer of different thicknesses at 8 kN: (A) 1 mm, (B) 3 mm, (C) 5 mm, (D) 10 mm; The stress is taken at nodes along a line situated close to the interface at a distance $\frac{t_a}{10}$ from the lower adherends (where t_a: adhesive thickness, Figure 5.16)

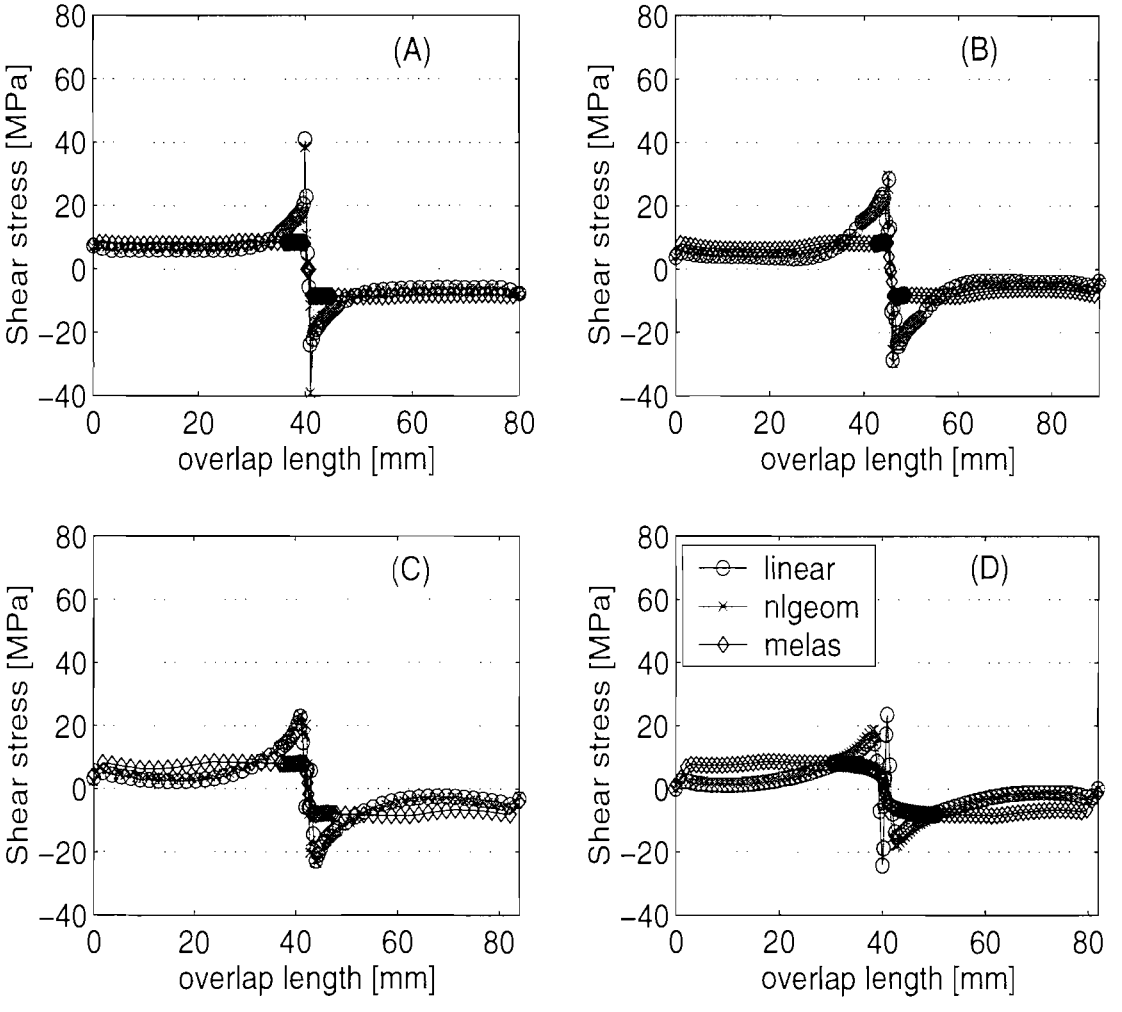

Figure 5.20: Shear stress in butt strap adhesive layer of different thicknesses at 8 kN: (A) 1 mm, (B) 3 mm, (C) 5 mm, (D) 10 mm; The stress is taken at nodes along a line situated close to the interface at a distance $\frac{t_a}{10}$ from the lower adherends (where t_a: adhesive thickness, Figure 5.16)

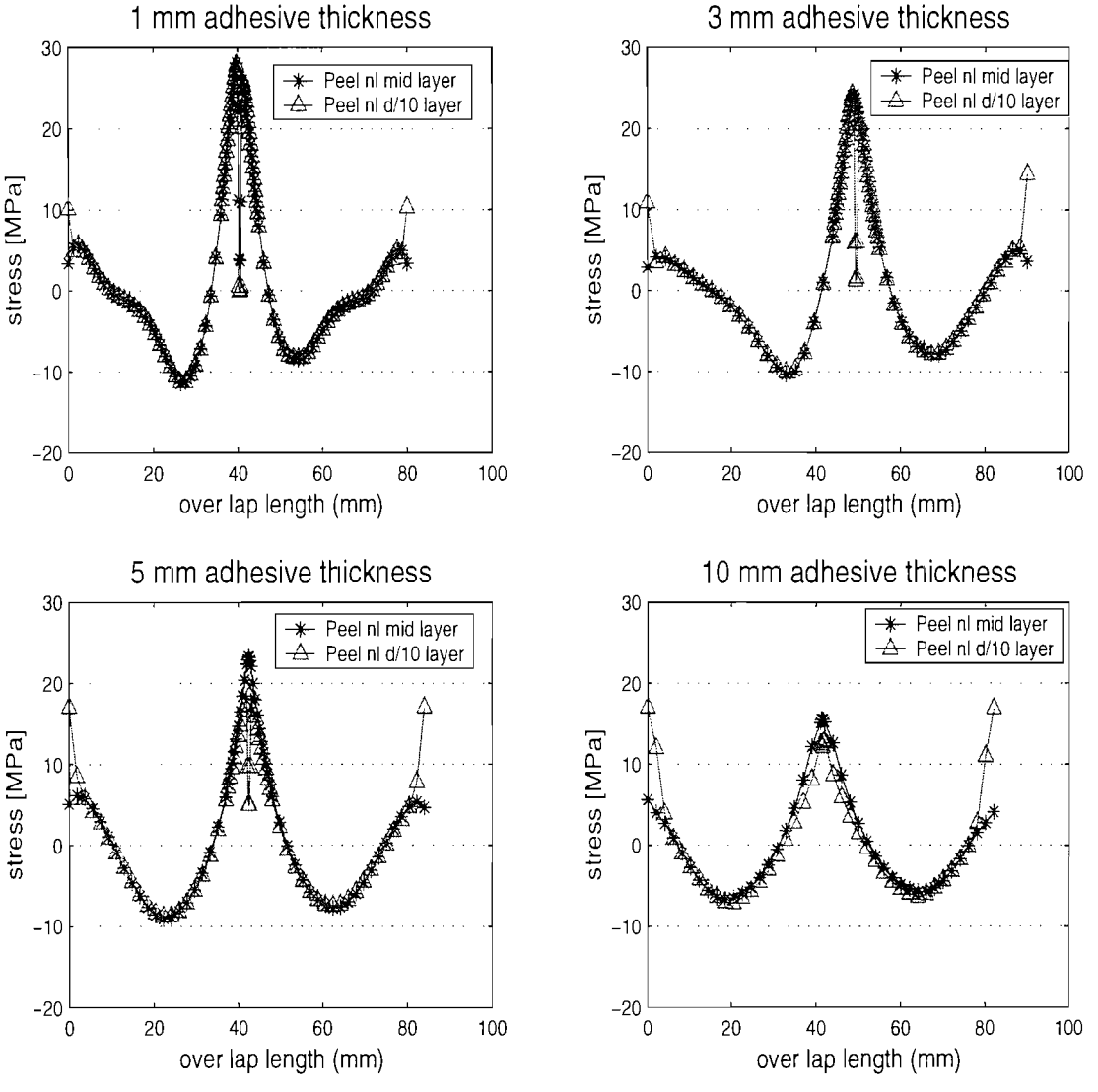

Figure 5.21: Normal stress profile in adhesive layer of butt strap joint at different locations through the thickness for a non-linear model at 8 kN

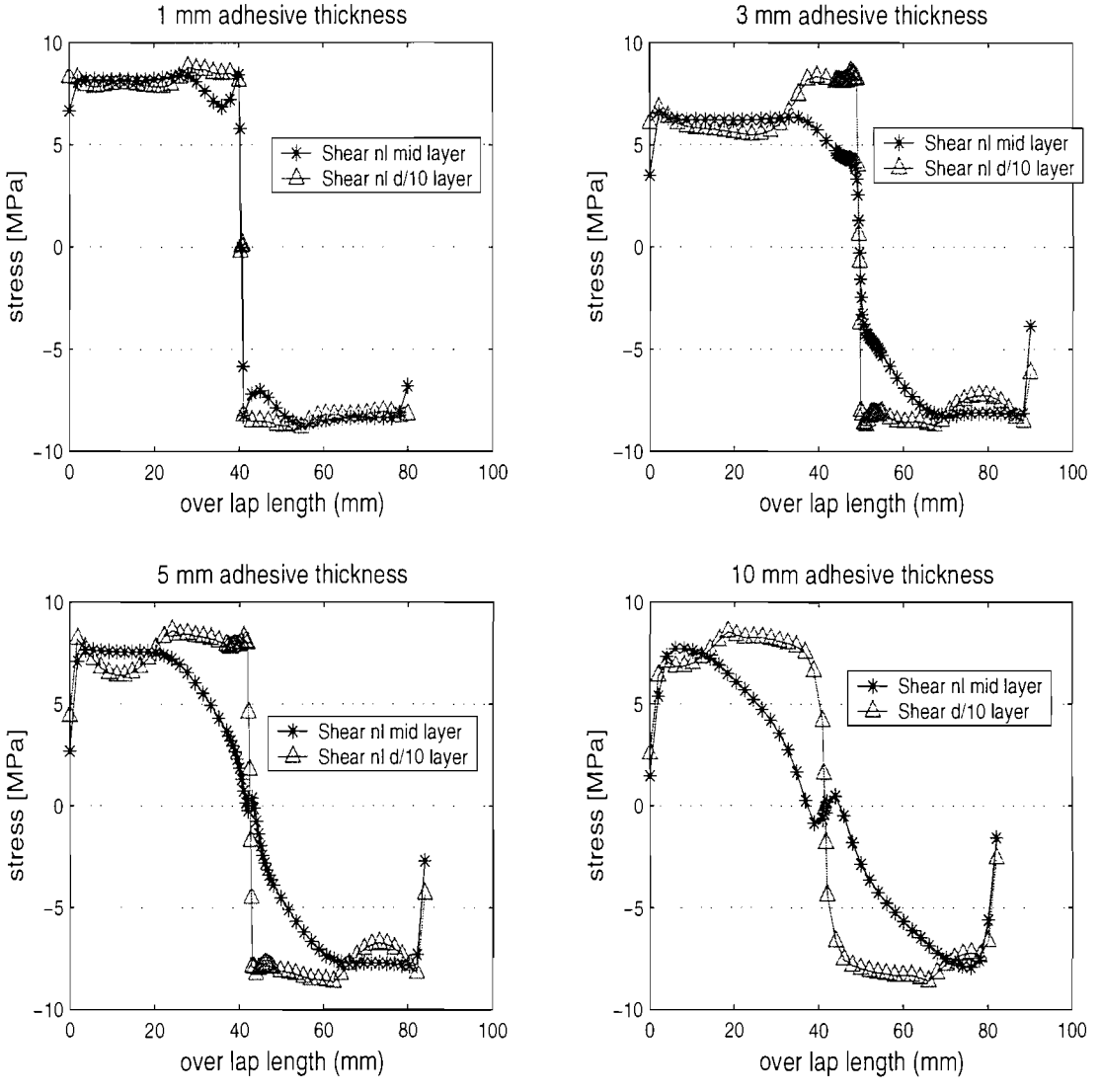

Figure 5.22: Shear stress profile in adhesive layer of butt strap joint at different locations for a non-linear model at 8 kN

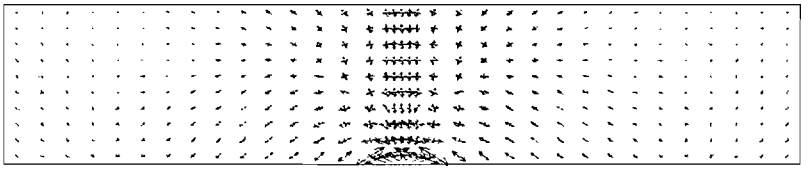

Figure 5.23: Principal stress direction at the free surface of joints B. This corresponds to the area surrounding the gap where the mesh is refined

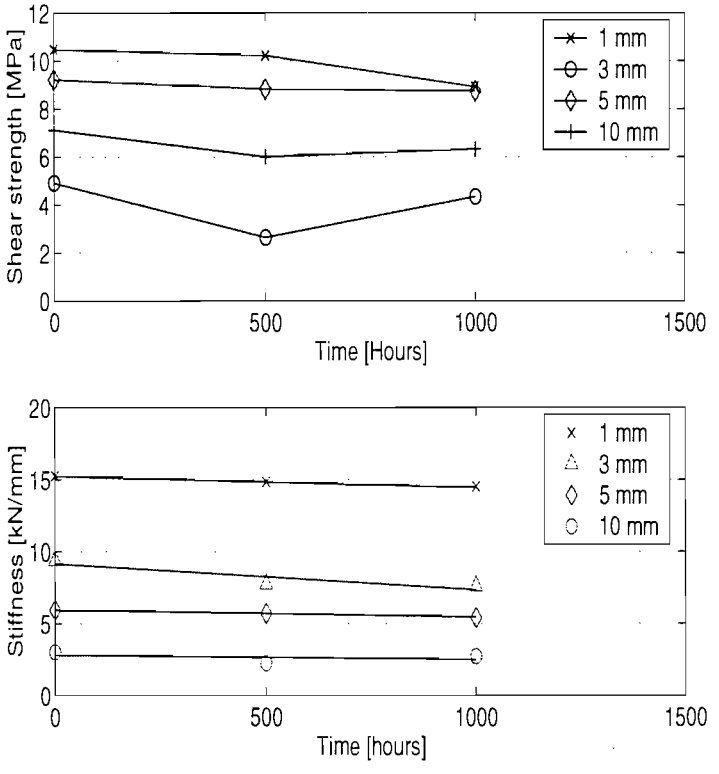

Figure 5.24: Influence of ageing: (a) on the strength, (b) on the stiffness of butt strap joints

Chapter 6

Fracture-based assessment of adhesive system

6.1 Introduction - Objectives

Chapter 5 was dedicated to the analysis of joints that were considered ideally without any defect. However, in some situations, because of the intrinsic nature of the adhesive material, initial defects in bonded joints can arise from voids created during the production or from damage during subsequent service. If the defect appears in a highly stressed region (eg at the edge of a lap joint, as seen in Chapter 2 section 2.2.1 and Chapter 5 section 5.4), the crack may propagate to give a major deterioration in performance and leading eventually to a catastrophic failure if no repair is carried out. It is therefore necessary to consider an analysis of such case.

The assessment of the behaviour of adhesive joints having cracks relies on fracture mechanics concepts presented in Chapter 2 and Appendix A. The idea of fracture mechanics approach is that damage in a structure can be tolerated up to a certain level of load or crack length. Hence it is necessary to assess this level of tolerance before the design process. In most structures, the predominant and most damaging mode is the mode I, hence the focus of this Chapter will be the characterisation of mode I fracture toughness of bonded joints with different adherends. A popular specimen used to characterise this tensile opening mode of adhesive joint is the Double Cantilever Beam (DCB) presented Figure 6.1 and using the Linear Elastic Fracture Mechanics (LEFM) concept.

Much research has been carried out on specimens involving different adherends such as aluminium alloys, steel or composites, using different geometrical configurations: simple DCB specimens, DCB specimens with end blocks or TDCB specimens (Ta-

pered Double Cantilever Beam). The most popular and easy to manufacture is the simple DCB specimen shown in Figure 6.1. Section 2.3 in Chapter 2 presented a general review on the use of fracture mechanics for adhesive joints and particularly joints with different adherends and pointed out the lack of data concerning joints with different metallic adherends.

The aim of this chapter is to characterise the crack growth in adhesive joints with both identical adherends and adherend imbalance through an experimental programme and analytical and numerical models. This involves defining a critical energy release rate and also defining what sort of influence the adherends have on the crack growth and the fracture toughness. Furthermore, as for the butt strap joint in Chapter 5, the influence of ageing on the cracked joint will be investigated too.

6.2 Experimental programme

The objective of the experimental programme is to generate a series of (load; crack length) data and load deflection curves that will enable the derivation of the critical fracture energy that is necessary for the crack to propagate.

6.2.1 Geometry and Materials

Figure 6.1 shows DCB specification in the case where both adherend materials are identical. In the general case where adherends have different material properties, the thickness h of each adherend has to be defined such that they both present an identical flexural rigidity to obtain a similar crack velocity as stated by (Bell & Kinloch 1997) and so that the tensile force remains perpendicular to the crack surface. This is essential to ensure that pure mode I fracture mechanics occurs during the experiments and consequently avoid mixed mode failure (Boeman, Erdman, Klett & Lomax 1999).

The specimens were produced from a 370 $\times$ 250 mm plate: adherends were grit blasted, acetone wiped and the primer was applied prior to bonding. Specimens were finally cut in strips of 25 mm and holes were drilled at the position specified in Figure 6.1.

The test programme is summarised in Table 6.1: three different configurations were considered: Al 6082 and Al 6082 adherends, Al 6082 and Al 5083 adherends and Al 6082 and steel adherends. These three combinations were considered because it

is likely that these adherends are associated in this way in the design of the joints, as shown in Figures 3.6 and 3.7. Table 6.3 presents a summary of the variations the adhesive thickness for the different specimens. It can be noticed that significant variations are observed not only between the different sets of specimens but also along the adhesive bond of each specimen.

6.2.2 Ageing environment

In order to investigate the effects of water on the mechanical properties of the joint, an accelerating ageing test programme was carried out. The ageing conditions were considered in accordance with the British Standard BS EN 29 142:1993: Specimens were immersed in a bath of distilled water for 3 weeks (approximately 500 hours) at 40^{o} C.

Distilled water was chosen because it was considered to be more damaging for the adhesive bond than salt water (Albericci, cited by (Armstrong 1997)) but also for practical reasons as the level of the solution's salinity is tedious to keep steady (Earl 2001). The temperature was chosen because it accelerates the absorption mechanisms while keeping the environment below the glass transition temperature T_g of the adhesive (Earl 2001, Kinloch 1990).

6.2.3 Test set up

The test procedure was followed in accordance to British Standard BS 7991:2001 (BSI 2002*a*). The tests were carried out at room temperature using a 100 kN Instron universal-testing machine operated in displacement control at a constant rate of 0.003 mm/sec, Figure 6.2. The design of the grip used for the test is presented Figures 6.3. The load and cross head displacement were recorded throughout the test, the length of the crack was monitored visually using a magnifying glass and via a trip of graph paper place under the adhesive bond. The corresponding load and displacement were noted and the test was stopped after about 80 mm of crack propagation to avoid any finite beam effect that could influence the fracture toughness values. Measurement of the machine compliance was done in order to get corrected cross head displacement values. This is of importance because if a testing machine deflects too much, the strain energy stored in the machine will be available to feed the crack and would lead to a crack instability (Atkins & Mai 1985).

6.3 Tests results

6.3.1 Locus of failure

After the test, each specimen was cut transversally to allow the observation of the locus of failure. This was to ensure whether the crack propagated within the adhesive, at the interface of the adherend or alternatively cohesively and adhesively.

6.3.1.1 Unaged specimens

Almost all of the samples presented a cohesive mode of failure in the adhesive with some spots where failure was observed close to the interface with the primer. Figures 6.4 to 6.6. This shows a good adhesive system (ie adhesive / primer / surface preparation) because no interfacial failure was noticed: in this case, the interlocking between the adhesive system shows its good performance. Although all the fracture modes were generally consistent, voids were observed in all the specimens as presented in Figures 6.4.

The crack path was observed after the test to assess whether the crack propagated along one or the other adherend interface or consistently through the mid layer of the adhesive. In the case of a DCB with steel and Al 6082, PTFE film being stuck on steel adherend, it is clear that the crack "drops" towards Al 6082 substrate and propagates close to the aluminium interface Figure 6.6 (b). As both adherends exhibit the same flexural rigidity, this phenomenon cannot be explained in terms of mechanical behaviour but rather in terms of adhesion and surface energy: the fracture follows the path of the weakest interlocking of both bonds. For the DCB with Al 6082 and Al5083 adherends, the crack propagates in the adhesive in a cohesive manner with random waves (wavy cohesive failure as defined by Liechti in reference (Pocius & Dillard 2002) page 61). The DCB made with both Al 6082 adherend also exhibited a wavy cohesive crack through the adhesive but with higher amplitude. Observation of the locus of failure actually showed that large voids spotted the adhesive bond.

6.3.1.2 Aged specimens

The specimens were tested soon after being dried with a cloth. Test conditions were similar to the test conditions of unaged specimens. Locus of failure and propagation pattern were monitored after the test as for the unaged joints.

In the case of the Al 6082/Al 5083 adherend combination, the crack propagated consistently in the adhesive layer with random oscillations. It was noticed that the adhesive layer was thinner than the unaged series (less than the specified 1 mm). For this reason, it was more difficult to distinguish failure propagation close to either the Al 6082 or the Al 5083 interface. For the steel/Al 6082 configuration, adhesive failure only occurred at the edges of the steel interface for 1 or 2 mm due to steel corrosion (Figure 6.9). In the center of the overlap, the crack propagated cohesively close to the Al 6082 interface as for the unaged specimens. The crack path in the Al 6082/Al 6082 joint was as randomly oscillatory as the previous series of DCB joints.

The locus of failure of aged specimens, in the case of aluminium combinations, was cohesive. No visual evidence of water ingression was observed on either the tip or the side edges of the DCB samples. Failure mode of steel to aluminium was adhesive at the edges and the tip due to corrosion of the steel but it was cohesive in the centre of the joint but close to the aluminium interface. This suggests that water corroded the steel interface damaging and weakening the interlocking bond between the adhesive-primer system and the adherend. This shows the distance up to which water affects the integrity of the joint in a 3 week period.

6.3.2 Load displacement behaviour

Once the crack was initiated all the load displacement curves of the DCB specimens tested showed similar trends as presented in Figure 6.10. Three phases can describe the curve:

- A linear part, preceded sometimes by non-linear behaviour due to the system testing machine - test fixtures. The linear part is followed by a non-linear zone where a peak is reached around 2.5 kN.
- The load then decreases with increasing vertical displacement non-linearly until recording process is stopped.
- The last part of the curve is linear, corresponding to the unloading phase to zero load (as opposed to zero displacement).

The load displacement curves for the Al 6082 / Al 6082 adherends (Figure 6.10 (b)) show different trends compared to either the Al 6082 / Al 5083 adherends or the Steel / Al 6082 adherends' cases. Indeed, the decreasing load phase in Figure 6.10 (b) is more wavy than the other two. In this respect, voids observed in Figure 6.4 on

Al 6082 / Al 6082 specimens can explain this phenomenon: drops of load observed in the Figure could be due to the presence of voids in the adhesive layer.

This type of curve also allows the determination of some parameters used for the post processing analysis, such as compliance of the specimen and whether permanent deformation occurs in the substrate at the end of the test, (BSI 2002*a*).

The initial non-linearity is not taken into account and in order to eliminate its effect, a linear extrapolation is done up to 95 % of the maximum load, usually taken as the end of the linear behaviour. The point that crosses this line and the vertical displacement axis is compared to the crossing point between the unloading line and this same axis in order to assess whether plasticity occurred in the adherend: this value is named δ_{offset}. Plasticity in the adherend is considered to occur if the ratio between δ_{offset} and the maximum vertical displacement value δ_{max} is less or equal to 5 % (Moore, Pavant & Williams 2001, BSI 2002*a*).

The DCB specimens made with Al 5083 and Al 6082 adherends, all presented permanent deformation after the test, $\delta_{offset}/\delta_{max}$ averaging 0.11. For the DCB made with Al 6082 adherends this ratio was 0.17 and for the DCB made with steel and Al 6082 it was 0.16.

Visual observations enabled the assessment of the adhesive bond quality and how a crack propagates when subjected to pure mode I of fracture. The following section will consider the data post processing with analytical models to assess crack propagation in terms of energy released.

6.4 Analytical modelling

The redistribution of stress in a body caused by the introduction of a crack or notch may be solved with analytical methods of linear elastic fracture mechanics (LEFM). LEFM assumes that a linear elastic body contains a sharp crack and then describes the change of energy which occurs when such a body undergoes an increase in crack area. The parameter of most fundamental importance is the energy release rate G or fracture toughness, which is defined as the rate of energy released by the crack growth:

$$G = \frac{\partial U}{\partial A} \tag{6.1}$$

where ∂U is the energy change and ∂A is the variation of area. It is this energy released which is available to drive the crack growth and overcomes the critical fracture resistance G_c. Therefore at fracture.

$$G = \frac{1}{B}\frac{\partial U}{\partial a} \tag{6.2}$$

Where B is the width of the specimen and ∂a the variation of crack length. G is determined by the loading and geometry of the cracked body while G_c can be considered as a material property and is the energy per unit area necessary to create a new surface area of the crack: it is called the fracture toughness.

A fracture mechanics analysis can be done by different methods, direct or indirect (Moore et al. 2001):

- Resistance curve description (R-curve).
- Minimum energy value.
- Onset of non-linearity in load deflection curves.

The first two are direct methods while the third is an indirect but more reproducible method.

The critical fracture energy can be represented by the R-curve and can be calculated with three analytical methods. These methods are namely: Simple Beam Theory (SBT), Corrected Beam Theory (CBT) and Experimental Compliance Method (ECM). Their concept and associated equations are described in Appendix A.

An R-curve provides a comprehensive description of the evolution of G_c when the crack propagates and the following sections describe the different post-processing steps gone through to assess the fracture toughness of the adhesive system considered.

6.4.1 Conditions of application

Linear Elastic Fracture Mechanics can only be applied under certain conditions, ie linear load deflection behaviour and small deformation at the crack tip compared to the in-plane dimension of the specimen. This is called the condition of small scale yielding and expressed by the following relationship:

$$B, a, (W - a) \geq 2.5 \left(\frac{EG_c}{\sigma_c^2} \right) \tag{6.3}$$

Where:
B is the width of the specimen,
a is the length of the crack,
W, is the effective length of the specimen,
(W - a) is called the ligament,
G_c is the critical fracture energy,
σ_c the yield stress of the adhesive.

6.4.2 Crack initiation

As the initial debonding area is initially modelled by a PTFE film, it is necessary to ensure that the film will not influence the crack propagation values, this is why a crack initiation is carried out (Blackman et al. 2003, Moore et al. 2001). Initial crack growth was conducted until the crack was seen to be moving by 1 or 2 mm. One set of data (crack length and corresponding load) was recorded and the specimen was unloaded. From this set, the energy corresponding to the crack initiation is calculated from Equations A.9, A.10 and A.12 in Appendix A.

Figures 6.11 and 6.12 present a summary of minimum energy for different combinations of adherends and different analytical methods in the case of aged an unaged specimens. This energy is calculated from equations A.9 to A.12 and corresponds to the first value recorded during the test when the onset of the crack was observed moving.

These figures show that the mininum energy required to open the crack is less in the case of steel / aluminium joints than for the Al 6082 / Al 6082 and Al 6082 / Al 5083 joints that present similar results. Also, SBT presents consistent results, although much more conservative, compared to the two other methods. Considering results from unaged and aged DCB tests, it is seen that environmental degradation results in a lowering of fracture energy to initiate the crack. Comparing the minimum energy of unaged and aged DCB specimens, the figures also show that the mininum energy to initiate and open the crack is substantially lower in the case of environmental degradation. This suggests that the water ingression increases internal pressure in the bulk adhesive facilitating crack opening.

It is also important to compare minimum energies when using specimens with PTFE insert as opposed to specimens with a pre-crack. Unlike (Blackman et al. 2003), it was observed that the energy required to open the crack from the insert is higher than the energy necessary to open the crack from mode I pre-crack by about 10%. They explained their results by the fact that the PTFE film produced a sharp initial crack that yielded lower initiation values than obtained after pre-crack. In the scope of the study, the adhesive used was less brittle than the one used in reference (Blackman et al. 2003); this could explain the discrepancies in the results.

6.4.3 Mean crack propagation

Resistance curves (R-curves), representing the fracture energy versus the crack propagation, were drawn in order to derive the mean crack propagation with the three different methods proposed. These propagation values will be taken as the critical fracture toughness G_{Ic}.

Figures 6.13 presents examples of R-curves. The data points from that figure are calculated from equations A.9 to A.12 via a spreadsheet, an example of which is presented in Appendix B. Tables 6.4 to 6.5 present the averaged values of fracture toughness for the five specimens of each combination of adherends.

From Figures 6.14 it can be seen that the adhesive considered presents a relatively high toughness for an adhesive: averaging between 1600 J/m^2 and 3500 J/m^2 depending on the method and the substrate considered. A material like steel presents a typical toughness of about 30 kJ/m^2 whereas a very brittle material like glass has a fracture toughness of 0.01 kJ/m^2 and tough polymers have a fracture toughness of about 4kJ/m^2 (Atkins & Mai 1985).

From equation 6.3, it can be seen that, the value at the right hand side of the relation is equal to 13.1 mm, while B = 25 mm, 26 mm $\leq$ a $\leq$ 120 mm and 249 mm $\leq$ W - a $\leq$ 344 mm during the test. Hence the condition of small scale yielding are respected.

6.4.3.1 Comparison of analytical methods

Generally speaking, the trend of the fracture toughness using CBT or ECM are similar presenting a brief increase of energy at the first millimetres of the crack tip followed by a plateau region. This plateau region in some cases decays slowly when the ECM method is used. The SBT method shows also a plateau region but with a

less sharper rise at the initiation of propagation.

For all specimens tested, the values of G_{Ic} deduced from CBT and ECM are in good agreement but the values deduced from SBT are substantially lower than those calculated employing the CBT and ECM approaches. This is because the simple beam theory does not take into account the rotation of the beam at the end and induced bending effects are neglected (Moore et al. 2001, Ripling et al. 1970).

Also, it is observed from Figure 6.15 that the SBT method has less variations and scatter than the CBT and ECM methods. From Figures 6.14, the average energy derived from the SBT method shows a standard deviation which is less than standard deviation observed in the case of CBT and ECM methods. In terms of R-curve, Figure 6.15 shows that the SBT and CBT methods present G_c values that are more constant with respect to crack growth than the ECM method.

6.4.3.2 Influence of ageing

Figure 6.16 shows an example of R-curves for aged specimens and different adherends and Figure 6.17 summaries the average fracture energy. The loss in the critical fracture energy between unaged and aged specimens varies between 26 % and 82 % depending on the method chosen. This means that environmental degradation by water affects the integrity of the interface causing changes in the value of G_{Ic}. Furthermore, these tests suggest the predominance of degradation by water over the influence of heat. Indeed, increase of temperature usually implies increase of material ductility and thus fracture toughness as stated by (Anderson 1995), which is not the case in the present study.

Also, it is noted that environmental degradation introduces a non-negligible scatter in the resistance curves. It was observed that, when comparing results sorted by adherend combination (i.e. comparing the 5 specimens of each series Al 6082/Al6082, Al 6082/Al 5083 or Steel/Al6082), results were in reasonably good agreement when the specimens were unaged. But when comparing the same series with aged specimens, the results did not correlate as well as with the non-aged series.

6.5 Numerical modelling

The previous section proposed the use of analytical models to predict fracture in simple adhesive joints subjected to mode I. These methods cannot be applied in the

case of more complex structures, but a numerical analysis can help to overcome this problem. Before using this tool for complex joints, it is necessary to validate the model and compare the results to those presented in Section 6.4. The aim of this section is to perform a finite element analysis of DCB specimens in order to derive the R-curves of a joint for each combination of adherends and to compare it to the analytical solutions presented in the previous section.

6.5.1 Finite element models

Three different models were investigated corresponding to the three different configurations of DCB specimens tested. The first configuration with an Al 6082/Al 5083 combination presents a geometrical symmetry but a mechanical imbalance. Therefore a complete finite element model was used. Figures 6.18 to 6.20. The second configuration tested presented both geometrical and mechanical imbalance with steel and Al 6082 adherends, Figure 6.21. The last combination of DCB was modelled with symmetrical considerations, as the joint was made with Al 6082 adherends. Figure 6.22.

The adhesive layer was modeled with PLANE82 elements whereas the adherend material was modeled with PLANE82 between the pin hole and the crack tip and with PLANE2 elements ahead of the crack tip. This enabled to get a good refinement in the finite element model around the crack tip and avoid too many calculations anywhere else. These elements are similar in their formulation (structural solid elements) and are compatible together: PLANE2 is a triangular 6-node structural element and PLANE82 is an 8-node structural element. They both have two degrees of freedom at each node: horizontal u_x and vertical u_y displacement. The crack tip, because of a singularity in the solution (the stress varies in $1/\sqrt{r}$, where r is the radial distance from the crack tip), had to be modelled with a special element, named singular element, that has to be quadratic with the midside nodes placed at the quarter points (Ansys 2002). Twenty four of these elements surrounded the crack tip.

For each data point from the experimental results (i.e. load and crack length), a finite element analysis was performed assuming plane strain conditions, to derive the critical stress intensity factor K_{Ic} and then the corresponding critical fracture energy value G_{Ic} given by the following relation:

$$G_{Ic} = \frac{K_I^2}{E_a}(1 - \nu^2)$$

Where E_a and ν are the Young's modulus and the Poisson ratio of the adhesive respectively.

The stress intensity factor value K_{Ic} was computed using KCALC function from the ANSYS software package. This function calculates the mixed mode stress intensity factors from nodal displacements at the crack tip but is limited to linear elastic problems with a homogeneous, isotropic material near the crack region (Ansys 2002).

Also, the J-integral function, described in Appendix A, was used to assess the fracture energy of the joint in the cases when the adhesive had linear and non-linear material properties. Each G_{Ic} and J_c value was then compared to analytical results.

6.5.2 Convergence analysis

A sensitivity analysis of the G_{Ic} and J values to the mesh density was carried out to check that there was convergence of the results with mesh refinement. The analysis was carried out for one model and a single set of (load ; crack length) values the reason being that the other models were based on the same as the one checked for convergence. Table 6.6 summarises this analysis and shows that convergence is obtained with the KCALC and the J-integral methods for a model with approximately 11500 nodes.

6.5.3 Results

Figure 6.23 presents an example of the fracture energy results given by the K-CALC and the J-integral functions from experimental data that was representative of each combination. The trend of fracture energy given by this numerical method follows exactly the same trend as the fracture energy given by SBT method but with a higher magnitude. As expected, the J-integral with the linear adhesive properties gives the same results as G_{Ic} calculated with the KCALC function. With non-linear material properties, modelled with a multi-linear elastic method, the results are lower than with the other methods.

Also, it is observed from Figure 6.23, that in the case of a steel/aluminium combination, deviation between SBT method and finite element method is minimal compared

to an aluminium/aluminium joint combination. As for the analytical models, fracture toughness was found to be less in the case where steel substrate is used than when aluminium is used.

6.6 Discussion

6.6.1 Influence of adherends and adhesive thickness

It is apparent from both analytical and numerical models, that the average energy release rate varies with the adherends used. Generally speaking, G_c values depend on geometrical factors such as the width of the joint or the adhesive thickness (Kinloch & Shaw 1981, Kinloch 1990) or factors such as the curing rate of the adhesive and surface preparation (Blackman et al. 2001). However, in the case studied, the same surface preparation was applied to all the adherends and the curing rate of the joint was done at ambient temperature, 21°C. Concerning the thickness of adhesive, the nominal thickness was 1 mm; however Table 6.3 shows that a non negligible scatter is observed between the original and the actual value for the different combinations. The DCB specimens made with Al 6082 adherends present the highest adhesive thickness (1.45 mm thickness near the PTFE film) compared to the DCB made with Steel and Al 6082 (1.26 mm) or Al 6082 and Al 5083 (0.65 mm). The DCB specimens with aluminium 5000 and 6000 series present a noticeably thin adhesive layer, by a ratio of 2 compared to the other DCB specimens.

What can be said from Tables 6.3 and 6.4 is that, comparing line 1 and 3 of each table, the adhesive thickness influences the fracture toughness of the joints in the limit of 0.6 mm and 1.4 mm because the substrate Al 5083 and Al 6082 present similar properties. Comparing the line 2 with line 1 only, it can be said that in this case, the adherend materials influence the value of the fracture toughness of the joint. Although these results are similar to the one found by (Yan et al. 2001a) who showed that fracture toughness of joints increases with decreasing substrate Young's modulus, many studies (Kinloch & Shaw 1981, Wang et al. 1978) have highlighted that a complex relation exists between the adhesive thickness and the energy release rate.

To further understand the mechanisms of crack propagation, a linear stress analysis was carried out to investigate the influence of the stress field surrounding the crack tip on the crack opening of the joint. For the three different combinations of the DCB (Steel/Al 6082, Al 6082/Al 5083 and Al 6082/Al 6082), the stress was computed in the case when the crack has propagated and the stress is calculated for a

set of (load; crack length) values taken from the experimental results. The load was the same for the three models (1370 N), but the corresponding crack length a from experiments was specific to each specimen.

Figure 6.24 shows the stress profile on a logarithmic scale ahead of the crack for the different combinations of adherends. Close to the crack tip, the normal stress σ_{22} follows the classical behaviour of $\frac{1}{\sqrt{r}}$ near the singularity, where r is the distance from the tip, for a very short distance up to approximately 0.06 mm. After this point a more complex behaviour is observed: the stress decreases until 0.3 mm to increase slowly up to about 2 mm away from the tip and decreases again more sharply. The trends of the curve for the three combinations of adherend are very similar but the steel to aluminium combination presents a lower stress magnitude compare to both aluminium combinations.

Similar numerical analysis were carried out on aluminium alloy and steel DCB by (Yan et al. 2001a) and steel and CFRP DCB by (Bell & Kinloch 1997, Blackman et al. 2001). A similar stress profile was found but no extremum in the normal stress was reported, ie, in the present case, more distortion in the stress field ahead of the crack tip is observed. What must be noticed from this graph is that the higher opening stress is associated with the steel-aluminium adherend, this means that even if the adherends have the same flexural rigidity (EI), the material mismatch still influences the state of stress in the adhesive.

6.6.2 Influence of ageing

Qualitatively, the ageing process affects the interlocking between the adhesive system and the adherends in the case where a steel adherend is used. This leads to adhesive failure at the edges and the tip of the specimens. Also, Figure 6.16 shows that the rise of the R-curves is less sharp when aged specimens are considered, this is emphasized in the case of steel to aluminium DCB joints. Eventually, flatter R-curves suggest that the adhesive bond compliance is reduced influencing less the results.

Quantitatively, the accelerated ageing process showed a decrease in fracture toughness compared to unaged conditions, Table 6.7. (Veazie, Robinson & Shivakumar 2004) observed more than 50 % reduction in fracture toughness in the case of sandwich composites after 5000 h. The reduction of G_{Ic} values from one DCB combination to an other are similar at about 35 %, Table 6.7. This similar reduction of

fracture energy regardless of the adherend suggests that the adhesive failure observed on steel to aluminium joints do not influence the magnitude of G_{Ic}.

6.6.3 Influence of calculation method

For analytical solutions, Table 6.4 and Figure 6.23 show that CBT and ECM methods are in good agreement, whereas SBT method gives substantially lower results than the corrected theories. These results are similar to those presented by (Blackman et al. 1991, Moore et al. 2001, Blackman et al. 2003) who explained this different results by the fact that the SBT method failed to take into account the crack tip root rotation effects. Furthermore, it can be noticed that the the fracture toughness tends to decrease with the Experimental Compliance method while it remains more constant with the CBT method. This decrease should not happen as G_{Ic} should remain independent of the crack length. (Blackman et al. 2003) found that this decrease was due to the compliance (or stiffness) of the testing machine and proposed a correction factor taking into account this effect. In this study, this correction factor was taken into account in the derivation of G_{Ic} values with CBT and ECM methods but the decrease remained accentuated.

A reason for the different results can be found in the equations modelling the compliance of the system for the different methods CBT and ECM methods. The compliance is given by the ratio of the vertical displacement δ_{corr} and the corresponding load F:

$$C = \frac{\delta_{corr}}{F} \tag{6.4}$$

For the CBT and ECM methods this gives respectively (Moore et al. 2001):

$$C = k_1 (a + \Delta)^3 \tag{6.5}$$

$$C = k_2 a^n \tag{6.6}$$

With k_1, k_2 constants including geometrical parameters and the elastic moduli and n and Δ being found experimentally (BSI 2002*a*). For Al 6082 / Al 6082 combination, $n = 1.95 \pm 0.19$, for the Al 5083 / Al 6082 $n = 2.03 \pm 0.15$ and for Steel to Al 6082 $n = 2.35 \pm 0.15$. Hence, it can be seen that the compliance is modelled with a power law of 3 with the CBT method while it is modelled with $1.95 < n < 2.35$ with the ECM method. Figure 6.13 (c) shows that good agreement is found between ECM

and CBT methods when n = 2.35 ie closer to 3.

The results given by the R-curves from the K-CALC function, lie between the conservative ones from SBT and the more realistic ones from the CBT and ECM methods whereas using the J-integral assuming non-linear elastic material gives the most conservative results of the 5 methods. Similar studies on Aluminium DCB and steel DCB specimen using the critical fracture energy and the J-integral method by (Yan et al. 2001a) showed that the critical J-integral is also lower than the critical energy release rate G_c. This is due to material non-linearity that allows material plasticity hence reducing the level of stress surrounding the crack tip and the energy release rate. However, it can be noticed from Figure 6.23 that this latter method gives a steadier plateau region, while the SBT and KCALC methods are slightly rising. In other words, the standard deviation of the propagation values is less when the J-integral is used which means that the method is more reliable.

Furthermore, unlike (Blackman et al. 2003) who successfully used correction factor to take the compliance of the testing machine into account to obtained R-curves independent of the crack length, this study showed that the bondline can no longer be neglected in the calculation of the fracture toughness of the joint. If a closed form solution is to be used for a relatively thick bondline, it has to take into account the presence of the adhesive in its formulation. In this respect, the use of finite element solution happened to give better results (ie the fracture toughness is independent of the crack length) than the analytical solution though more conservative.

6.7 Conclusion

This Chapter addressed the fracture behaviour of double cantilever beam specimens bonding different combinations of adherends with a semi rigid adhesive. The fracture toughness of the adhesive system was characterised according to three different analytical methods; a finite element approach was used to correlate these results.

This study has emphasized the following key points:

- The role of the adhesive bond is important in determining the compliance of the system during the test. This led in some cases to fracture toughness results dependent on crack length which should not happen.
- Experimental and analytical results suggest that the influence of the adhesive

thickness is more dominant than the influence of different adherend combinations. An analysis of the stress field surrounding the crack tip showed that the stress field presents different magnitude depending on the adherend used, although they had similar flexural rigidity.

- Each series of aged specimen showed a similar rate of toughness reduction. In the case of steel adherend, this loss of fracture toughness was accompanied with adhesive failure at the steel interface due to the corrosion of the metal.

- This comparison between different methods therefore provides an envelope for a design criterion for a defect tolerance approach that will be investigated in Chapter 8. In terms of analytical methods, the corrected beam theory method was found to be the most suitable and accurate to calculate the energy release rate G_{Ic}.

Tables

Test method	Sample material specifications	Number of specimens
Mode I fracture mechanics at ambient conditions	Al 6082 / Al 5083	5
	Al 6082 / Steel	5
	Al 6082 / Al 5083	5
Mode I fracture mechanics after ageing	Al 6082 / Al 5083	5
	Al 6082 / Steel	5
	Al 6082 / Al 5083	5

Table 6.1: DCB Test matrix

Adherend system	L [mm]	h_1 [mm]	h_2 [mm]	t_a [mm]	a_0 [mm]
Al 6082 / Al 6082	370	12	12	1	51
Al 6082 / Steel	370	8	12	1	51
Al 6082 / Al 5083	370	12	12	1	51

Table 6.2: Nominal dimensions of the DCB specimens. these refers to Figure 6.1

Adherend system	crack tip [mm]	root of the beam [mm]	average thickness along the beam [mm]
Al 6082 / Al 6082	1.45 ± 0.04	1.31 ± 0.05	1.38 ± 0.07
Al 6082 / Steel	1.32 ± 0.05	1.20 ± 0.06	1.26 ± 0.08
Al 6082 / Al 5083	0.74 ± 0.03	0.51 ± 0.03	0.64 ± 0.11

Table 6.3: Summary of adhesive thickness of DCB specimens

Adherend system	G_{Ic} SBT $[J/m^2]$	G_{Ic} CBT $[J/m^2]$	G_{Ic} ECM $[J/m^2]$
Al 6082 / Al 6082	1678 ± 137	3742 ± 723	3663 ± 830
Al 6082 / Steel	1693 ± 88	2659 ± 110	2615 ± 117
Al 6082 / Al 5083	1565 ± 63	3063 ± 173	3001 ± 190

Table 6.4: Summary of fracture toughness of non aged specimens DCB specimens

Adherend system	G_{Ic} SBT $[J/m^2]$	G_{Ic} CBT $[J/m^2]$	G_{Ic} ECM $[J/m^2]$
Al 6082 / Al 6082	1103 ± 350	2607 ± 310	2534 ± 291
Al 6082 / Steel	1263 ± 743	1725 ± 302	1582 ± 332
Al 6082 / Al 5083	1037 ± 519	1956 ± 424	1885 ± 399

Table 6.5: Summary of DCB test results for aged specimens

Number of nodes	G_{Ic} K-CALC $[J/m^2]$	J $[J/m^2]$
6920	303	301
7545	308	293
8785	306	291
11422	306	303
12941	306	305

Table 6.6: Summary of variations of calculated fracture energy with mesh refinement

	Simple Beam Theory	Corrected Beam Theory	Experimental Compliance Method
Al 6082 / Al 6082	34 %	30 %	31 %
Al 6082 / Steel	26 %	35 %	39 %
Al 6082 / Al 5083	33 %	36 %	37 %

Table 6.7: Loss of toughness due to accelerated ageing with respect to the analytical methods and the adherend system

Figures

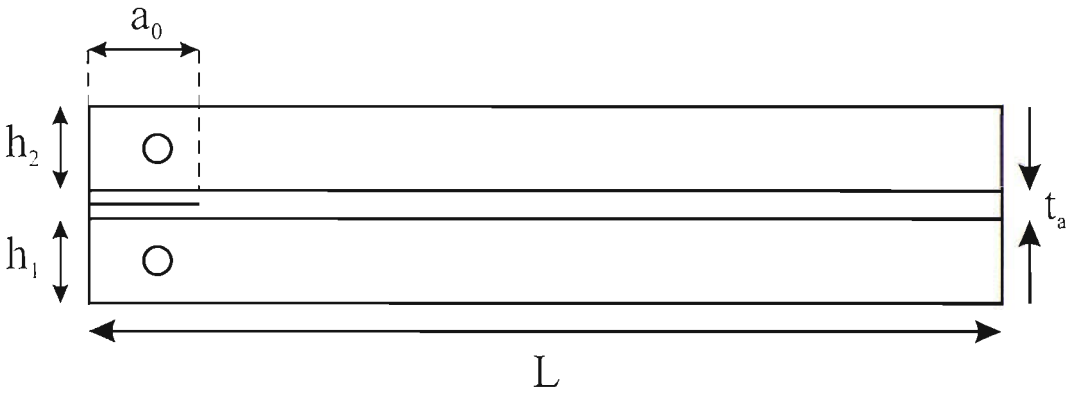

Figure 6.1: DCB specifications. see Table 6.2 for the dimensions

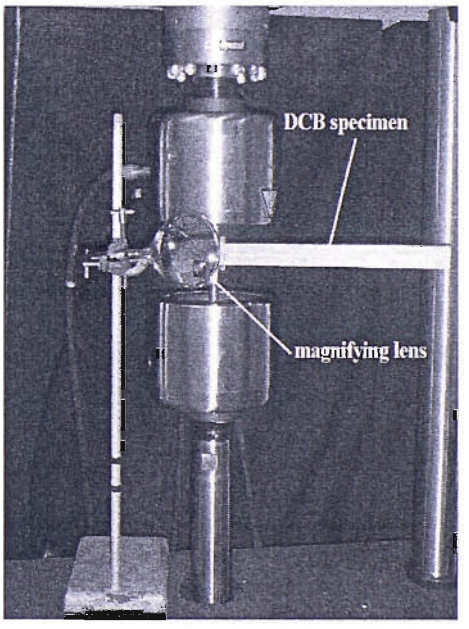

Figure 6.2: Setup of DCB test

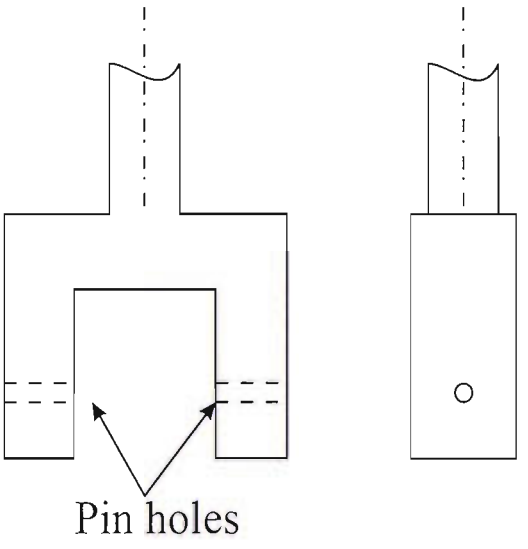

Figure 6.3: DCB test fixtures

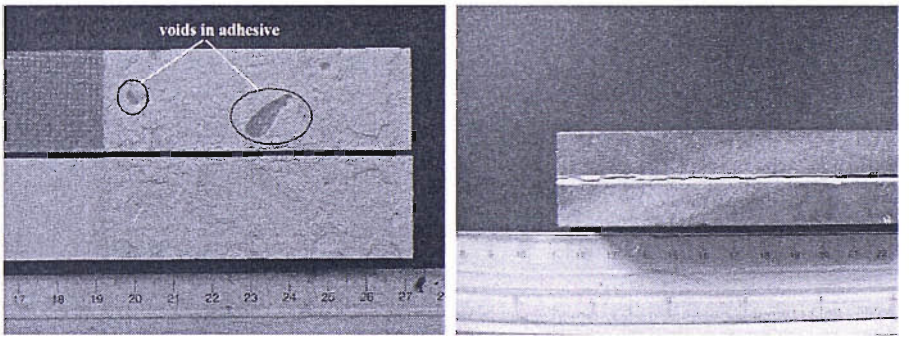

(a) (b)

Figure 6.4: Failure mode of unaged DCB specimens with Al 6082 / Al 6082

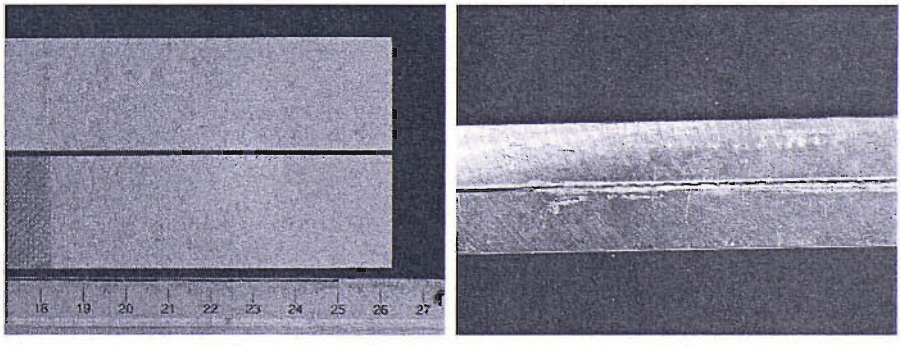

(a) (b)

Figure 6.5: Failure mode of unaged DCB specimens with Al 5083 / Al 6082

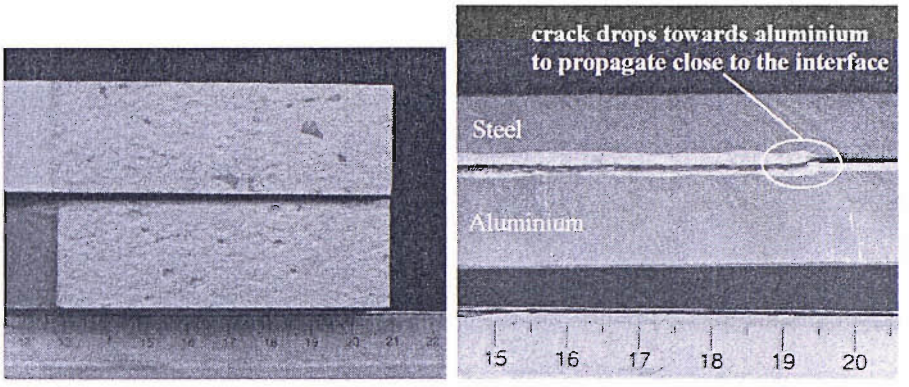

(a) (b)

Figure 6.6: Failure mode of unaged DCB specimens with Steel / Al 6082

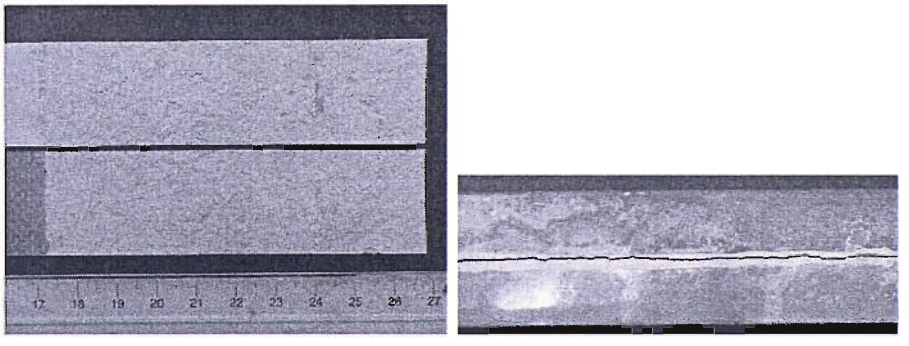

(a) (b)

Figure 6.7: Failure mode of aged DCB specimens. Al 6082 / Al 6082

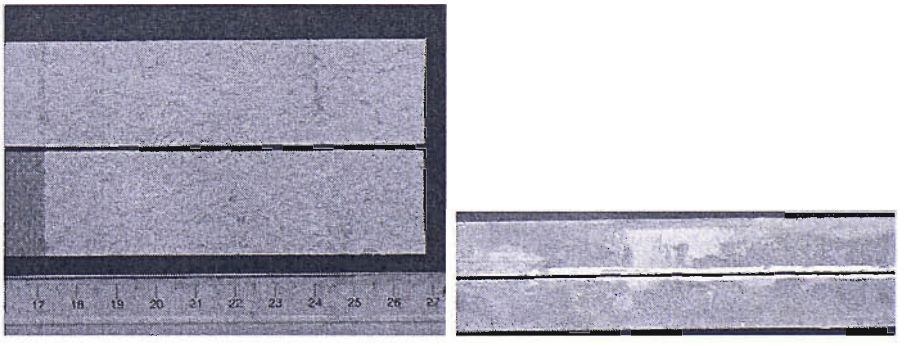

(a) (b)

Figure 6.8: Failure mode of aged DCB specimens Al 6082 / Al 5083

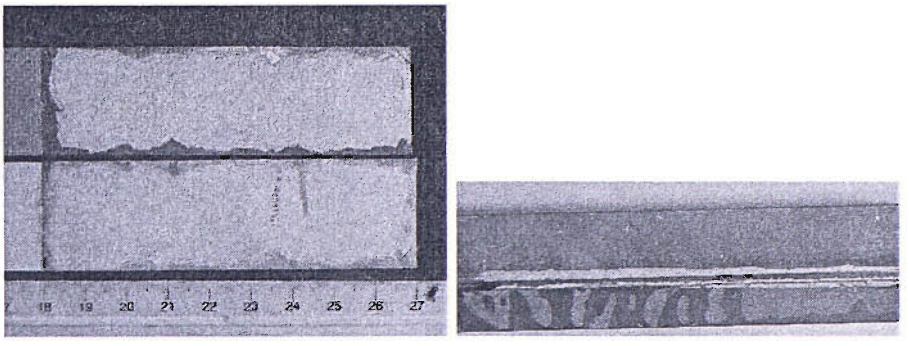

(a) (b)

Figure 6.9: Failure mode of aged DCB specimens. Al 6082 / Steel)

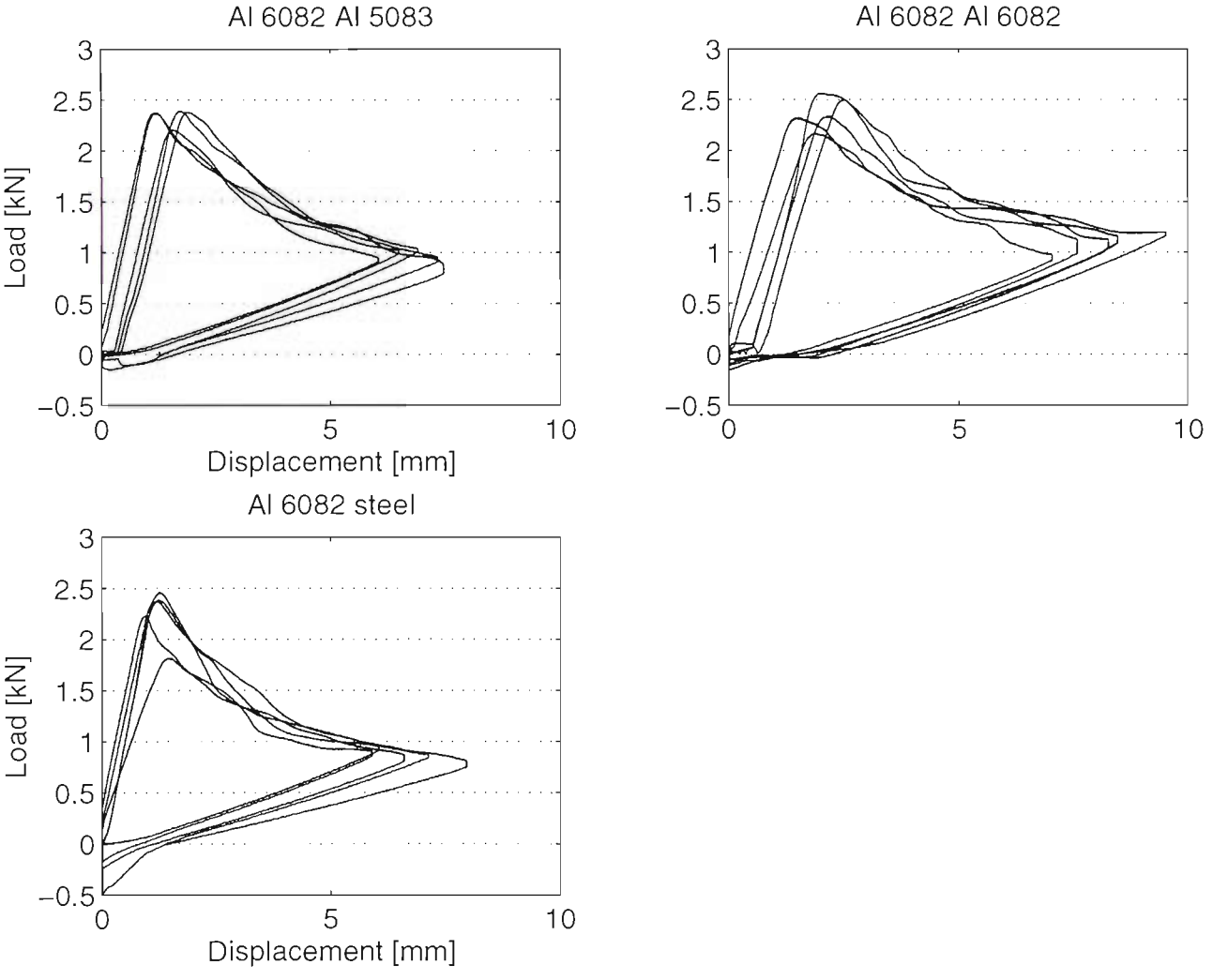

Figure 6.10: Load displacement curves of the different DCB specimens tested

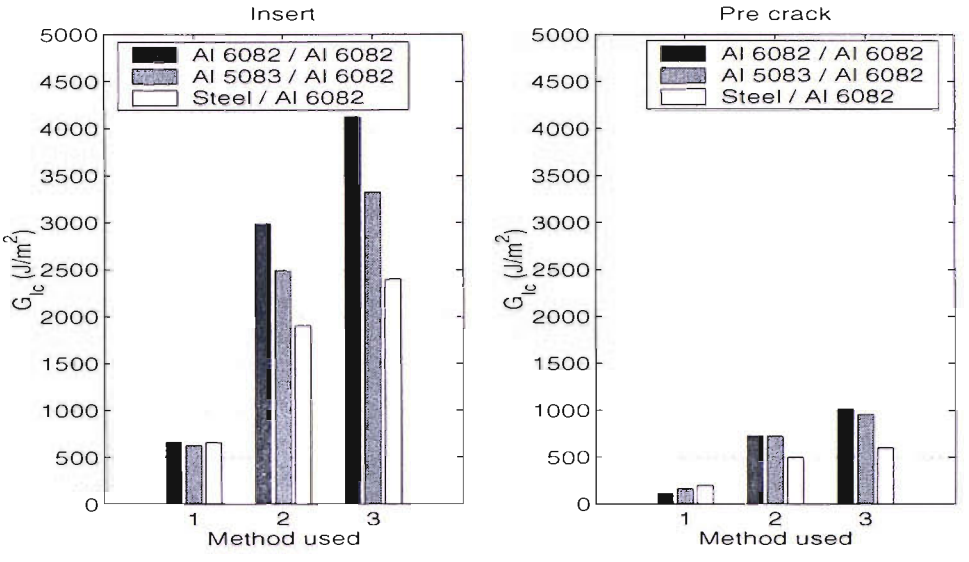

Figure 6.11: Minimum fracture energy of DCB specimen from insert and pre crack: non aged specimens. (1): SBT method. (2): CBT method. (3): ECM method

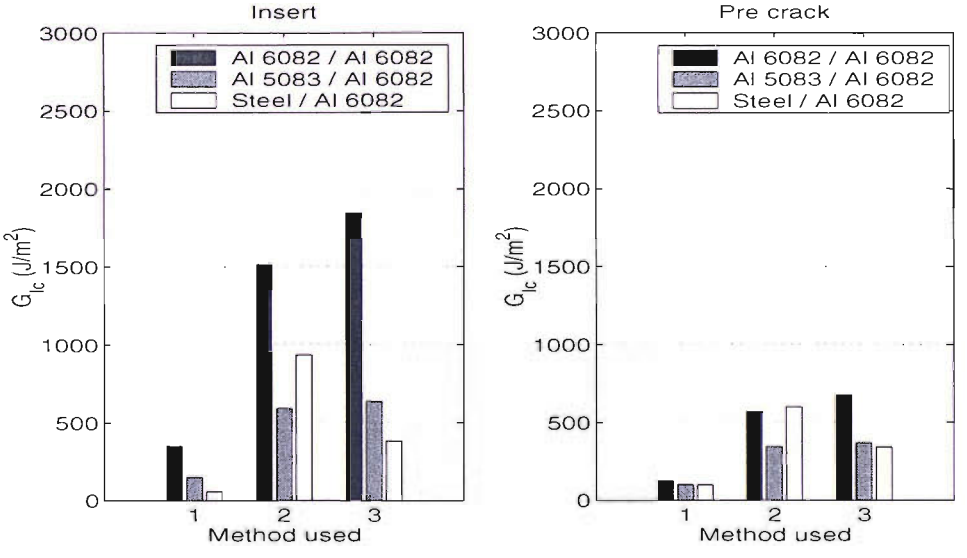

Figure 6.12: Minimum fracture energy of DCB specimen from insert and pre crack: aged specimens. (1): SBT method, (2): CBT method. (3): ECM method

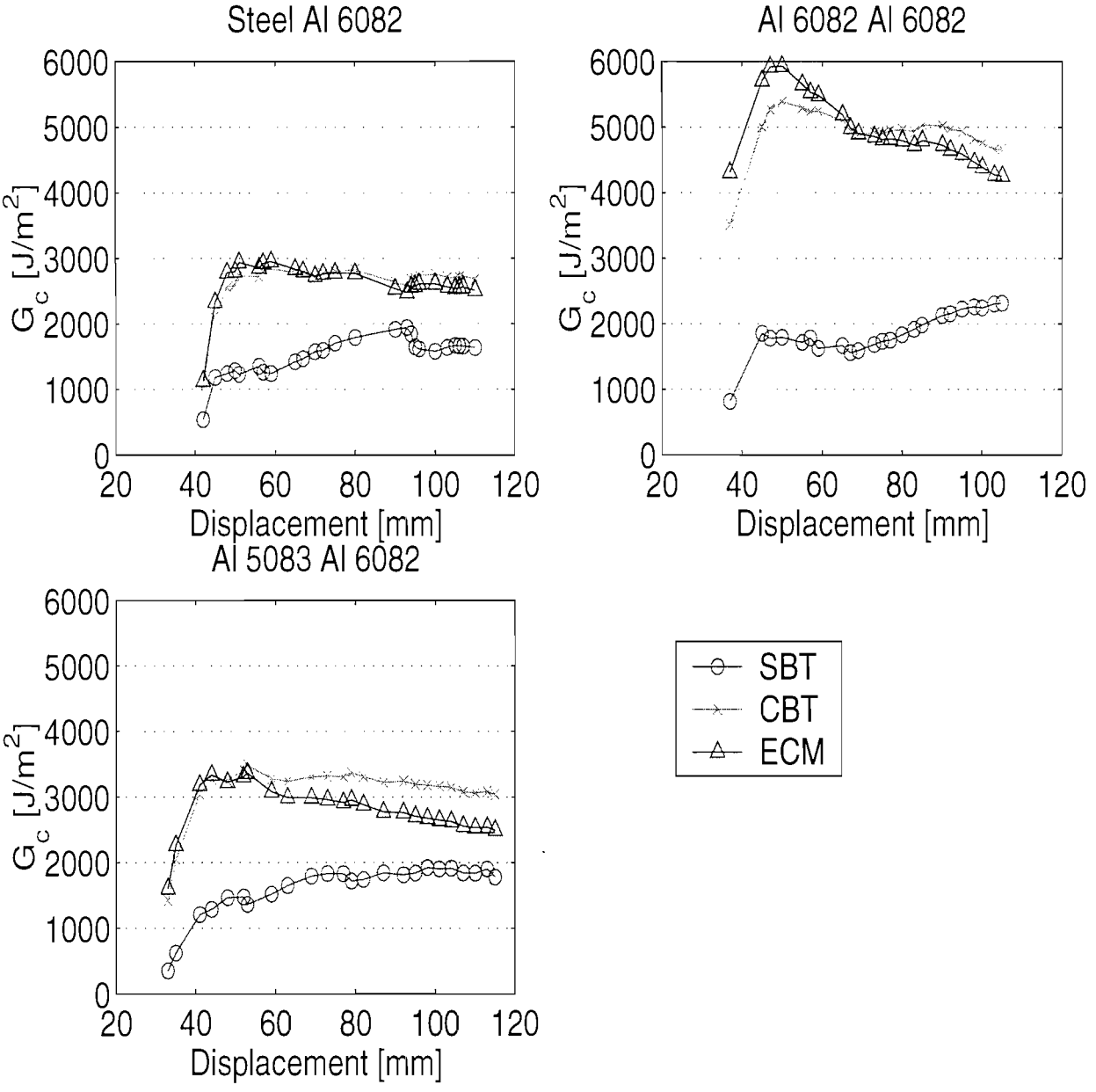

Figure 6.13: Typical resistance curves of unaged DCB specimens: analytical methods

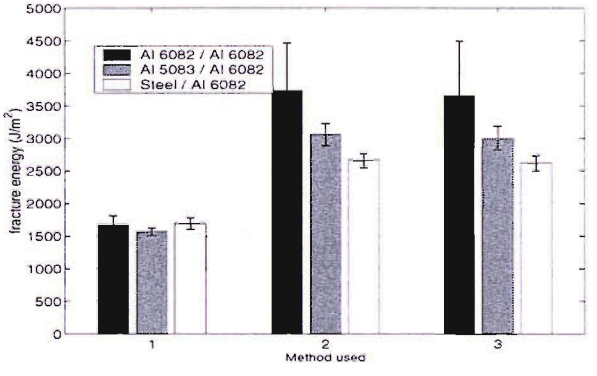

Figure 6.14: Average fracture toughness of unaged DCB specimens. (1): SBT method, (2): CBT method, (3): ECM method

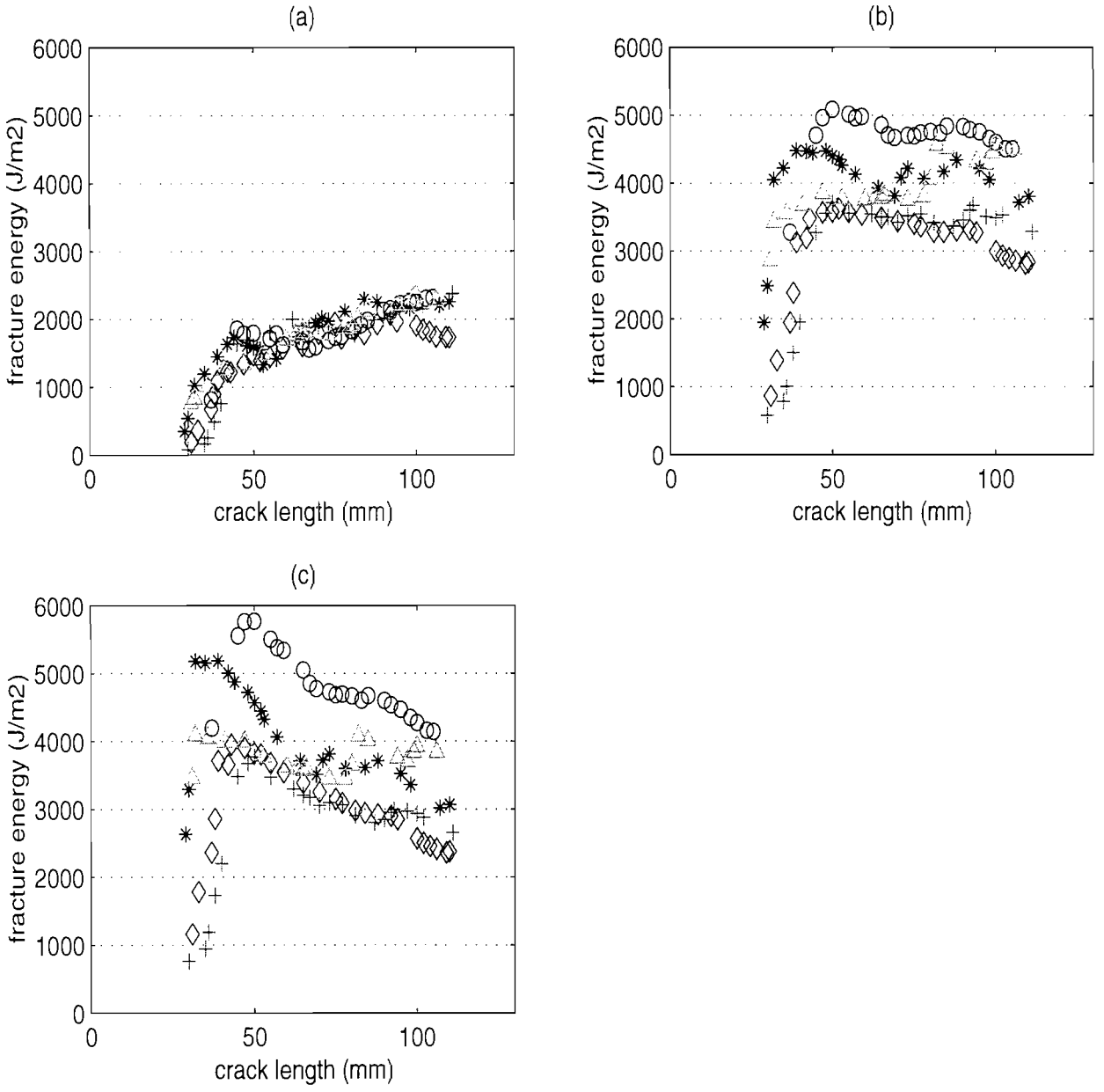

Figure 6.15: Comparison of R-curves of DCB with Al 6082 adherends from different methods (a): SBT method, (b): CBT method, (c): ECM method. Each curve corresponds to a specimen tested

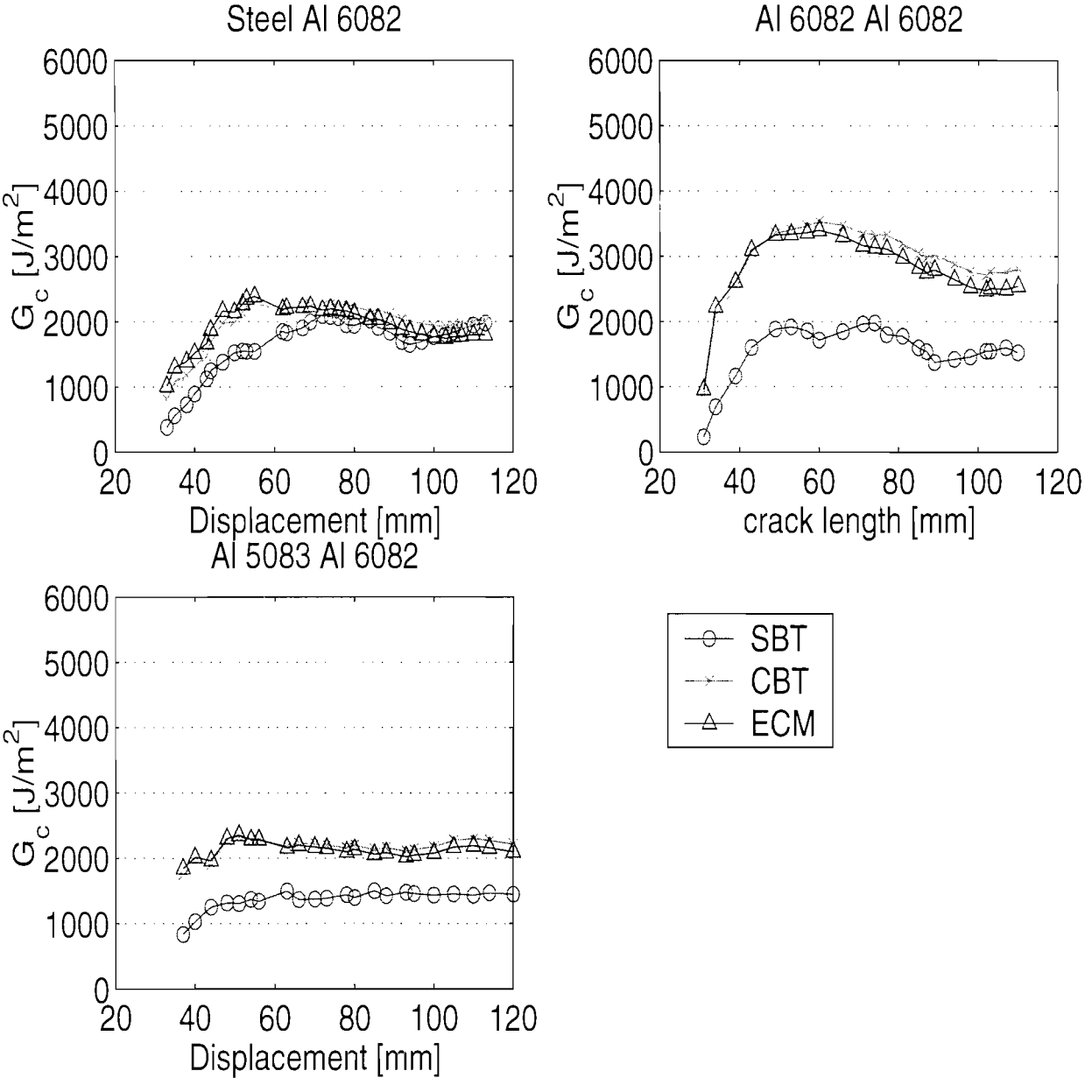

Figure 6.16: Typical resistance curves of aged DCB specimens: analytical methods

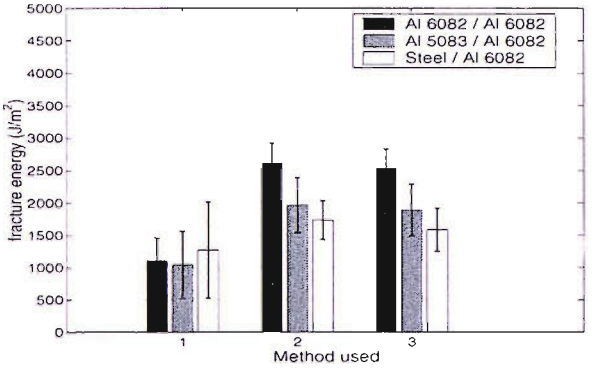

Figure 6.17: Average fracture toughness of aged DCB specimens. (1): SBT method. (2): CBT method. (3): ECM method

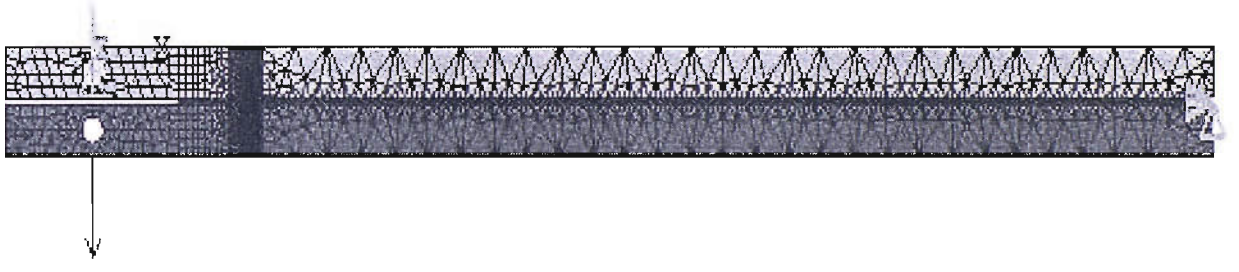

Figure 6.18: Finite element model of Double Cantilever Beam with Al 5083 and Al 6082 substrates

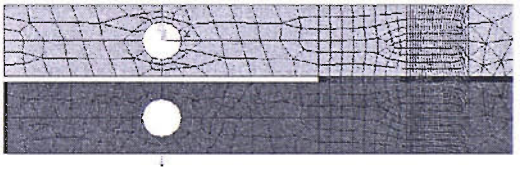

Figure 6.19: Finite element model of Double Cantilever Beam: detail of mesh

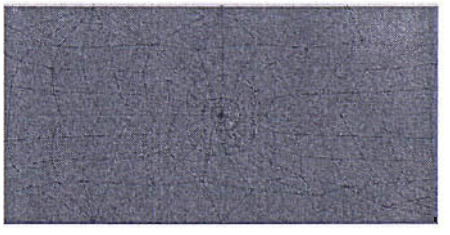

Figure 6.20: Finite element model of Double Cantilever Beam: detail of crack tip mesh

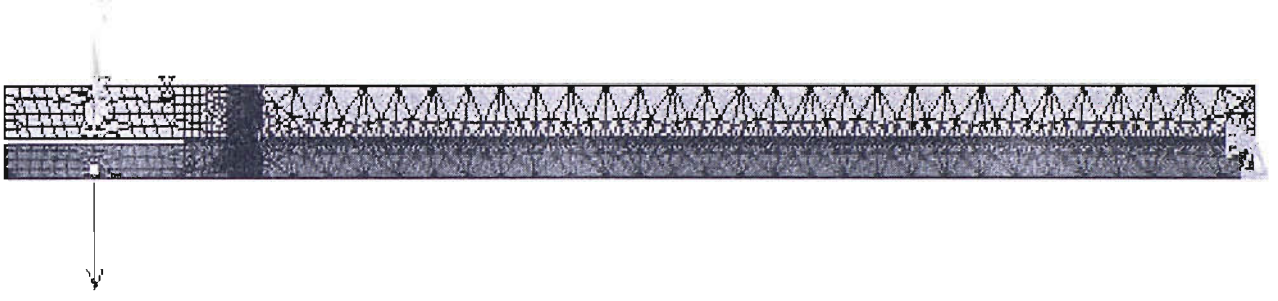

Figure 6.21: Finite element model of Double Cantilever Beam with steel and Al 6082 substrates

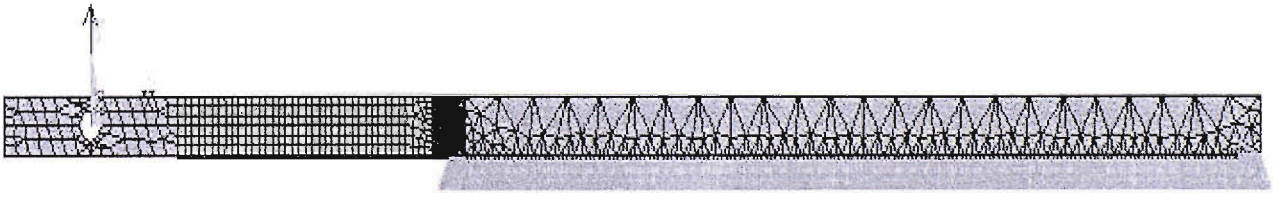

Figure 6.22: Symmetrical finite element model of Double Cantilever Beam with Al 6082 substrates

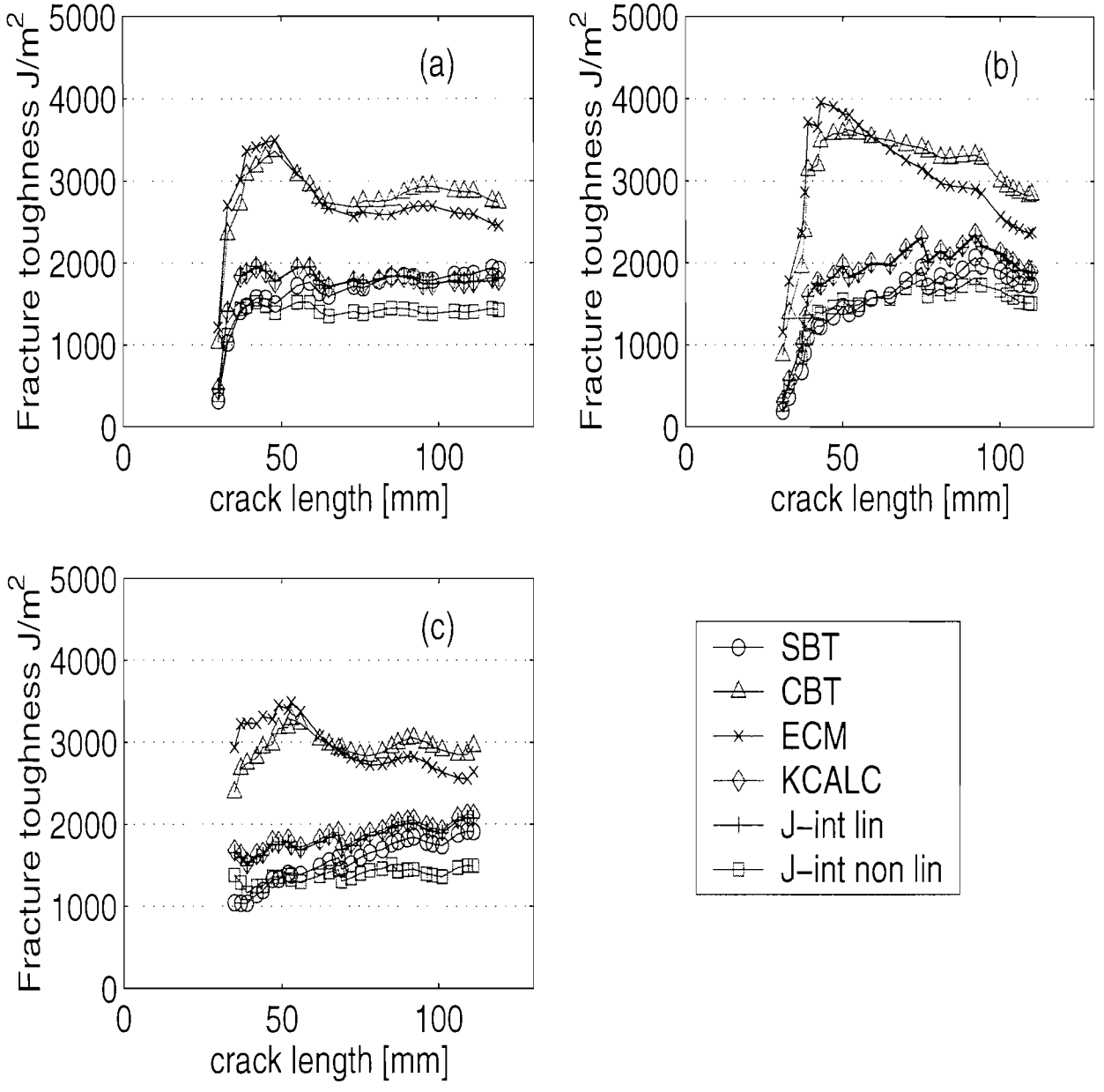

Figure 6.23: Typical resistance curves of unaged DCB specimens: analytical and numerical methods. (a) steel-Al 6082 substrates, (b) Al 6082-Al 6082 substrates, (c) Al 6082-Al 5083 substrates

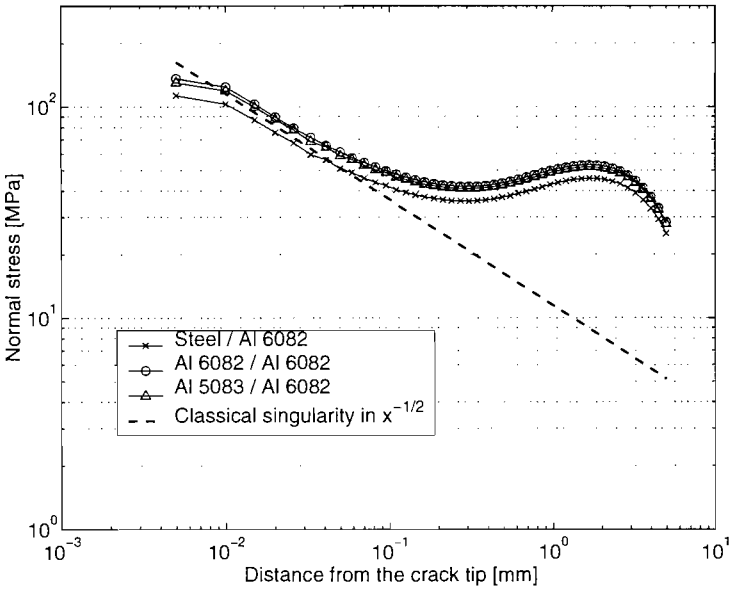

Figure 6.24: Stress profile ahead of the crack tip of DCB specimens for different combinations of adherends; F= 1370 N

Chapter 7

Strength of structural joints

7.1 Introduction

During the service life of a ship, wave and wind pressure induce tension, compression and bending forces in the structure. Regulation bodies such as Det Norske Veritas (DNV 2001) define ultimate loading conditions that ship structures must sustain while in service. So far, adhesive joints have been designed to transfer load by compression and shear usually joining thin plates and this technology is well established. However in the context of the marine industry, the structures and the plating used could be radically different and so would the joint designs. Hence, the aim of this Chapter is to investigate the viability of adhesive bonding concept for large joints in a marine environment through the study of structural joints based on joints designed for the aluminium superstructure presented in Chapter 3. It will present work carried out to characterise the tensile behaviour of structural joints, by experimental test programme and explain their failure mechanisms through a finite element analysis.

Having previously presented the local approach and characterised the adhesive system in terms of strength and fracture toughness, this chapter presents the third step of the study. Once this local approach was done, the following step is to assess the strength of more complex joints that can be used in a ship. The objective of this chapter is to characterise the tensile and flexural strength of structural joints, considered damage free, through an experimental test programme and explain its failure mechanisms through a finite element analysis.

7.2 Geometries and materials

7.2.1 Joint design

Two different bonded joint designs were proposed as possible fastening configuration for the superstructure Figure 3.1. They are namely, steel-to-aluminium connections and aluminium-to-aluminium connections, respectively named joint A and B. These joints are similar in terms of design as they are extruded box sections adhesively bonded based on a double butt strap configuration.

Joint A is a joint between the deck of the ship and the aluminium framed superstructure as presented in reference (Cantrill et al. 2004) and Figures 3.1 to 3.6 in Chapter 4. It consists of an aluminium box section beam located on a raised steel L section reinforced by an aluminium flat plate as a strap between the the two sections in order to transmit the load by tension/compression and shear. However, for practical reasons (cost and fabrication) it was easier to manufacture and test a simplified design than the original one. Therefore, representative models were produced for testing purposes, Figure 7.1 (a).

The joints were manufactured in 500 mm lengths, and were cut up into 80mm long test sections using a horizontal band saw. The procedure was relatively straightforward with the joint between the two box sections being made before bonding on the straps. The standard procedure for surface preparation and joint spacing was followed.

However, during the grinding of the steel end faces, it was observed that a highly polished surface finish was being produced. This may have contributed to areas of adhesive failure found in the structural tests. The polished surfaces were a result of grinding a hardened surface, most probably produced by the welding of the end assembly.

As the superstructure described in reference (Cantrill et al. 2004) is modular, connection B joins each aluminium-framed module to the other. It is made of two extruded aluminium beams (6082 alloy series) adhesively bonded and reinforced with two aluminium straps (Al 5083 alloy series) so as to be similar to a symmetrical double butt strap joint to transmit the load by shear. Material and geometrical specifications are presented in Figure 7.1 (b).

The bonding procedure for these configurations was similar to the one described above for steel to aluminium connections. In the following, the steel to aluminium connection and the aluminum to aluminium connections will be named joint A and joint B respectively.

7.2.2 Materials

The selected adhesive is a Plexus product named MA 550. It is a two-part methacrylate adhesive designed for structural bonding of thermoplastic, metal and composite assemblies. Tests carried out by Centre Technique d'Arcueil (CTA) (Weitzenböck et al. 2004a) on the bulk adhesive, gave the results presented in Figure 3.3. Although this adhesive is considered as a rigid adhesive with a Young's modulus of 309 MPa, it can be seen that linear portion of the mechanical behaviour is fairly restricted in both tensile and shear mode.

The adherends used are mild steel and aluminium alloys 6082 and 5083 series. The material properties of the adhesive and these adherends are presented in Table 3.1.

7.3 Experimental modelling

The experimental programme was set up in order to assess the tensile strength of the joints and identify their modes of failure in tension. As it has been shown by a numerical analysis of the global superstructure (Jarry, Shenoi, Kapadia & Miao 2004), the joints were likely to undergo tensile loads in a worst-case scenario at the corner end of the structure. Therefore, it was of interest to assess the ultimate tensile strength of the joint to evaluate the safety margin for the bonded structure. Also it was decided to assess the strength of the joint subjected to a constant bending moment in the direction of the extrusion, Figure C.1. These latter tests, though they provided an indication about the failure mode and bending behaviour of the joints, could not be analysed with numerical models in the scope of this study and hence, are only presented in Appendix C.

The specimens A and B were tested on FORTRESS (Flexible Orthogonal Rig for Testing Real Ship and boat Structures designed by Read (Shenoi, Read & Hawkins 1995)) equipped with an hydraulic ram controlled by an 8800 Instron controller. The ram could produce 130 kN at maximum hydraulic pressure and the specific load was aquired via a 250 kN load cell. The displacement of the crosshead was recorded by a Linear Variable Differential Transducer (LVDT). Figure 7.2 give

an overview of the experimental setup.

In terms of mechanical behaviour, the results are presented in Figure 7.3 (a) and (b) and Table 7.2 summarises the tensile stiffness and ultimate tensile load of the specimens tested.

The trend of the load-deflection curves for joints A can be summarised by two distinct behaviours. One where the linear portion is limited in the range of 0 to 2 mm followed by clear non linear region leading to brittle failure. The other one where the linear portion of the curve is extended up to 4 mm and the non-linear region leading to failure is shorter than in the previous case. The tensile behaviours of joints B are presented in Figure 7.3 (b). After a non-linear part due to take up of play, the behaviour of the joint is relatively linear between 0 and 40 kN where onset of non-linearity is observed. After that point, the joint starts to behave in the non-linear domain up to an ultimate load at about 50 kN, followed by a catastrophic failure of the joint. It can be noticed that failure is also not complete because the load level did not reach zero: the joint can still sustain a certain level of load but with a degraded stiffness as indicated in Figure 7.3 (b). Comparing these two sets of joint behaviours, it can seen that joint B presents more consistent results than joint A and that the non-linear domain of joint B is usually more accentuated than for the other one.

Table 7.2 shows that the result of the load at failure for joint A are fairly consistent at about 70 kN. The linear limit is estimated to be at about 30 kN. The average deflection at failure for these joints is about 5.5 mm but with some discrepancies. The results for joint B are also consistent for four specimens whereas a fifth one presents a remarkable lower load to failure that was discarded for the results in Table 7.2, it gives an average ultimate load of about 50 kN. The linear limit is estimated to be at 40 kN. The average deflection at the corresponding failure load is estimated at 4 mm. A the onset of non-linearity. It is clear that joints A are stronger that joints B by almost 30% and the onset of non-linearity occurs earlier for joint A than joint B. The deflection at failure is higher in the case of joint A compared to joint B.

A fair agreement between the estimated averaged stiffness for joints A as shown by Table 7.2, but a common onset of non-linearity was not evident to locate because of the disparity in the behaviour of the joints, Figure 7.3 (a). To estimate the tensile stiffness of the joint, the portion of the curve between 0 and 1mm was considered.

ignoring the initial non-linearity due to the take up of play. With this method, the averaged stiffness was estimated to be 15 kN/mm. For joint B, the same method was considered to obtain the averaged stiffness. The stiffness of four specimens is in good agreement as seen in Figure 7.3 (b), whereas a fifth specimen is slightly stiffer than the others (this one has not been taken into consideration). It is noticeable that joint A has a higher averaged stiffness than joint B. This can be explained by the higher flexural rigidity of the steel-to-aluminium joint.

In terms of locus of failure, all the joints failed consistently in the same pattern as shown in Figures 7.4 (a) and (b). Visual observations also indicate that failure occurred mainly cohesively within the adhesive but alternatively close to the steel or the aluminium adherend, as shown in the Figure 7.4 (b). However, for one of the specimens, failure initiated in the aluminium strap rather than in the corner of the aluminium box and the steel plate. The reason for this difference is that it was observed that the adhesive bond between the aluminium strap and the two boxes was 3 times thicker than the adhesive bond between the steel plate and the aluminium box. A typical mode of failure of joint B can be seen in Figures 7.5 (a) and (b). Some voids can be observed in the bond line but failure mainly occurred close to the adherend, although still in a cohesive mode. Figures 7.4 and 7.5 suggest that failure initiates in the corner ends of the joints and then propagates in perpendicular directions towards the free surface of the strap and along the face of the box sections. In one case of joint B, cracks were observed at the opposite corner of the joint where actual failure was observed, showing a good symmetrical loading. The failure patterns are similar for both joints but it was noticed that joints B failed more consistently close to the adherend.

7.4 Numerical modelling

7.4.1 Finite element details and boundary conditions

In order to clarify the mechanisms of tensile failure of these complex joints, a finite element analysis was carried out using ANSYS package. The model consists of PLANE82 elements from the ANSYS library, they are 2-D 8-Node structural solid elements usually used to model 2-dimensional metallic structure. It is defined by eight nodes having two degrees of freedom at each node: translations in the nodal x- and y- directions (u_x and u_y). The adhesive is isotropic and the analysis carried out assuming plane strain conditions. Indeed, in the superstructure (Cantrill et al. 2004) the x- and y- plane dimensions are considered much smaller than the third one,

justifying the use of plane strain conditions. Figures 7.6 and 7.7 present typical finite element models for these connections.

7.4.2 Convergence analysis

As for the butt strap joint models, the convergence of the results needed to be checked for the structural joints. This analysis was based on the stress in the adhesive bond and particularly close to the corner end of the adherends where stress concentration is likely to occur, according to the experimental results described previously in Section 7.3.

The procedure to obtain an increasing number of nodes was as follows: for a given load, the number of elements along the straps (AB) and along the faces (CD) was increased together with the number of elements through the adhesive and adherend thickness to avoid too high element aspect ratios that would produce suspect results. The results are presented in Figures 7.8 and 7.9.

It can be seen that for deck-to-superstructure joint model the normal and shear stresses reach an asymptotic value after the third iteration corresponding to approximately 20,000 nodes. The unit-to-unit joint model the stresses reach their asymptotic values after 15,000 nodes in the model.

As a result, in both models on which the study will be based, the adhesive layer has 10 elements through the 3 mm thickness in order to investigate the stress in the middle of the bond and close to the interface where failure was shown to occur. In the case of joint A, due to the geometry of the joint itself, the mesh could not be defined regularly all along the adhesive bond, the model has approximately 18,000 nodes. At the corner of the joint, the aspect ratio of the element is 1, whereas along CD the aspect ratio is about 5. In the case of joint B, the aspect ratio is 6 along CD, 1 around the corner and 4 for the elements along the straps, the model has approximately 15,000 nodes.

7.4.3 Tensile stiffness

The first step was to characterise the stiffness of the finite element model and compare it to experimental results to ensure that the model is compatible with the experiments.

The FORTRESS rig on which tests were carried out, was shown to have a certain stiffness that allowed it to deform significantly beyond a certain load level. It is therefore important to take this stiffness into account in the boundary conditions of the finite element model. The experimental procedure to characterise the stiffness of the rig and then the spring element constant was carried out by (Boyd 2005). To measure this stiffness, a steel bar was loaded to a certain level. The deflection between the reaction face and the load cell and the deflection between the two specimen fixings were recorded with transducers while the bar was strain gauged to directly obtain its stiffness. The stiffness constant of the rig was estimated to be 20 kN/mm, the fixtures had a stiffness of 160 kN/mm and the steel bar 3000 kN/mm. Spring elements with the stiffness constant corresponding to the rig were then added to the model of the joint.

The stiffness of the finite element models was obtained by applying 1 mm displacement on one side of the joint and taking the resultant reaction force. Even though the stiffness of the rig was taken into account, the finite element model was still found to be stiffer than the experimental one. For joint A, the stiffness of the finite element model is 17.5 kN/mm whereas the experiment presents an average stiffness of 15.0 kN/mm, Table 7.2. For joint B, the FE results give a stiffness of 16.6 kN/mm to be compared to the averaged 14.2 kN/mm given by the experiment.

7.4.4 Stress profile in the adhesive bond

Prior to focusing on the failure prediction of the joint, it was necessary to carry out a stress analysis in the adhesive layer to find areas where stress concentration was likely to cause failure of the joint.

A direct observation of the specimen geometry and of the test results strongly suggested that failure initiated in one of the corner ends of the box adherends. Also, experimental results have shown that failure in the adhesive bond occurred cohesively close to the adherend, Figures 7.4 and 7.5. Therefore, it was chosen to observe the stress profile in the adhesive bond from both a distance of $\frac{t_a}{10}$ and $\frac{t_a}{2}$, where t_a is the adhesive bond thickness, in order also to characterise the variations of stress through the thickness of the joint at the failure loads 70 kN and 50 kN for joints A and B respectively.

Figure 7.10 presents the tensile stress and the shear stress profiles along the adhesive bond at 70 kN for joints A. The tensile stress is almost constant and close to zero

along CD with significant peaks towards the corner ends of the aluminium box section. It is noticeable that a peak occurs on one side at the corner position whereas on the other side, the main peak occurs 10 mm away from the sharp corner, whereas a secondary one develops at the corner position. Figure 7.11 gives a more precise idea of the tensile stress SX along CD and C'D', ie at two different positions through the adhesive thickness. Figure 7.11 also shows that the peaks of tensile stress varies between 37 MPa and 32 MPa depending on the position through the adhesive bond from which the stress was calculated.

Similarly, the stress profile in the adhesive layer was observed for joint B. The load level was chosen at 50 kN the average failure load, Figure 7.3 (b).Figure 7.12 shows the tensile stress and the shear stress in the adhesive layer close to the adherend: in the strap (along A'B', see Figure 7.7) and the so called vertical adhesive layer between the two extruded aluminium box sections (C'D'). By symmetry, the stress would be the same in the opposite strap of the joint.

The tensile stress is negligible along CD rapidly increasing towards the corner ends and as expected, the peak of stress occurs at the corner end of the joint. Along AB, a small peak is observed at the free surface (at about 10 MPa) and a higher one occurs at the middle of the overlap (at about 17 MPa). The shear stress is constant and much lower than the tensile stress all along the adhesive bonds except at the corner ends where a complex profile is observed.

A comparison between the tensile stress (SX) at $\frac{t_a}{10}$ (along C'D') and the one in the middle of the adhesive layer (CD) ($\frac{t_a}{2}$) is shown in Figure 7.13. The drop of stress magnitude between $\frac{t_a}{10}$ and $\frac{t_a}{2}$ is not significant: from 38 MPa to 37 MPa.

7.5 Discussion

7.5.1 Stiffness of the specimens

Figures 7.3 (a) and (b) show that the average stiffness deduced from the experiments and the stiffness found via the finite element model are in reasonably good agreement. The numerical models of joints A and B are respectively 14% and 6.5% stiffer than the experimental models. For joint A, the higher difference between the models can be explained by the adhesive thickness.

The experimental results have shown that the stiffness of the steel-to-aluminium

joint is higher than the one of the aluminium joint. Numerical models show different stiffnesses (17.5 and 16.6 kN/mm respectively) that are higher than the experimental models which is a common feature for finite element model as the bond is ideal. Comparing the increase of stiffness between the aluminium joint and the steel-to-aluminum in both experimental and numerical model, it is found that it is of 5 % for both models.

7.5.2 Stress profile in the adhesive

As far as joint A is concerned, Figure 7.10 shows that the normal stress along A'B' presents significant variations around the junction between the strap and the two box sections. Tensile stress is observed towards the free surface of the joint: as the strap slightly bends and the box tends to squeeze, the adhesive will stretch with the combination of these two effects. However, compressive stress occurs at 80 mm and 95-100 mm: at the junction between the strap, the aluminium and the steel boxes, the load path encounters stiffer adherends with the transverse faces of the aluminium and the steel boxes, the adhesive is then compressed between the strap and the box frame. The tensile stress observed around 90 mm is likely to be due to a combination of the stretching of the joint and the strap that tends to retains the adhesive that is more bulky.

Along C'D' and CD, the tensile stress is almost constant and close to zero because of load equilibrium. The peaks of stress near the corners are due to the geometry of the joint: similar profile are found in double strap joints. (Adams et al. 1997, Mitra & Ghosh 1995). For joint B, similar explanations can be given for the stress profile along both adhesive layers. However, due to the geometry and the symmetry of joint, more conventional profiles are observed.

Figures 7.10 and 7.12 show that joints A and B present similar peak of stress at similar location in the adhesive bond at respectively 70 kN and 50 kN. Hence, it can be deduced that as the adhesive thicknesses are the same, it is the adherend stiffness (via its thickness) that influences the stress in the bond. Indeed, joint A was made with thicker and stiffer adherends than joint B (twice as thick, as mentioned in Figure 7.1), therefore it could transfer more loads than the other with lower stress in the adhesive.

7.5.3 Comparison between FEA and experiments

7.5.3.1 Background

As stated at the beginning of the section, according to the experimental failure of the specimens, it was assumed that failure initiated at the corner of the joint due to the sharp angle of the box adherend. In terms of failure location and initiation, the finite element and experimental models seem to be in good agreement for both joint designs: they showed stress concentration at a similar location and predict a failure due to tensile stress.

The magnitude of the stress at the experimental failure load, does not reflect a realistic level at failure. Indeed, the ultimate tensile stress to failure for the bulk adhesive material was recorded to be at about 14 MPa, the maximum tensile stress shown by the finite element model is 36 MPa, which is far beyond the experimental tensile adhesive failure. The reason being that in reality, the adhesive yields before failure that decreases the level of stress: this is not taken into account when linear finite element analysis is considered. Several researchers have tried to tackle this problem introducing different adhesive failure criteria. Authors such as (Adams & Peppiatt 1974) and (Harris & Adams 1984) suggested a criterion based on the maximum principal stress whereas (Hart-Smith 1973) suggested a criterion based on the maximum normal stress. These criteria can only be applied to simple joints like single lap joints. A criterion such as the Von Mises one could be applied but with a certain inaccuracy as it does not take into account the difference in the tensile and compressive yield strength and the dependence of the yielding on the hydrostatic component of the applied stress that occurs in the case of polymer materials. Hence (Raghava, Cadell & Yeh 1973) proposed a criterion based on a modified Von Mises yielding criterion taking into account the conditions stated above.

However, Brede *et al* cited by (Weitzenböck et al. 2004a) considered that in a shipyard environment, these criteria could be difficult to implement with in-house or commercial finite element codes. They therefore developed a pragmatic approach based on a combination of experimental and numerical results that claimed good results. The method is employed here and described in Appendix D.

7.5.3.2 Application

In the present study, the simple joint geometry considered is the butt strap joint with 3 mm adhesive thickness which analysis was presented in Chapter 5. This 3

mm adhesive joint was considered because it has a similar adhesive thickness as the one specified for the steel-to-aluminium connection.

The line of length $d = 3$ mm was defined from the middle node of the adhesive bondline, Figure 5.16. The different stress components calculated and averaged along this line are summarised in Table 7.3 in the first row. Then failure occurs if any of the shear, tensile stress or principal and equivalent stress exceeds 26.2 MPa, 17.31 MPa, 57.7 MPa or 37.29 MPa respectively. This ensures a conservative criterion as averaged values are considered in the simple design while maximum values are considered for the complex design. Also, it should be noticed that the stresses considered for that criterion will not be reached in the real structure as plastic flow develops in the adhesive.

The most critical area was identified to be the bottom corner end in the joint, therefore this area will be considered for the design failure load. Table 7.3 records the maximum stresses along the line considered. At 70 kN, the maximum tensile SX stress is 36 MPa which is higher than the design value of 26.21 MPa shown in Table 7.3. The same procedure was followed again for 60 kN and 50 kN: at 60 kN the tensile stress is still above the design criterion whilst at 50 kN the maximum tensile SX stress is found to be 26 MPa. This is the first parameter to reach its critical value, before the shear or principal stress.

For the joint B, the different stress components computed and averaged along this line are summarised in the first row of Table 7.4. Earlier, the most critical area was also identified to be the corner end in the joint, therefore this area is also considered for the design failure load. Numerically, it was found that at 53 kN, the maximum tensile SX stress was 40.1 MPa which is higher than the normal stress design value 26.21 MPa, Table 7.3. The same procedure was followed again for 40 kN and 35 kN: at 40 kN the tensile stress is still above the design criterion whilst at 35 kN the maximum tensile SX stress is found to be 26.1 MPa. This is the first parameter to reach its critical value (before, the shear or principal stress). Table 7.3 summarises the different critical stress values in both the local joint design and the structural joint designs mentioned above.

7.6 Conclusion

This chapter investigated the behaviour of structural joints made with aluminium only and aluminium and steel that could be used in a high speed craft, through a strength approach. Experimental and numerical results gave some insight into the mode of failure and the failure mechanisms of box section joint designs made with this combination of materials.

From this study, the following conclusions can be drawn:

- Tensile test results showed cohesive failure in the adhesive close to one adherend and suggested that stress concentrations occurred at the corners of the joints. Finite element analysis showed that failure of the joint is mainly due to tensile stress rather than shear stress due to the large faces of the butt.
- The thickness of adherends influences the tensile strength via the state of stress in the adhesive. Although, joint B presented a larger bond thickness than joint A overall, an average of 30 % loss of strength was observed between these two joints.
- Influence of the position in the adhesive layer on the stress magnitude, showed that it only affects the stress values at the corner ends, ie at singularity points.
- An empirical failure criterion was applied that provided conservative results useful for the design of complex bonded structures. It showed that failure of the joint was due to tensile stress.

Tables

Joint	t_1	t_2	t_3	t_4	t_5	t_6	t_7	t_8
A	3.3 ±0.2	2.6 ±0.1	2.6 ±0.2	2.7 ±0.4	2.5 ±0.5	2.7 ±0.2	1.9 ±0.3	3.4 ±0.4
B	2.3 ±0.1	2.2 ±0.2	2.1 ±0.2	2.5 ±0.2	2.8 ±0.3	2.9 ±0.2	–	–

Table 7.1: Average dimensions of adhesive bond at different locations. t_1 to t_8 refer to Figure 7.1

	Ultimate load [kN]	Average stiffness [kN/mm]	FE stiffness [kN/mm]
Deck to superstructure	71.6 ± 2.4	15.0 ± 1.2	17.5
Unit to unit	51.1 ± 2.6	14.2 ± 0.8	16.6

Table 7.2: Average ultimate tensile strength and stiffness of structural joints

	Mean SY	Mean SXY	Mean S1	Mean SEQV	Max SY (SX)	Max SXY	Max S1	Max SEQV
Butt strap 3 mm	**26.2**	17.3	57.7	37.3				
Steel to aluminium connection: 70 kN					36.7	4.0	38.1	20.8
Steel to aluminium connection: 60 kN					32.2	3.5	33.1	16.9
Steel to aluminium connection: 50 kN					**26.0**	2.9	27.1	14.8

Table 7.3: Stress values for failure criterion in steel to aluminium connection (all values in MPa)

	Mean SY	Mean SXY	Mean S1	Mean SEQV	Max SY (SX)	Max SXY	Max S1	Max SEQV
Butt strap 3 mm	**26.21**	17.31	57.70	37.29				
Aluminium to aluminium connection: 53 kN					40.11	9.96	44.00	21.48
Aluminium to aluminium connection: 40 kN					29.88	7.42	32.77	16.00
Aluminium to aluminium connection: 35 kN					**26.14**	6.49	28.67	14.00

Table 7.4: Average and maximum stress values for failure criterion in aluminium to aluminium connection (all values in MPa)

Figures

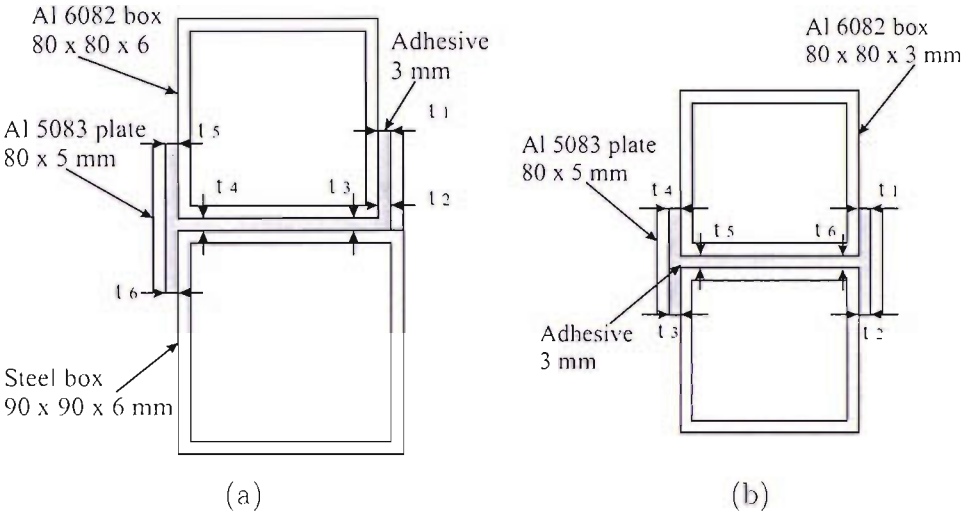

Figure 7.1: Sketch of structural joint specimens: (a) Steel to aluminium connections (joint A). (b) Aluminium to aluminium connection (joint B): The sketch is not to scale, dimensions showed are nominal ones. t_1 to t_6 refer to Table 7.1.

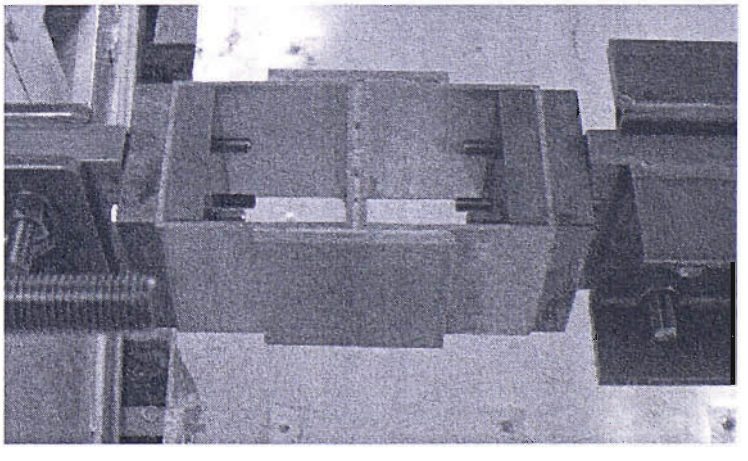

Figure 7.2: Experimental setup for structural joints test

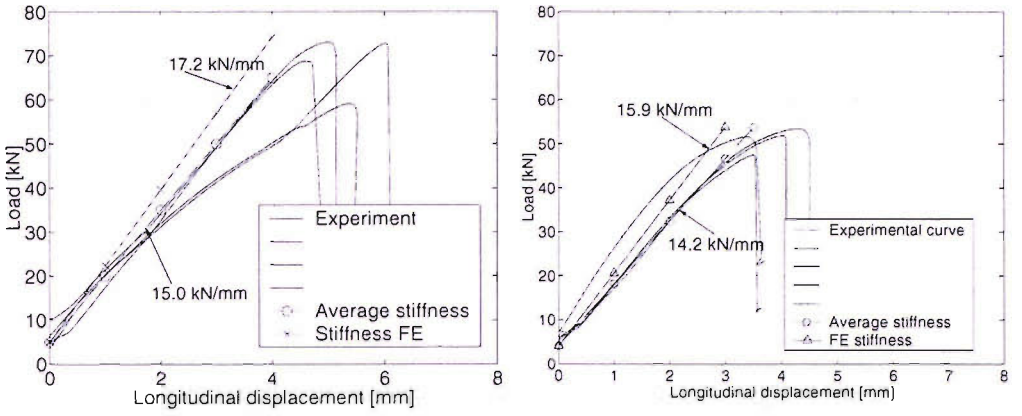

(a) (b)

Figure 7.3: Tensile behaviour of structural joints: (a) joint A, (b) joint B.

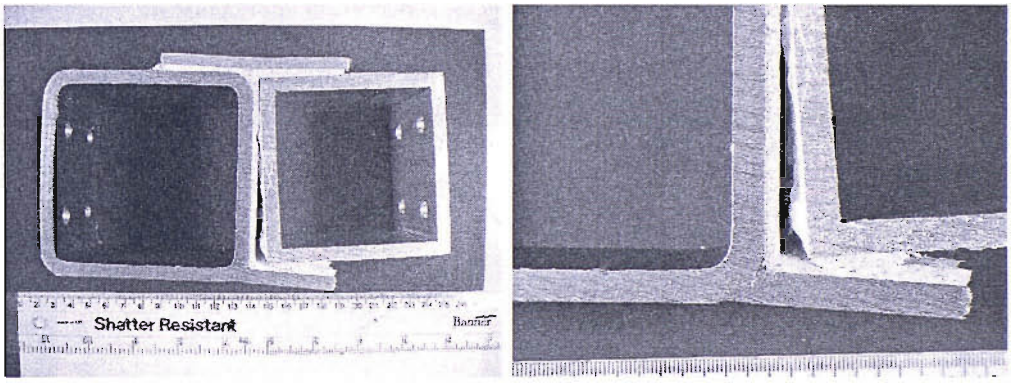

(a) (b)

Figure 7.4: Typical tensile mode of failure of deck to superstructure joint: unaged specimens.

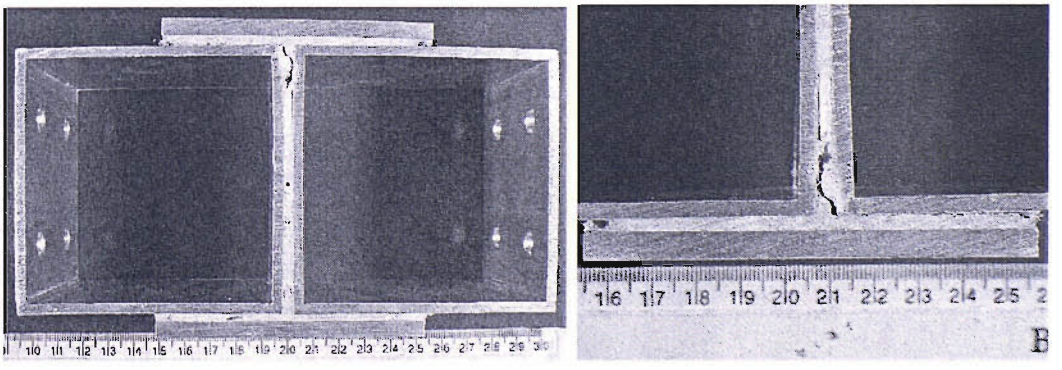

(a) (b)

Figure 7.5: Typical Failure in aluminium to aluminium connection in tension.

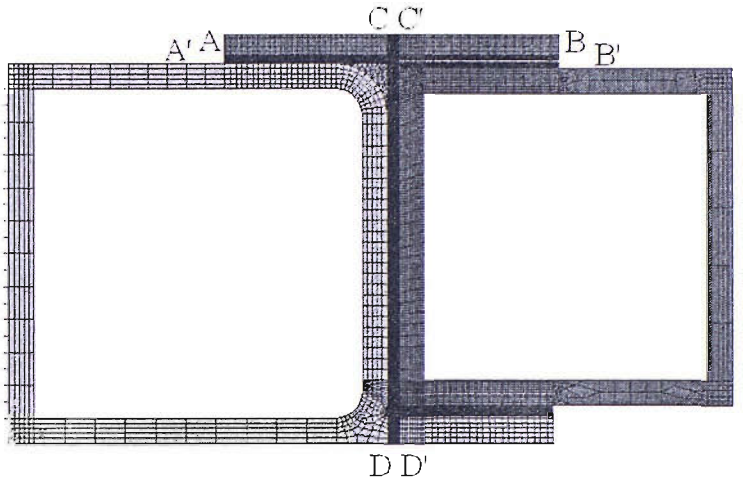

Figure 7.6: Overview of finite element model of steel to aluminium connection

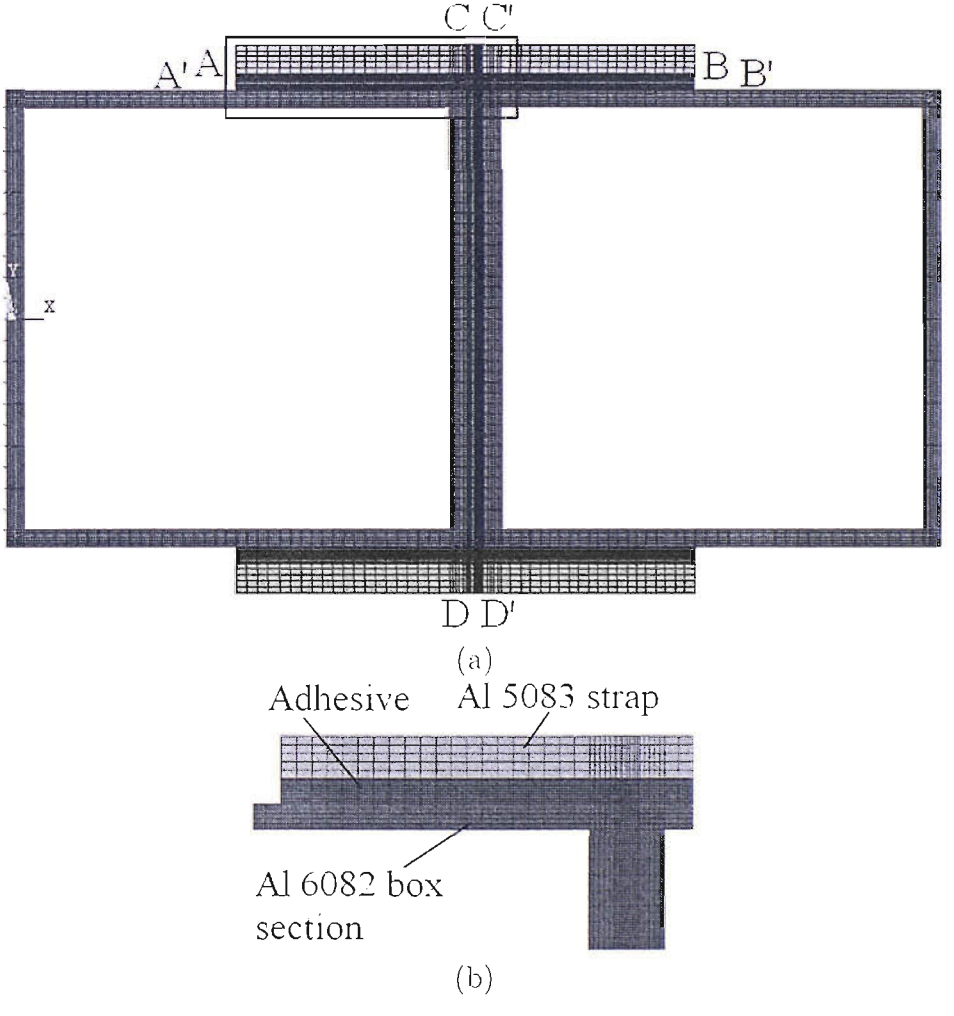

Figure 7.7: Finite element model of aluminium to aluminium connection: (a) global view, (b) view of the adhesive mesh.

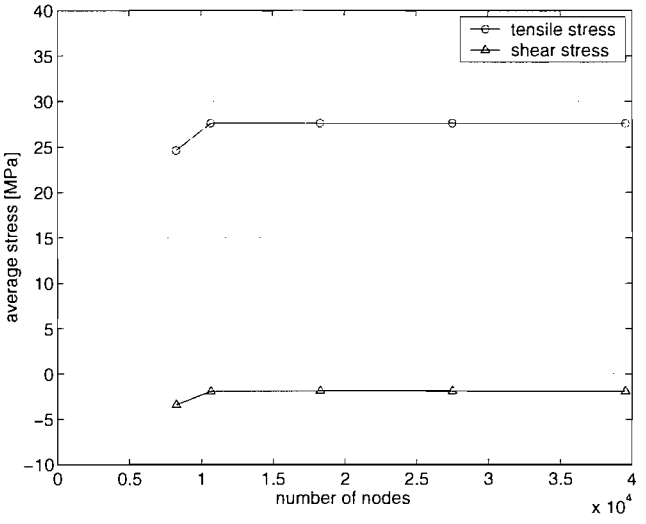

Figure 7.8: Convergence of the stress in the adhesive bond of steel-to-aluminium joint

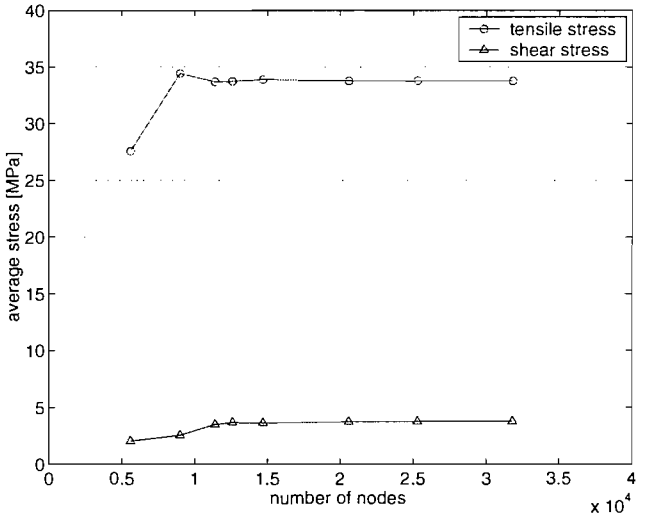

Figure 7.9: Convergence of the stress in the adhesive bond of aluminium-to-aluminum joint

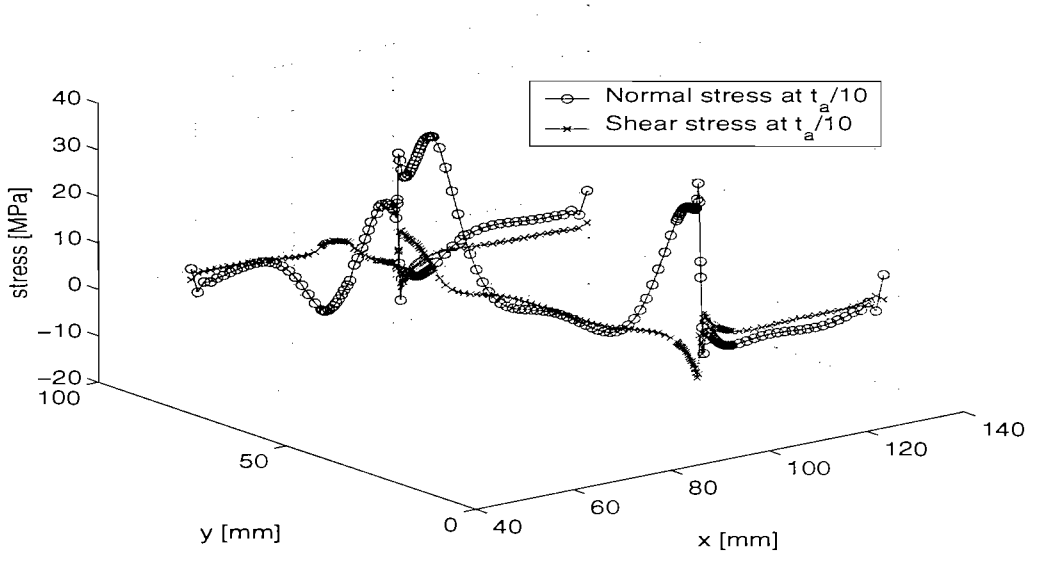

Figure 7.10: Tensile stress in joint A at 70 kN taken at $\frac{t_a}{10}$ from aluminium box section. x- and y- directions refer to x- and y- axis mentioned in Figure 7.6.

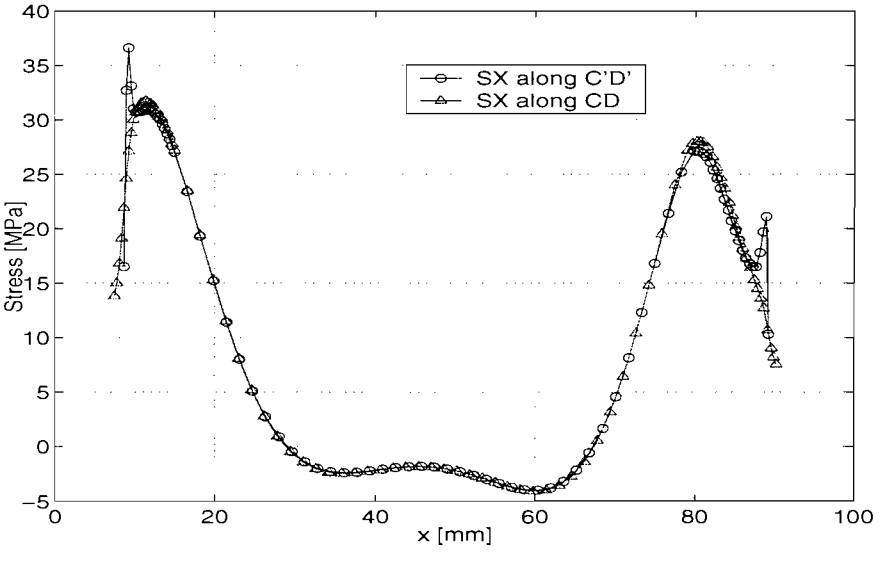

Figure 7.11: Comparison of tensile stress along the adhesive layer along CD and C'D' at 70 kN.

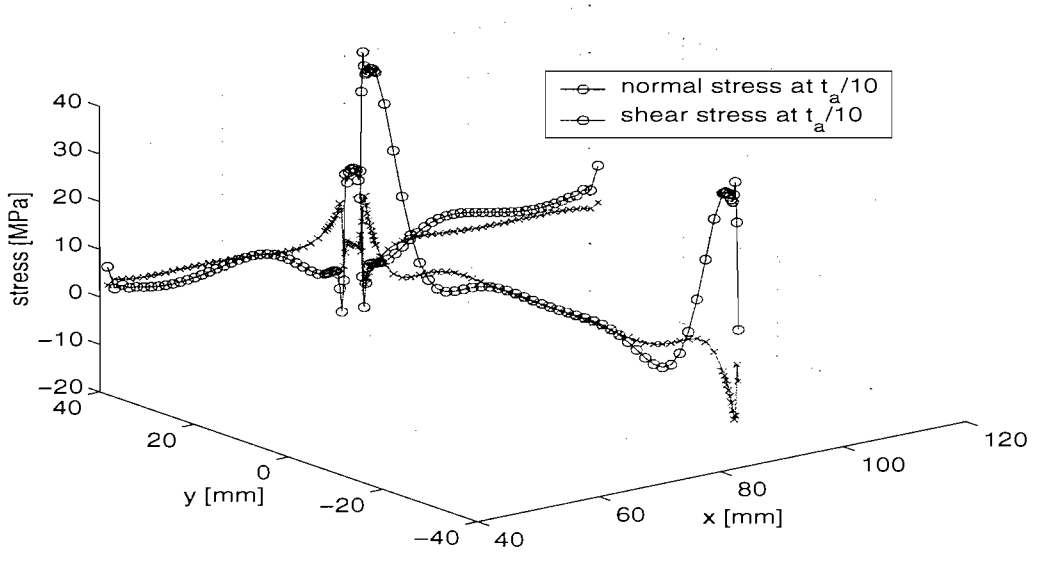

Figure 7.12: Normal stress profile in adhesive layer of joint B, at a distance ($\frac{t_a}{10}$ from adherend) at 50 kN. x- and y- directions refer to x- and y- axis mentioned in Figure 7.7

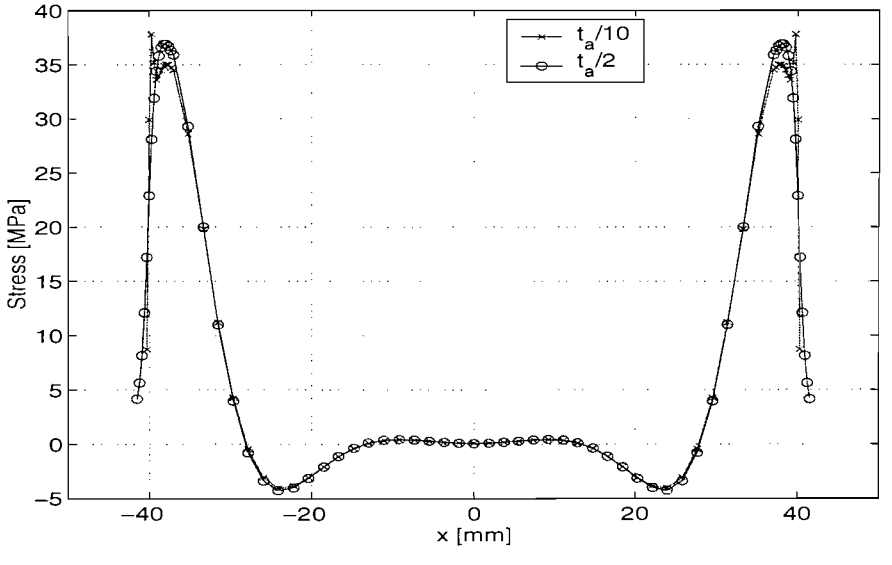

Figure 7.13: Tensile stress in adhesive layer along CD and C'D' in joint B at 50 kN.

Chapter 8

Assessment of defect tolerance criteria in bonded ship structural elements

8.1 Introduction – Objectives

Typical bonding conditions in a shipyard environment, as shown by Figure 8.1 are subjected to dust and other small scraps and can lead to defects included in the bondline during the manufacturing process of the adhesive joints. Also, in Chapter 6 it was shown that even if the joint is made in laboratory conditions and the bondline is potentially defect free, voids occur during the application of the adhesive. The reason being that in reality, intrinsically an adhesive material is not homogeneous and isotropic and in large and thick bonding areas voids would inevitably occur. As an example, Figure 8.2 shows that in some DCB specimens voids could be up to 15 mm of length, and could develop and produce major cracks during in-service conditions that are harmful for the integrity of the structure. In the case of the structural joints studied in Chapter 7, it was therefore important to explore and propose a defect tolerance approach for structural adhesive joints.

The objectives of this chapter are twofold:

- For a series of load levels, and different crack lengths, determine at which critical length the crack would propagate without control,
- For a series of loads and one crack length, investigate the influence of the crack position through the adhesive thickness of the joint.

This will enable the determination of the critical length at which the crack would propagate with instability. This defect tolerance criterion together with Non De-

structive Test (NDT) would provide an important tool to prevent catastrophic failure of the bonded joints.

8.2 Fracture criterion

In Chapter 6 both linear elastic fracture mechanics (LEFM) and non-linear elastic fracture mechanics were used to calculate the mode I fracture toughness G_{Ic} of DCB joints specimens. Due to the simplicity of the joint, three analytical methods were used to directly obtain G_{Ic} while it was obtained via the stress intensity factor K and the contour integral J when FEA was considered. However, it was shown that the results given by the J integral were more conservative than the one given by linear elastic theory and more time consuming to obtain. Moreover, the regime in which the fracture mechanics study is carried out in this chapter is considered to be linear for both the aluminum-to-aluminium joint and the steel-to-aluminium joints. Figures 7.3. Therefore, this particular study is limited to the case of LEFM.

As the joints studied here were too complex to be considered by an analytical solution, the fracture energy G was obtained via a finite element analysis and the stress intensity factor K, which calculation is outlined in Appendix A. The relation between the two parameters is:

$$G = \frac{(1-\nu^2)K^2}{E_a} \tag{8.1}$$

Where E_a and ν are the Young's modulus and the Poisson ratio of the adhesive respectively. The defect will be growing when G will be more than G_{Ic} the critical fracture energy in mode I obtained in Chapter 6. The fracture criterion used for the steel-to-aluminum connection will be the lowest fracture toughness value of the steel-to-aluminium DCB specimens. G_{Ic} = 1693 J/m^2. The fracture criterion for the aluminium-to-aluminium connection will be the fracture toughness obtained for Al 6082-Al 6082 DCB combination G_{Ic} = 1678 J/m^2.

It is important to notice that the fracture toughness derived in Chapter 6 is only valid for joints with 1 mm adhesive thickness. The assumption that those experimental values would be the same for thicker adhesive bonds (typically 3 mm as specified for the design of the structural joints) can be argued. Indeed, conflicting results were observed and discussed concerning the rise of fracture toughness with adhesive thickness that was found difficult to predict with a simple law (Kinloch & Shaw 1981, Daghyani et al. 1995, Yan et al. 2001a); this will be discussed in Section

8.5. Hence, in order to have a relevant mean of comparison between the fracture energy developed by the crack of a structural joint and the data from Chapter 6, the joints were analysed for both 1 and 3 mm adhesive bond.

Also the study will only focus on damage solely due to mode I fracture. However, it will be briefly outlined that this is not the only mode that occurs during the fracture process in this complex joint design.

8.3 Finite element details

8.3.1 Geometry and material

The geometries of the joints are the same as those presented for the strength behaviour of the structural joints in Chapter 7. It has been adapted in order to include a region where a crack is embedded. Figures 8.3 to 8.5. This region is modelled with six-noded triangular elements that have their midside node at the quarter point and are suitable to model singularities (Ansys 2002). These elements could be easily connected to 8-noded quadrangular elements used elsewhere in the model.

As for the strength approach study, the materials (adhesive and metals) are considered to have linear properties, listed in Table 3.1 and to be homogeneous and isotropic. Plane strain conditions are assumed as the height and width dimensions (x- and y- directions respectively) are much smaller than the depth of the joints.

During the analysis, it was observed that the crack faces at the left hand side were crossing each other: the vertical (-y) displacements of some nodes of the bottom face were greater than the displacement of nodes from the top face. This singularity is not physically possible and was discussed by (Phillips, Shenoi & Moss 1999) in the case of fracture mechanics applied to T-joints. In this study, the method used to overcome the problem was to include gap elements between the nodes that initially crossed each other: these elements have a certain stiffness in compression but not in tension. The element does not affect the system while it is in tension but prevent any situation of interpenetration of elements. To make sure that these elements artificially inserted at the crack faces did not affect the post-processing results, the compatibility of these elements with the model was checked. They were shown not to significantly affect the value of the fracture energy: for example, with a crack length of 50 mm, G = 721 J/m^2 without gap element, whereas G = 719 J/m^2 with gap elements, which represent an acceptable 2.8% difference in the results.

8.3.2 Loads and boundary conditions

Four different load levels were considered for the aluminium-to-aluminium connection and three for the steel-to-aluminium connection. In the case of the aluminium-to-aluminium connection they are: 20, 30, 35 and 40 kN. In the case of the steel-to-aluminium connection, they are: 30, 40 and 50 kN. These levels were chosen because they remain in the linear domain of the joint behaviours and are sufficiently high to assume that a crack would be likely to propagate at this level.

In terms of boundary conditions, each joint is rigidly fixed on one side following the same conditions presented in Chapter 7.

8.3.3 Position and length of the crack

In Chapter 7 the experimental programme and the strength analysis of the structural elements have identified the stress concentration areas to be close to the corner end of the joints, which is a singularity in itself. Therefore these areas are prone to crack development and propagation and the crack model was positioned with one of its tips positioned where the tensile stress is maximum. This tip remained at its position throughout the sensitivity analysis whilst the opposite crack tip changed with the length of the crack.

Four different crack lengths were considered, namely: 5, 10, 15 and 20 mm. These were chosen because it was reasonable to assume that such length of void would occur during the manufacturing process. Indeed, according to observations made after the different tests on butt strap joints, structural joints and DCB specimens, large voids were sometimes spotted. Figure 8.2 shows the type of voids that can be encountered during the application of the adhesive. Such voids are likely to generate cracks that could propagate in extreme conditions.

8.3.4 Mesh sensitivity analysis

Like the previous analysis on local and structural joint models, a sensitivity of the results to the mesh density was carried out to check the convergence of the model. The analysis was done for a single set of (load : crack length) values for each joint design the crack length being the larger one to ensure that the model would converge even for smaller cracks. Tables 8.1 and 8.2 present an summary of the variation of fracture energy of the cracked joints with the density of the mesh. It can be seen that the convergence is obtained each time for a model with approximately 27 000

nodes.

8.4 Parametric analysis

This analysis will enable the observation of the sensitivity of the fracture energy to the variation of different parameters such as the length of the crack, the position of the crack tip through the thickness of the adhesive and the adhesive thickness of both joints.

The influence of adhesive thickness in the fracture energy of the joint was particularly important to observe because of the lack of experimental data. Indeed, as mentioned in Section 8.2 conflicting results were obtained with regards to whether an optimum adhesive bond (ie a maximum fracture energy for a given thickness) can be reached for the fracture toughness.

8.4.1 Steel-to-aluminium connection

8.4.1.1 Variations of crack length

The energy release rate at the crack tip close to the adherend corner was calculated for a crack placed 0.5 mm away from the aluminium box adherend, ie very close to the interface. Figure 8.6 shows the variations of the fracture toughness at the crack tip of a steel to aluminium connection for different load values. The critical value of the fracture toughness for the adhesive is assumed to be 1693 J/m^2, Table 6.4.

It can be seen that the energy release rate of the crack increases with increasing crack length and increasing load. According to the figure, the critical fracture energy is reached for a crack length of 19 mm at 20 kN, 10.5 mm at 30 kN and 6 mm at 40 kN. Beyond these lengths, the crack is likely to propagate in the adhesive layer if it is occured 0.5 mm away from the aluminium box adherend.

8.4.1.2 Variations of crack position

A crack of constant length of 5 mm was inserted in the adhesive bond and the energy release rate was calculated for different positions through the thickness of the bondline from the middle of the adhesive layer (1.5 mm) to the interface with the aluminium adherend (2.5 mm). Figure 8.7 shows the variation of the critical fracture energy at the crack tip with the position of the crack.

The fracture energy increases with increasing load and also increases as the crack gets closer to the adherend interface (increasing "crack position"). In this particular case (a crack length of 5 mm), it can be seen that the crack is not likely to propagate at any load level between 20 and 40 kN as the value of the srain energy release rate remains below the fracture toughness value.

Table 8.3 presents the stress intensity factors obtained for modes I and II and the corresponding ratios for different crack positions through the adhesive bond. It can be seen that this ratio varies between 10 and 63. As the fracture energy varies with the square of the stress intensity factor (Equation A.17, Appendix A), this ratio increases in the same manner. Hence it can be seen that mode II fracture energy at the crack tip is more than a 100 times less than mode I fracture energy at this location.

8.4.1.3 Variations of adhesive thickness

The variation of fracture energy at the tip of a crack was observed for joints with 1 and 3 mm adhesive bond thickness respectively. The model with 1 mm bond ensures a relevant comparison with the experimental data obtained in Chapter 6 while the model with a 3 mm adhesive thickness enables a comparison with the latter.

Figure 8.8 shows the variation of fracture energy for a crack embeded in the adhesive bond. The crack is positioned along the middle of the adhesive layer and the tip at the point where the stress is maximum (see Chapter 7 Figure 7.11). Hence, it was possible to compare this value for different adhesive thicknesses.

Generally speaking, it can be observed that the level of fracture energy is higher for the joint with the 3 mm bond than for the 1 mm bond. More specifically, the energy increases almost linearly between 5 and 20 mm for a 3 mm joint whereas for the 1 mm adhesive joint this increase is more progressive.

8.4.2 Aluminium-to-aluminium connection

8.4.2.1 Variations of crack length

A similar procedure to the steel-to-aluminium connection was carried out to calculate the fracture energy at the crack tip inserted in the adhesive bond of joint. The energy release rate was calculated for a crack placed 0.5 mm away from one of the aluminium box adherends, ie very close to the interface. Figure 8.9 shows the

variations of the fracture toughness at the crack tip of a aluminum-to-aluminium connection for different load values. The critical value of the fracture toughness for the adhesive is assumed to be 1693 J/m^2.

From Figure 8.9 it can be seen that the energy release rate of the crack increases with increasing crack length and increasing load. According to the figure, the critical fracture energy is not reached for a crack length between 5 mm and 20 mm at 20 kN. However, at 30 kN the critical fracture energy is reached for a crack 6 mm in length and at a higher load, the energy release rate is beyond the the fracture toughness of the adhesive for any crack length above 5 mm. Hence, at 20 kN the crack is not likely to propagate in the range of crack lengths considered and at a given crack positioned 0.5 mm away from the adherend. For any load level above 30 kN, the crack is likely to propagate above a length of 6 mm.

8.4.2.2 Variations of crack position

Like for steel-to-aluminium connection, a crack of constant length of 5 mm was inserted in the adhesive bond and the energy release rate was calculated for different positions through the thickness of the bondline from the middle of the adhesive layer (1.5 mm) to the interface with the aluminium adherend (2.5 mm). By symmetry similar results would be obtained if cracks were inserted under 1.5 mm. Figure 8.10 shows the variation of the critical fracture energy at the crack tip with the position of the crack.

The fracture energy increases with increasing load and also increases while the crack get closer to the adherend interface (increasing "crack position"). In this particular case (a crack length of 5 mm), unlike for the steel-to-aluminium connection it can be seen that the crack is not likely to propagate at 20 and 30 kN as the fracture energy remains below the limit of 1693 J/m^2 for the given crack length. However at 35 kN, the critical fracture energy is reached for a 5 mm crack positioned 0.4 mm away from the middle of the adhesive layer (1.9 mm on the graph). Above 35 kN, the fracture energy is beyond the fracture toughness and the crack is likely to propagate regardless of its position through the adhesive thickness.

Although, the joint is loaded symmetrically in tension, it is likely, because of the corner geometry, that mode II fracture would occur at the crack tip. Hence, both stress intensity factors were recorded for a 5 mm crack length at different positions through the thickness at 30 kN. Table 8.4 shows the results obtained and the ratio

between both stress intensity factors K_I and K_{II}. This ratio varies between 338 and 4, consequently, for the same reason as the one exposed in Section 8.4.1.2 the mode II component of the fracture energy can be neglected compared to the mode I energy in the total fracture energy release rate.

8.4.2.3 Variations of adhesive thickness

For the same reason as for the steel-to-aluminium connection, the variation of fracture energy at the tip of a crack was observed for joints with 1 and 3 mm adhesive bond thickness.

Figure 8.11 shows the variation of fracture energy for a crack embeded in the adhesive bond of joints with 1 and 3 mm thickness respectively. The crack is positioned along the middle of the adhesive layer and the tip at the point where the stress is maximum (see Chapter 7 Figure 7.13).

It is observed that the level of fracture energy is higher for the joint with the 3 mm bond than for the 1 mm bond but much more significantly than in the case of the steel-to-aluminium connection. Between 5 mm and 10 mm, the energy increases sharply while this increase is less pronounced between 10 and 20 mm; this is particularly significant at high load levels.

8.5 Discussion

8.5.1 Influence of adherend stiffness

For a given load, as seen in Chapter 7, the stresses are higher in the aluminium-to-aluminium connection because of the thinner adherend material. This higher internal stress implied a higher fracture energy values at the crack tip. At 40 kN, in the case of steel-to-aluminium connection, the fracture energy goes from 677.44 J/m^2 for a crack of 5 mm to 1750 J/m^2 for a crack of 20 mm. In the case of the aluminium-to-aluminium connection, the fracture energy lies between 2615 J/m^2 and 5666 J/m^2 for the same crack lengths respectively.

8.5.2 Influence of crack length

Generally speaking, it was observed that greater crack lengths gave greater fracture energy values regardless of the joint design. More specifically, for a given load (40 kN for example), the crack propagation will occur sooner (i.e. for smaller crack length)

in the case of aluminium connections than in the case of steel to aluminium connections. Indeed, at 40 kN it was observed that the crack would start to propagate from an 18 mm crack length in the steel to aluminium connection, Figure 8.6, whereas it was likely to propagate for a crack smaller than 5 mm for aluminium-to-aluminium connecitons, Figure 8.9.

8.5.3 Influence of crack position

The crack position through the thickness of the adhesive bond was shown to have some influence on the value of the fracture energy at the tip of the crack but less than the crack length has. Indeed, the further the position from the corner singularity the lower the stress. Hence, for both joint designs, cracks inserted close to the interface with the aluminium, (i.e. the tip is close to the corner of the box section) produced higher fracture energy value than cracks inserted in the middle of the adhesive layer.

The influence of the crack position on the mode II fracture energy was analysed. It was shown that for each design, the closer the crack tip to the corner, the smaller the difference between the stress intensity factors K_I and K_{II}. However, Tables 8.3 and 8.4 show that these $\frac{K_I}{K_{II}}$ ratios do not followed the same trend. In the case of the steel-to-aluminium connection the ratio is comprised between 10 and 63, whereas in the case of the aluminium-to-aluminum connection, it is comprised between 4 and 338. In the case of the aluminium joint, the very high ratio found when the crack is inserted close to the middle of the adhesive layer is explained by the symmetry of the joint and the type of loading. Indeed, the perfect symmetry of the double butt strap joint implies the shear stress to be zero in the middle of the adhesive layer leading to pure mode I fracture without any mode II component. As the crack get closer to the corner singularity, mode II fracture energy occurs as shear appears due to the effect of the local geometry. In the case of the steel-to-aluminium joint, this phenomenon does not occur, because the joint is not symmetric and shear inevitably occurs, leading to a small mode II fracture energy at the crack tip. However, it should be noticed that this mode II component is negligible compared to the mode I component.

One of the limitations, in this study, is that the crack is considered straight and to propagate along a straight line. However, in Chapter 6 it was observed, Figure 6.4, that the crack oscillates through the adhesive bond. Indeed, the crack direction depends on the adherend geometry and type of loading. Hence it is dependent on the criterion chosen: if using the mode I fracture criterion (Chen, Dillard, Dillard

& Clarke 2002) the direction of the crack depends on the ratio between mode I and mode II fracture energies. If pure mode I is obtained the crack will propagate in a straight direction, if mixed mode occurs, the crack will oscillate. Figure 7.4(b) to some extend and Figure 7.5(b) more clearly show irregular cracks in the adhesive bond close to the corners of the joint. This suggests that a directionally unstable crack initiates at the corners with a mixed mode fracture and then stabilized in a straight direction close to the adherend/adhesive interface under pure mode I fracture.

8.5.4 Influence of adhesive thickness

It was stated earlier in Section 8.2 that it was likely that the fracture toughness of the adhesive joints changes with adhesive thickness. Indeed, the trend followed by the toughness with increasing adhesive thickness is subject to conflicting results (Chen et al. 2002, Daghyani et al. 1995). However, it is likely that mode I fracture toughness of 3 mm adhesive joints would be higher than the average value of 1693 J/m^2. Taking also into consideration that the method used to calculate the fracture energy gave the lowest values of the fracture toughness (Figures 6.14 and 6.23) compared to analytical solutions, this implies that using data from DCB specimens with a 1 mm adhesive thickness provides a very conservative criteria to predict fracture propagation.

From Figures 8.8 and 8.11 it can clearly be observed that the fracture energy is higher for 3 mm thick adhesive bonds than for 1 mm adhesive bonds. This can be explained in terms of adherend constraints (Kinloch & Shaw 1981, Daghyani et al. 1995): when the adhesive bond is thin there exists a relatively high constraint from the adherends whereas when the bond thickness increases the bond is less constrained. When the bond is thick, the degree of plastic deformation at the crack tip decreases and the energy release rate decreases.

8.6 Conclusion

This chapter has presented a fracture mechanics approach applied to complex joint designs to give an insight into the damage tolerance of these joints investigated for certain crack configurations. The following conclusions can be drawn:

- Areas prone to crack development and propagation are situated close to the corner of the joint where singularities occur.

- Mode I fracture energy was calculated for different crack lengths at different load levels for both joint designs. It was shown that steel-to-aluminium joints were more tolerant to damage than aluminium-to-aluminium joints since larger cracks and higher loads could be sustained without propagation.

- Numerical results suggest that the adhesive thickness of the joint influences the fracture energy developed by the crack as a higher thickness yields to higher fracture energy at the crack tip. Hence, taking the adhesive fracture toughness of 1 mm joint as a fracture criterion represent a conservative criterion that can be used for the failure prediction.

- The influence of the crack position through the thickness was investigated and it was found that the value of the fracture energy could vary from single to double at high load levels.

Tables

Number of nodes	Fracture energy G_I [J/m^2]
11 536	1365
16 145	1368
18 039	1346
19 439	1357
24 282	1360
28 665	1360

Table 8.1: Sensitivity of fracture energy of cracked steel-to-aluminium connection to mesh density

Number of nodes	Fracture energy G_I [J/m^2]
10 205	3872
18 991	3886
22 935	3916
27 731	3927
34 104	3928

Table 8.2: Sensitivity of fracture energy of cracked aluminium-to-aluminium connection to mesh density

Crack position [mm]	1.5	1.75	2.0	2.25	2.5
Mode I SIF K_I [N/m$^{3/2}$]	306010	316460	332210	355300	391480
Mode II SIF K_{II} [N/m$^{3/2}$]	17106	4984	7447	20738	38533
K_I / K_{II}	17.89	63.49	44.61	17.13	10.16

Table 8.3: Stress intensity factor at the crack tip of steel to aluminium connection at 30 kN

Crack position [mm]	1.5	1.75	2.0	2.25	2.5
Mode I SIF K_I [N/m$^{3/2}$]	689570	694470	710400	736120	769120
Mode II SIF K_{II} [N/m$^{3/2}$]	17106	3602	76954	124520	189080
K_I / K_{II}	338.14	192.8	9.23	5.91	4.07

Table 8.4: Stress intensity factor at the crack tip of aluminium-to-aluminium connection at 30 kN

Figures

Figure 8.1: Example of bonding process in shipyard conditions

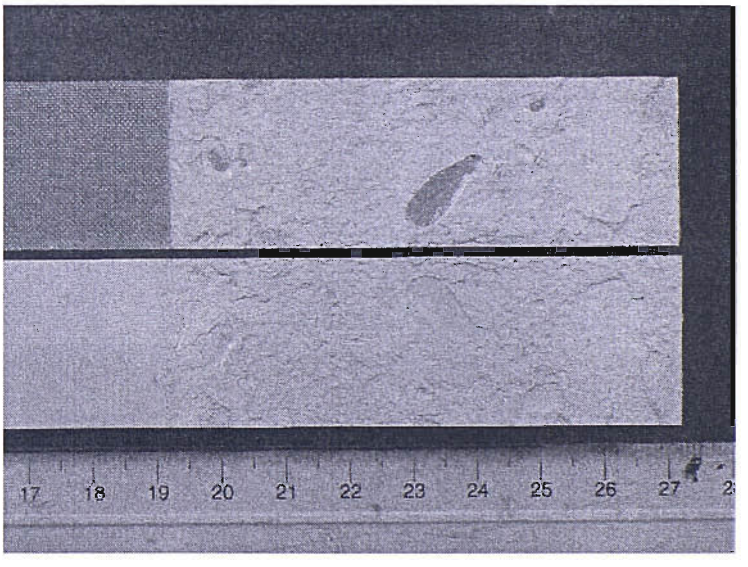

Figure 8.2: Example of voids encountered in the adhesive bond

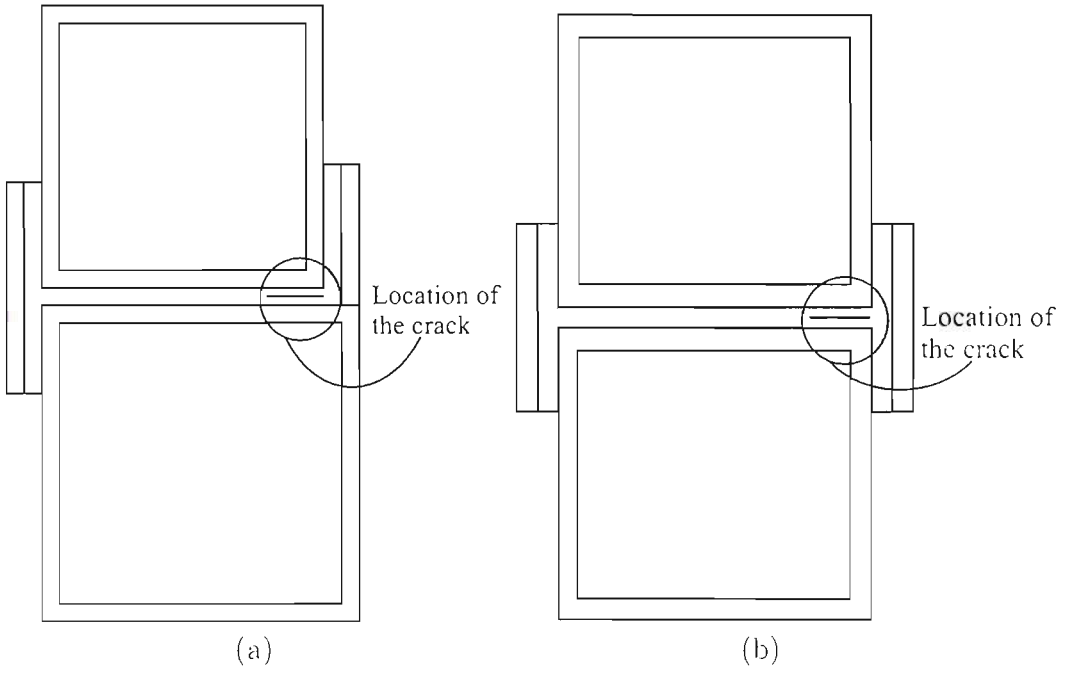

Figure 8.3: Position of the crack inserted in the adhesive bond of structural joints: (a) steel to aluminium connection, (b) aluminium-to-aluminium connection

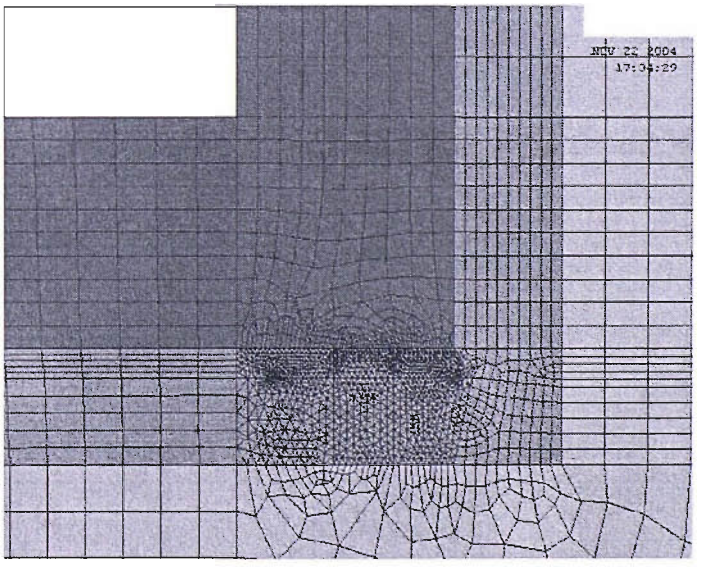

Figure 8.4: Mesh detail of crack inserted in steel-to-aluminium connection

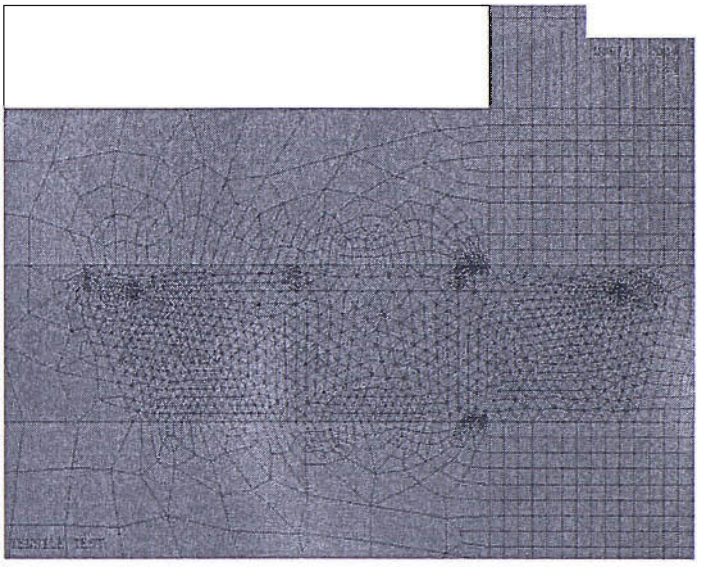

Figure 8.5: Mesh detail of crack inserted in aluminium-to-aluminium connection

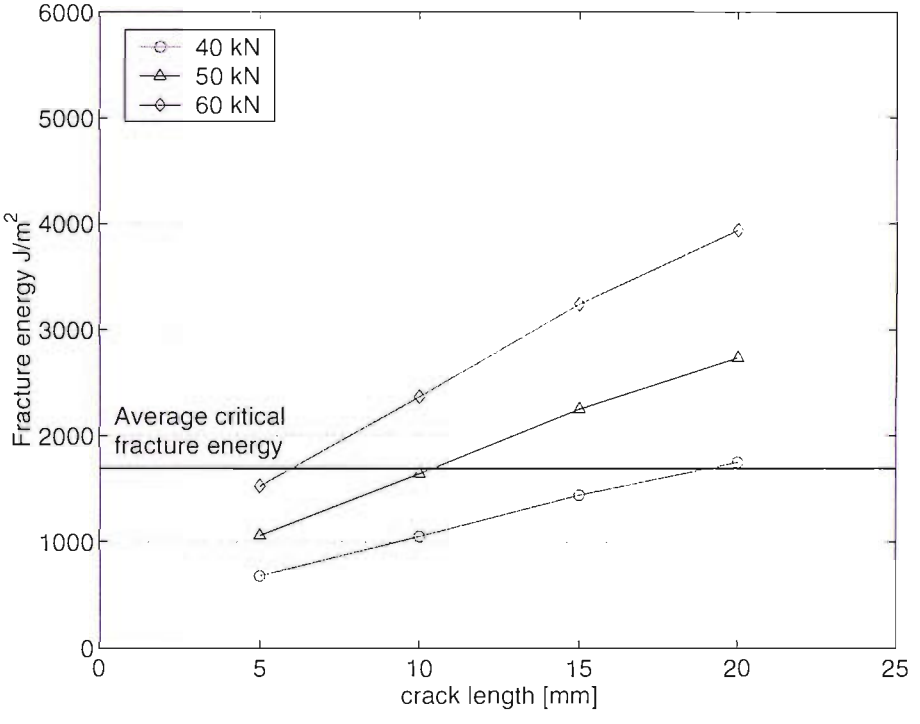

Figure 8.6: Variation of fracture toughness with the length of a crack embedded in the adhesive bond of a steel-to-aluminium connection

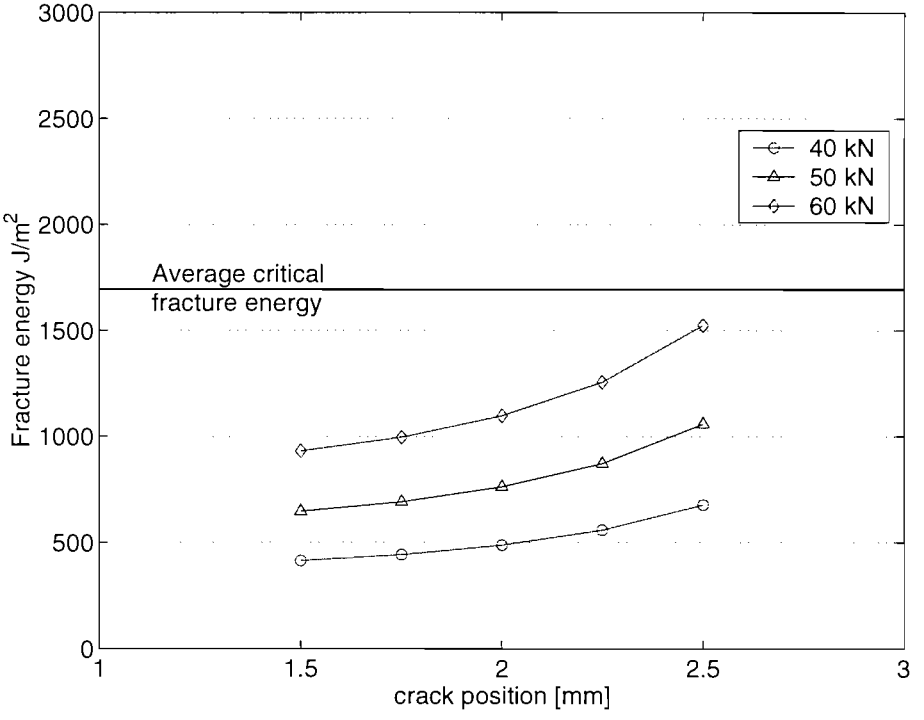

Figure 8.7: Variation of fracture energy with the position of a crack embedded in the adhesive bond of a steel-to-aluminium connection

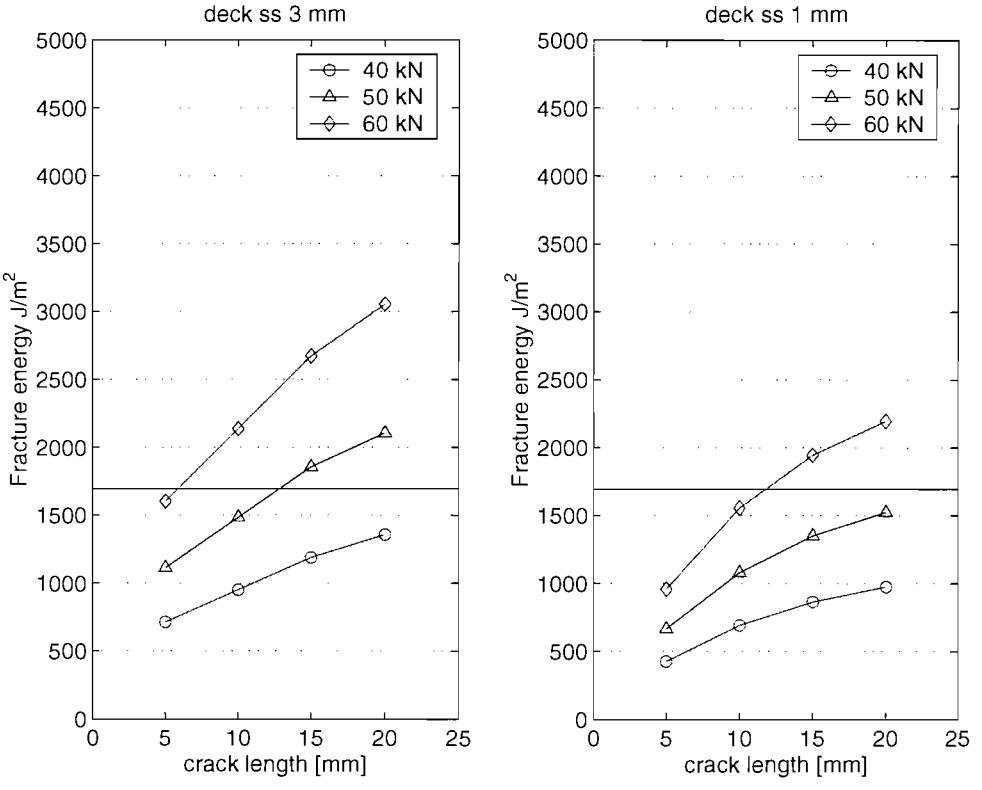

Figure 8.8: Variation of fracture energy with the length of a crack embedded in the adhesive bond of a steel-to-aluminium connection

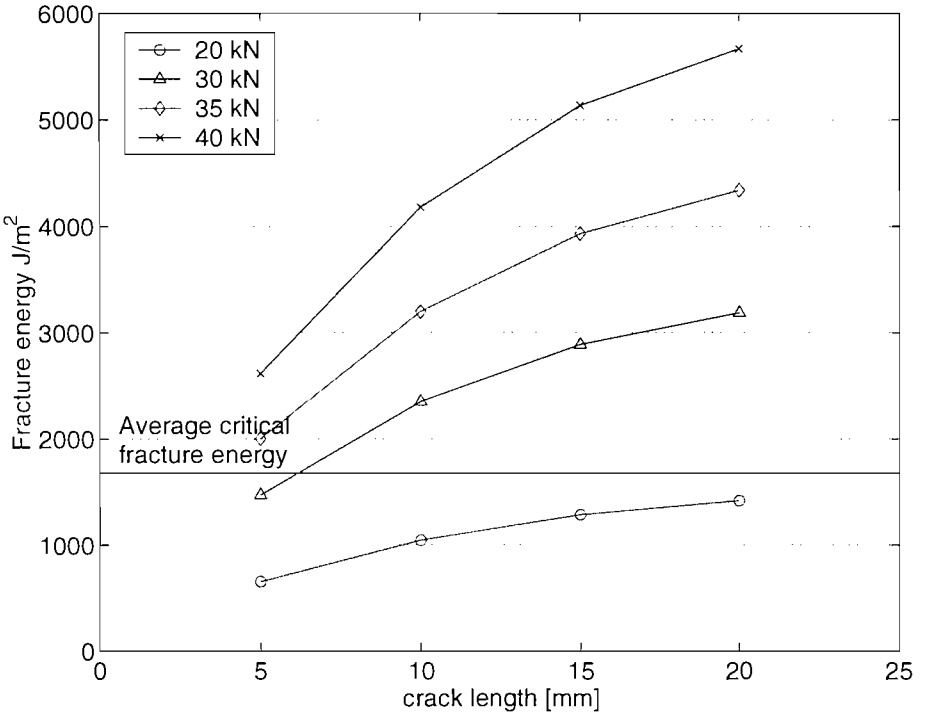

Figure 8.9: Variation of fracture energy with the length of a crack embedded in the adhesive bond of a aluminium-to-aluminium connection

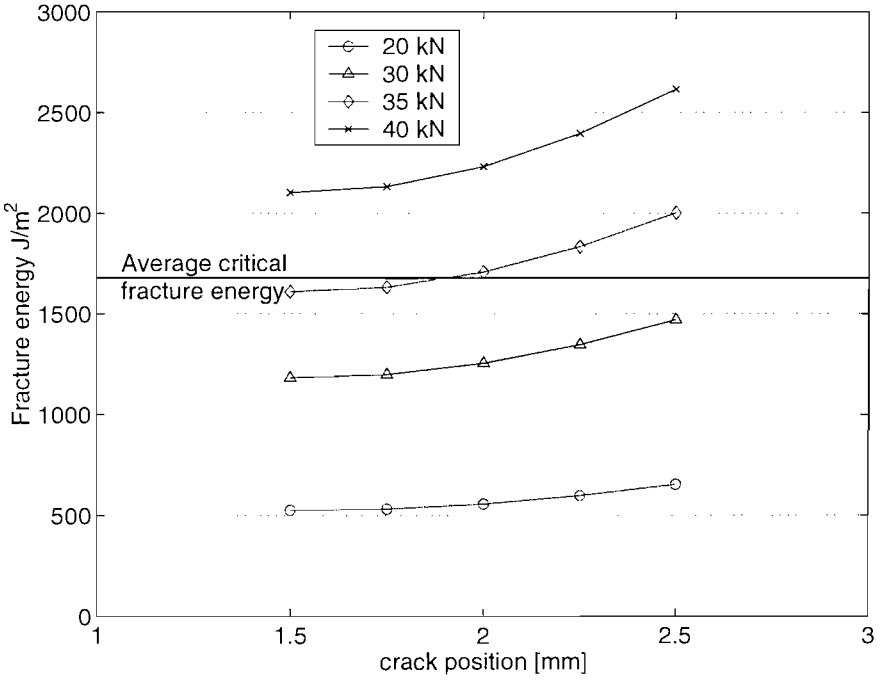

Figure 8.10: Variation of fracture energy with the position of a crack embedded in the adhesive bond of a aluminium-to-aluminium connection. 1.5 mm corresponds to the middle of the adhesive layer

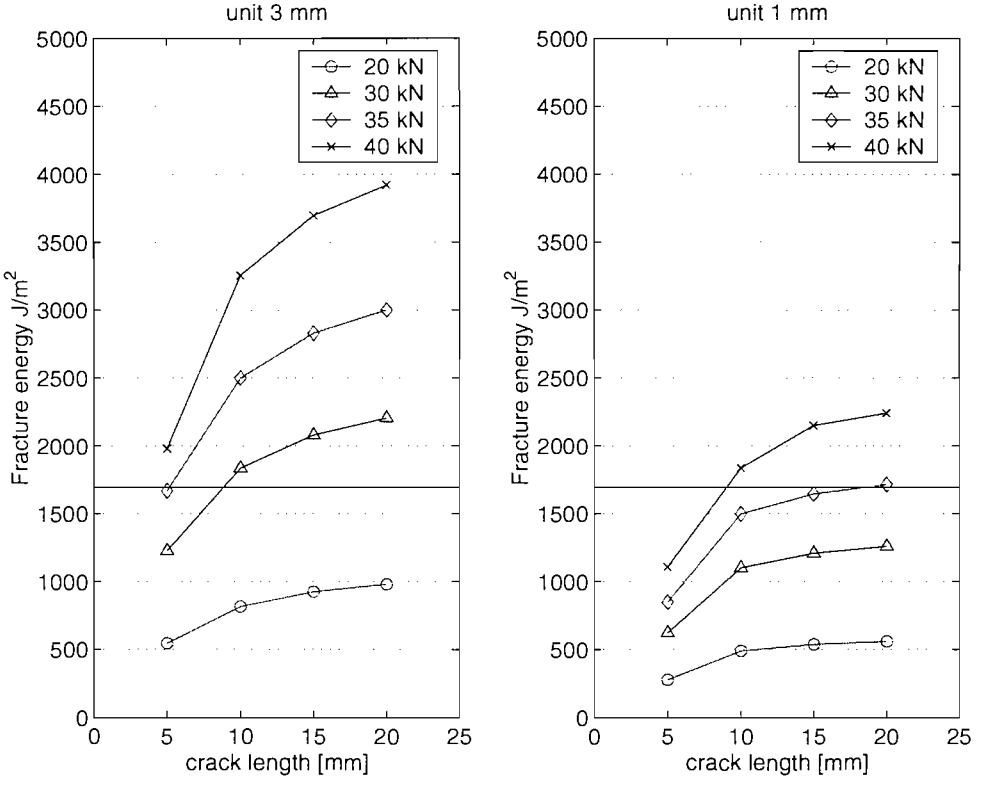

Figure 8.11: Variation of fracture energy with the length of a crack embedded in the adhesive bond of a aluminium-to-aluminium connection

Chapter 9

Discussion

9.1 Introduction

The previous Chapters have focused on the behaviour, analysis of failure and stresses in adhesive joints considered for the fabrication of a marine structure. These represent the different steps of the methodology presented in Chapter 4. The approach adopted for the assessment of the bonded superstructure problem is based on the flowchart presented in Figure 4.1. Although, this method is applied to the particular example of the superstructure of a ship, it could be seen as a more general approach when adhesive bonding is considered for a marine structure.

A similar method to the one presented here was used by (Loscombe 1990) in the study of structural design of SWATH (Small Waterplane Area Twin Hull) ships. In first instance an analytical model was considered to study a box-like ship, then a global FE analysis of the ship was carried out followed by a more precise mesh of local areas. Another study by (Di, Kelly, Chowdhury, Goss & Berkovits 1997) investigated the fatigue behaviour of an aluminium welded catamaran: the global model was used to investigate areas where further local study needed to be done on structural elements leading to a more detailed analysis on some welded connections. An embedding procedure was proposed that allowed an analysis of each sub-model independent of the boundary conditions of the higher level model. Recently (Wang et al. 2004) described a global to local approach using submodelling techniques in order to incorporate adhesive bonding in the design of large structures. Their analysis requires detailed joint analysis to incorporate either hyperelastic or spring elements with equivalent joints stiffness.

The early steps described in the chart were not actually carried out by this author but are presented for the sake of illustration. The results when borrowed from other

authors, are acknowledged subsequently. These steps though very important in the design stage were outlined in Chapter 4, Section 4.2. However, this chapter will mainly focus on the second half of the chart that forms the bulk of the work carried out for this thesis.

9.2 Global structural model

The global finite element model of the superstructure that is used as a case study was prepared by Dr. Shihua Miao during the Bondship project (Bondship 2003). The structural analysis of this superstructure was carried out on the assumption that the load transfer is achieved through the beams and frames. The honeycomb plating, which is bonded to the stiffeners, is assumed not to carry any load. It is assumed that the main deck of the ship is fixed and consequently there is no interaction between the ship hull and the superstructure.

Finite element analysis has been carried out using the ANSYS package. In the package library, element BEAM44 was chosen for the frame structure. BEAM44 is a 3D beam element that has six degrees of freedom at each end, three in translation and three in rotation. The material property of the aluminium sections is assumed to be E = 71 GPa, $\nu = 0.35$.

9.2.1 The Boundary Conditions

The superstructure is rigidly fixed to the main deck of the ship hull since it is assumed that there is no interaction or deformation between the superstructure and the ship hull. Thus every node of the finite element mesh at this location is constrained in the three directions.

9.2.2 The Applied Loads

As a short superstructure (less than 50m) it is not required to withstand bending/compression loads. The main loads experienced by the structure are then: the weight of the structure itself, the weight of the equipment and the personnel and those due to environmental conditions such as the wind pressure.

Two load cases representing two possible worst-case scenari were investigated as an example and presented here:

- One case where the side and bridge pressures are considered (asymmetric case), Figure 9.1,
- one case where the front and bridge pressures are considered (symmetric case), Figure 9.2.

The distribution of the pressure is linear from the bottom to the top of the superstructure. Uniform pressure is also imposed on the bridge floor. These pressures are applied according to DNV rules (DNV 2001).

9.2.3 The Output of FEA

Figure 9.3 shows the nodal load response to side pressure on the port side and Figure 9.4 shows the nodal load response to front pressure at the front of the superstructure. The results are given in the global coordinate of the superstructure and x = 0 corresponds to the origin of the coordinate system, see Figure 9.1. In all directions, a positive value corresponds to a tensile load while a negative value corresponds to a compressive load.

In the first case, it can be seen that the load response is negligible in the x direction due to the loading configuration. The most significant loads found are the forces in the z- direction and in a lesser extend in the y- direction where they are mainly compressive. In the second case, the load response is negligible in the y- direction and constant and compressive in the x- direction due to the loading configuration too. In the z- direction, the load response is mainly compressive along the beam with sharp increase yielding to high tensile loads at the edges of the superstructure. These relatively high tensile loads found at the extremity of the superstructure may be explained by the singularity of the point situated at the corner of the superstructure due to the discontinuity between the horizontal deck and the vertical superstructure (Evans 1983).

This global analysis has shown that loads are significantly high at the junction between the deck and the superstructure and if an adhesive bonding solution is to be considered a local analysis needs to be carried out. This therefore justify both numerical and experimental programme undertaken to investigate failure mode and failure mechanisms of deck-to-superstructure joints and the associated generic topologies.

9.3 Strength based criterion

9.3.1 Study of generic joint

The study of the strength of generic joints was the topic of Chapter 5. This phase essentially enabled an assessment of the adhesive system (adhesive/primer/surface preparation) together with the chosen adherends. A number of issues therefore needed to be considered: the adherend and adhesive materials, the surface preparation and the ageing process. One of the key issues in this study was the high tolerance in the adhesive application due to shipyard condition and the lack of trained workforce. This led indirectly to greater thickness of adhesive bond than specified in the original design (Cantrill et al. 2004) and therefore an investigation was needed to assess the loss of mechanical properties on generic joints.

The extensive experimental programme carried out on butt strap joints has helped to characterise the different modes of failure of the joint under unaged and aged conditions. Small adhesive layers led to cohesive failure while thicker adhesive bonds led to a more hybrid cohesive-adhesive failure. Also, the adhesive system was shown to be suitable for aluminium adherends whereas in the case of steel, a more careful surface preparation was deemed important. In terms of mechanical behaviour, the experimental programme has shown significant loss of strength and stiffness due to adhesive thickness increase. Although the realistic aspects of accelerated ageing of the joint could be argued, it still provides data concerning water ingress in the joint and it was possible to get indication of how the joint is weakened.

In terms of numerical modelling, finite element analysis was preferred to analytical formulation in order to assess the stress in the adhesive. The reason being that analytical models are usually restricted to simple joint like single lap joint with thin adhesive bonds and in some extent thin adherends. In this case, the butt strap joint geometry and the relatively thick adhesive bond prevented any analysis via closed form solution. Finite element analysis not only allowed a more accurate stress analysis, but also allowed to show the influence of geometric non-linearities as well as mechanical non-linearities in the stress profile of the joint loaded in tension. Unlike analytical models that consider a constant shear stress through the adhesive bond thickness (Volkersen 1938, Goland & Reissner 1944, Hart-Smith 1973), it was shown that it is no the case, Figure 5.22.

The accelerating ageing programme carried out on the joints cannot be related to

any realistic degradation process as it should have taken a much longer time to have the specimens service life conditions. However, the experiments gave an indication of the type degradation to be expected when the joints are immersed in a humid environment. In particular, they showed how damaging the effect can be to the strength of the joint, especially if the adhesive bond is poorly manufactured. In this respect, there is probably a need for the designer to envisage a solution to protect the joint against such environmental degradation when using adhesive bonding in a marine environment.

9.3.2 Study of structural joints

Once the adhesive system was characterised, a study of a structural component was carried out both experimentally and numerically. The experimental programme included tensile characterisation of joints under conditions consistent with those in highly loaded areas such as the deck to superstructure connection.

The experimental programme enabled the characterisation of failure modes and provided an insight into failure mechanisms of the joint loaded in tension. The failure mode was observed to be mainly cohesive with only a few samples showing areas where adhesive failure, indicating a relatively good adhesive system for this design. This was in good agreement with the observations made for the generic joints, especially showing adhesive failure on steel adherend, Figure C.4.

Due to the relative complexity of the joint design, finite element analysis was chosen to assess the stress along the adhesive bond and it was shown that a linear model would give sufficiently accurate results. The analysis showed the importance of correctly modelling the boundary conditions in order to get a good agreement between numerical and experimental data. The modelling results enabled location of the zone of high stress and confirmed the mechanism of failure suggested by the experiment.

The study has highlighted the role of the stiffness of the adherends in the strength of the joints. Indeed, the deck-to-superstructure joint was made with a 6 mm thick steel box and a 6 mm thick aluminium box, while the unit-to-unit joint was made with 3 mm thick aluminum boxes. Quantitatively, the steel-to-aluminium connections with a smaller bond area carried 30% more load than the aluminium-to-aluminium connection. However,this increase of strength translates into a weight penalty in the global structure.

The finite element analysis showed the predominance of tensile stress failure rather than shear in these joints. This can be explained because the bonding area between the two boxes is as large as the areas of the straps. Decreasing the area between the faces of the box sections would lead to peel failure in the strap as shown by Hart-Smith cited in (Pocius & Dillard 2002) instead of tensile failure.

In terms of joint design, these configurations are interesting in that they fail due to direct tensile stress and not by peel due to the large bonding area of the butt. However, the geometry of the joint made with extruded section and sharp corner leads to very localised high stress areas. these areas are minimized with increasing adherend thickness as seen for the steel-to-aluminium connection. A way to reduce these stress concentration would be done by rounding the corners of the aluminium boxes (Adams & Harris 1987).

9.3.3 Failure criterion

The practical failure criterion based on experiment and numerical results was applied to the adhesive joint, considering that with the adherend materials and thickness involved, the adhesive would fail before. This is the opposite approach to the one advocated by Hart-Smith in an aerospace environment where the adhesive bond must not be the weak link in the structure (Hart-Smith 1973).

The reason for the choice of such a criterion was that other criteria either fail to take into account all the mechanical aspects of polymeric material (Von Mises) or are not implemented in commercial finite element codes (Raghava). Therefore, a hybrid approach based on experimental and numerical analysis was considered appropriate for the study. The experimental data has the advantage to consider simple joints that take into account the adherends, the surface preparation, the adhesive thickness and in some extent the load transfer mechanism of the complex joint.

The method also avoids to face a stress singularity that increases indefinitely with refining mesh surrounding corners or free surface. It ensures a conservative criterion comparing averaged values from the generic joint analysis and peak values from the complex joint analysis.

9.4 Energy based criterion

9.4.1 Study of generic joint

The study of the fracture behaviour of generic joints was the topic of Chapter 6. This phase enabled the assessment of the fracture toughness of the adhesive system. A number of issues were considered such as the influence of the combination of different adherends and the influence of adhesive thickness variations. Although the former was an original axis of investigation, the latter was analysed because observation made before testing, showed that for a given specimen the thickness of the adhesive bond varied substantially around the nominal thickness originally specified as seen in Table 6.3. These variations of adhesive thickness were not as significant as the one considered for the butt strap joints but significant enough to observed changes in the results of the fracture toughness.

Comparing the analytical and numerical models applied to DCB specimens, it was shown that the analytical models gave much less conservative results than numerical models. The analytical results are however more realistic as they describe a fairly tough adhesive with a high fracture toughness. This is due to models that do not take into account rotation of the root of the beams: this was first highlighted and explained by (Williams 1989).

As for the butt strap joints, the accelerating ageing programme carried out on the DCB specimens cannot be related to any realistic degradation process. However, the experiments gave an indication of the type degradation to be expected when the joints are immersed in a humid environment.

9.4.2 Study of structural joints

Based on the data derived from the DCB test programme, an analysis of damaged structural joints was carried out to assess their damage tolerance. The analysis implied different crack lengths and different applied stress via the applied load level.

The fracture mechanics analysis of the structural joints, with a nominal adhesive thickness of 3 mm, based on fracture toughness of DCB specimens with 1 mm adhesive thickness can be argued. Indeed, few studies have shown that the fracture energy of joints with toughened epoxy adhesives was highly dependent on the adhesive thickness and difficult to characterise (Kinloch & Shaw 1981, Daghyani et al. 1995, Yan et al. 2001b) among others. For this reason, it was necessary to

consider the cases where the adhesive thickness is the same for both the generic joints and the structural joints. If data is not available for different thicknesses, the numerical results can only be used as a means of comparison. In this study, the results obtained indicate that the fracture energy developed by a joint with 3 mm adhesive is higher than for a joint with 1 mm. However, it is likely that experimental tests on thicker generic joints would show a rise in the fracture toughness of the joint (Daghyani et al. 1995, Yan et al. 2001b) and in this case the fracture criterion chosen is conservative.

9.5 Comparison

This study showed two different approaches to investigate the behaviour of structural adhesive joints. One approach considered the joint to be damage-free and uses a stress-based criterion to identify areas prone to stress concentration in the joint. Based on generic joint test and stress analysis results, the failure of the joint was investigated with a conservative criterion.

The second approach considered that defects can inevitably occur in an adhesive bond but can be tolerated up to a certain load level or crack length. Based on mode I fracture mechanics tests results, an energy based assessment of the structural joint was done considering different load levels and crack length using linear elastic fracture mechanics.

The last step described in Figure 4.1 is now to check the compatibility of the designed load with the global load response of the superstructure which a brief analysis has been carried out section 9.2.

Figure 9.4 shows that the maximum load to be expected is about 56 kN in the case of front pressure. Experimental tensile tests showed that the ultimate load capacity of the deck to superstructure joints is 70 kN. This is above the maximum load carried by the superstructure but ratio between these two values is rather small compared to usual safety factors encounter in the industry (Clarke 1996). However it should be borne in mind that the boundary conditions at the base of the superstructure (all the degrees of freedom are constrained) are very conservative. In reality part the forces will be relieved due to the elasticity of the connection between the deck and the superstructure (Chapman 1961). Hence, in first approximation, the ultimate static load applied to the steel-to-aluminium connection is compatible with

the global load response of the superstructure.

Figure 8.8 shows that the steel-to-aluminium connection with 1 mm adhesive thickness is damage tolerant up to 50 kN and a crack length of 20 mm. Beyond this load level and this crack length, it is likely that any crack would propagate catastrophically. If the thickness of the joint is 3 mm and the criterion is kept the same, the steel-to-aluminium connection is damage tolerant up to 40 kN and a crack length of 20 mm. This becomes a more conservative criterion and satisfies the compatibility with the global load response of the superstructure.

In terms of failure load, the two approaches gives similar results as Table 7.3 predicts a failure at 50 kN for the steel-to-aluminium connection and the Figure 8.8 also suggests that beyond this load level and a 10 mm crack the joint is likely to fail. However, it should be noticed that the stress analysis needs to be carried out before the fracture energy approach to locate the areas of stress concentration. Also, in this particular study, the fracture criterion was shown to be a much more sever failure criterion (ie conservative) than the stress-based criterion.

9.6 Summary

In terms of practical ship design, in a short and structurally ineffective superstructure, high forces are usually developed at the connection between the superstructure and the main hull if the same materials are used for both structures (Chalmers 1993, Chapman 1961). This study proposed an analysis of structural adhesive joints which could help to design such joints to relieve these high forces by using a low modulus material between the steel deck and the aluminium superstructure. In the particular case of the superstructure presented in Chapter 3, the application of the DNV High Speed Craft code stipulates that it is not required to withstand bending and compression load. However, realistically, the superstructure will transmit a minimum vertical and shear loads that will be done via the adhesive joint.

Figures

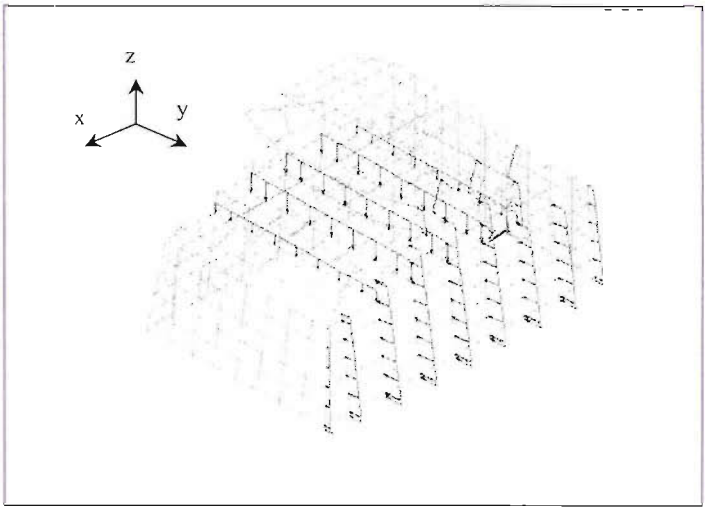

Figure 9.1: Superstructure subjected to side load pressure

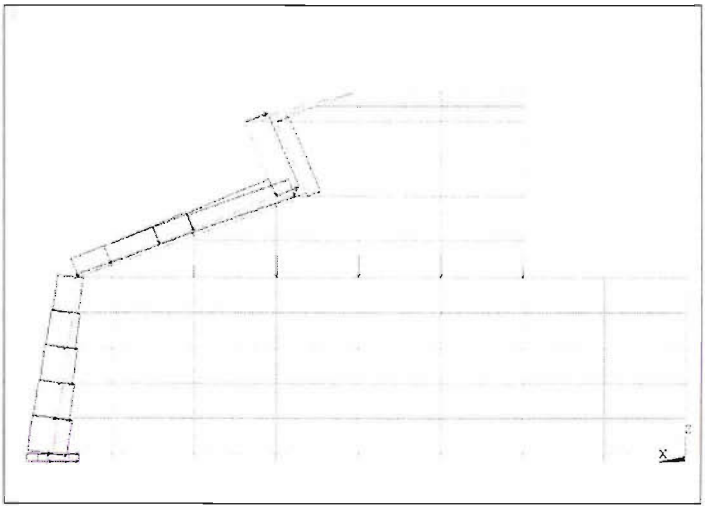

Figure 9.2: Superstructure subjected to front load pressure

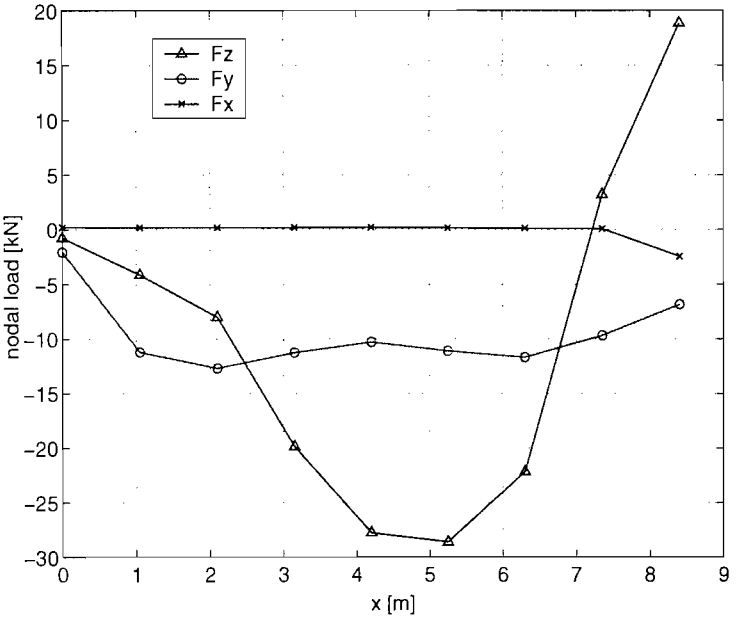

Figure 9.3: Nodal load response at the bottom of the superstructure to side pressure (portside)

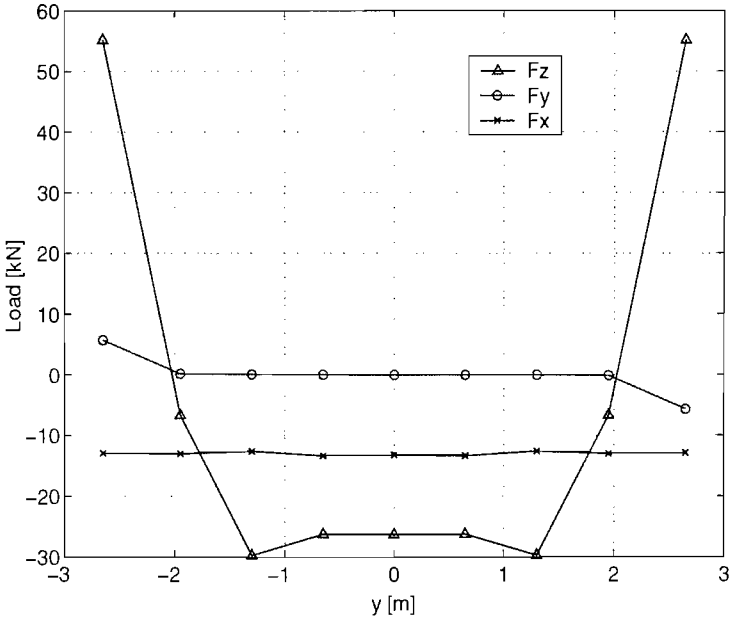

Figure 9.4: Nodal load response at the bottom of the superstructure to front pressure

Chapter 10

Further works

While this research has advanced knowledge with application of adhesive bonding technology to large structural application in shipbuilding, it has also highlighted the need to conduct further studies. These primary topics are briefly outlined below:

- In adhesive joint analysis, failure criteria have been a matter of investigation for some times because of the nature of the adhesive material and the stiffness mismatch in the joints. The strength-based criterion used in Chapters 5 and 7 was shown to be practical but involved several steps to be followed and experiments to be carried out. Hence it needs to be applied in the case of other adhesive joints applications with different joint design and different adhesive materials. Also, since it was shown to be time consuming, other criteria would need to be developed involving a more simple procedure for the designer.

- One of the topics of investigation in Chapters 5 and 6 was the influence of water on the degradation of the joint characteristics. The bath of distilled water in which the joints were immersed provided a convenient accelerated ageing environment, but the results obtained were very difficult to relate to reality. Immersing the specimens for a few months or a few years in an environmental chamber where the temperature, salt concentration and rate of humidity could vary would provide a more realistic solution. Hence, the atmosphere and the time scale would be comparable to weather conditions encountered in-service. This therefore warrants further study.

- The work carried out in Chapter 7 only investigated the static behaviour of structural joints. However, one of the reason for the reluctance of ship designers to consider adhesive bonding for structural elements is the lack of data concerning the long term-performance of joints in a marine environment, such as creep or fatigue due to dynamic load. Most of these performances can be

assessed in laboratory conditions but are time consuming and in-service conditions are not always reproduced. They can still provide valuable data about the mechanisms of joint degradation. In the particular case of the structural joints studied here, it should be interesting to assess the fatigue life of the joint at different frequencies and stress ratios in both tension-compression and bending. This would give a first estimate for the fatigue life of the superstructure itself.

- In terms of fracture behaviour of basic and structural joints, as stated above, experimental data are very important and hence it would be necessary to continue the work initiated on the fracture behaviour of thick adherend - thick adhesive joints. In particular, the analysis of damaged structural joints carried out in Chapter 8 was only based on the results of DCB joints with a nominal adhesive thickness Chapter 6. Future investigations on damaged joints need to consider DCB specimen with a bond thickness that corresponds to the bond of the structural joints. This would ensure a more precise criterion for the crack propagation in structural joints.

Chapter 11

Conclusion

This study focused on adhesively bonded joints with thick adherends and adhesive bonds to be used in a shipbuilding environment. It was based on a global-to-local analysis and compared two different approaches and failure criteria. The work addressed the strength of butt strap joints in different ageing environments and structural joints with marine grade adherends based on a double butt strap configuration. The fracture behaviour of the joints was assessed using Double Cantilever Beam specimens with both analytical and numerical models and this analysis was used to assess the damage tolerance of the structural joints defined above.

The local strength-based approach focused on three main issues concerning adhesive bonded single butt strap joints: the influence of adhesive thickness on the strength and behaviour of the joints, the influence of the combination of water and temperature and the influence of material non-linearity on the stress profile in the adhesive layer. The key aspects of the strength-based study concerned the characterisation of the mechanical behaviour of the joints and their mechanism of failure via experimental and numerical models.

The fracture mechanics analysis of bonded DCB specimens enabled the understanding on the defect resistance of the particular adhesive system used to bond different adherend materials. It gave an insight of the fracture behaviour of this particular adhesive system and specifically gave an envelope of fracture toughness values for the joint with different adherend materials.

The study of the behaviour of complex joints that could be used for structural purpose in a high speed craft involved experimental and numerical analysis. It enabled the characterisation of the behaviour of thick complex joints. It also highlighted the influence of the adherend stiffness in the state of stress in the adhesive and then

the strength of the joint. Finally, based on the data from the local joint design, a practical failure criterion based on experimental and numerical results was used and shown to be relevant to predict failure of the joint in a conservative way.

The energy-based assessment of structural joints was carried out using finite element models considering different lengths of crack, two adhesive thicknesses and different load levels. Based on data from generic DCB joints, this analysis enabled an assessment of the tolerance to damage of structural joints. For a given load or a given adhesive thickness, the study provided a range of crack lengths where the critical fracture energy is not reached and the joints considered to be safe.

In terms of design, this work provides a basis for a design approach to adhesive bonding of joints with both thick adherends and adhesive bond. It contributes to a better understanding of adhesively bonded structures in a marine environment and it helps to promote a more general access to this technology in that industry.

Appendix

Appendix A

Linear Elastic Fracture Mechanics concepts

A.1 Energy balance approach

A.1.1 Analytical methods

The first approach mentioned is based on the early work of (Griffith 1920) concerning cracks in glass materials and consider that a crack will grow when sufficient energy is released. In other words, crack will grow when all the work done by applied external forces and the elastic energy stored in the material is converted in elastic surface energy.

Generally speaking, for all loading systems, G can be defined as follows:

$$G = \frac{\partial U_{ext}}{\partial A} - \frac{\partial U_s}{\partial A} - \frac{\partial U_k}{\partial A} - \frac{\partial U_d}{\partial A} \tag{A.1}$$

For low rate testing, Uk =0 and if all the energy dissipation is local to the crack tip then Ud =0.

The energy changes are,

$$dU_{ext} = Pd\delta \tag{A.2}$$

and

$$U_s = \frac{1}{2}P.\delta \tag{A.3}$$

Therefore:

$$dU_s = \frac{1}{2}(Pd\delta + \delta dP) \tag{A.4}$$

hence,

$$G = \frac{1}{2}(P\frac{\partial \delta}{\partial a} - \delta\frac{\partial P}{\partial a}) \tag{A.5}$$

Since the compliance of the system is given by

$$\delta = C.P \tag{A.6}$$

and

$$du = CdP + PdC \tag{A.7}$$

the energy change can as well be expressed as follows:

$$G = \frac{P^2}{2B}\frac{\partial C}{\partial a} \tag{A.8}$$

This method enable to calculate the energy per unit area needed to enable a crack to propagate with respect to the main parameters of the test: load and corresponding crack length. It can be noted that this relationship does not take into account geometrical parameter of the specimen. The interest of this direct method (Kinloch 1990) is to get the value of G_c without any ambiguity that is found with the stress intensity factor approach.

In order to compute fracture energy G_I three analytical formulations are proposed in a test protocol from (Moore et al. 2001): simple beam theory, corrected beam theory and experimental compliance method.

For thin adhesive layer, using simple beam theory, the adhesive fracture energy can be expressed as follows (Ripling et al. 1970):

$$G_{Ic} = \frac{4P^2}{E_s B^2}\left(\frac{3a^2}{h^3} + \frac{1}{h}\right) \tag{A.9}$$

where E_s is the elastic modulus of the adherend and h the thickness of each adherend. The first term in bracket is due to the bending deflection and the second one is due to shear deflection which is usually negligible (Joshi, Gray, Banks, Haymar, Gilmore, Yates & Pethrick 1997, Ripling et al. 1970).

The simple beam theory is based on the assumption that the beam is built-in cantilever. This implies that by using the simple beam theory it is assumed that at cantilever root the slope and deflection are zero. However the forces and moment cause the end region to deform. This assumption therefore may result in an error.

The simple beam theory expression for the compliance of a perfectly built-in DCB specimen will underestimate the compliance as the beam is not perfectly built-in. A means of correcting for this effect is to treat the beam as containing a slightly longer crack length a $+\Delta$. Δ may be found experimentally by plotting the cube root of the compliance as a function of crack length a.

The fracture energy G_{Ic} derived from the Corrected Beam Theory is then given by:

$$G_{Ic} = \frac{3P\delta}{2B(a + |\Delta|)} \tag{A.10}$$

where P is the load, δ the displacement, a the crack length and B the width of the specimen.

The flexural modulus E_f of the DCB specimen can be calculated to check whether the test was carried out properly as a value independent of the crack length should be obtained via the following equation:

$$G_{Ic} = \frac{8(a + |\Delta|)^3}{CBh^3} \tag{A.11}$$

An alternative approach, given by the Experimental Compliance method, is to plot the logarithm of the compliance C versus the logarithm of the crack length a. The slop n of this plot is used to give G_{Ic}:

$$G_{Ic} = \frac{nP\delta}{2Ba} \tag{A.12}$$

where P is the load, δ the displacement, a the crack length and B the width of the specimen.

(Blackman et al. 1991) recommended during the analysis to employ all three methods. However if it is not possible for all methods to be used, they recommend that the ECM be used since this method together with the CBT are considered to be more accurate methods for determining the value of G_{Ic}.

A.1.2 Numerical method

As the previous methods described above are valid only for linear elastic materials, (Rice 1968) proposed a path independent integral based on the energy balance approach that can be applied in the case of materials with non-linear elastic behaviour. The corresponding parameter is J as opposed to G and is given by the following relation:

$$J = \oint_{\Gamma} W dy - \oint_{\Gamma} T \frac{\partial u}{\partial x} ds \tag{A.13}$$

Where:
Γ corresponds to an arbitrary path surrounding the crack tip,
W is the strain energy density,
$T = (\sigma_x n_x + \sigma_{xy} n_y \ ; \ \sigma_y n_y + \sigma_{xy} n_x)$ is the stress vector at the outer side of Γ,
u is the displacement vector,
x and y are the cartesian coordinates.
s is the arc of length along the integration line Γ.

In the case of linear elastic problems, the J-integral is exactly equal to the strain energy release rate G.

A.2 Stress intensity factor approach

An alternate approach proposed by (Irwin 1957) considers the stress field surrounding the crack tip to be characterised by a parameter called stress intensity factor K. This relates the stress intensity at the crack tip to the applied load and geometrical parameters. However, two approaches can be considered (Kinloch 1990): one where the crack is situated far from the interface between materials (ie in bulk materials) or when the crack is situated close to this interface that corresponds to bonded structures.

In the first case, the relation between the crack length, the applied stress and the K factor is given by:

$$\begin{pmatrix} \sigma_{11} \\ \tau_{12} \\ \sigma_{22} \end{pmatrix} = \frac{K_I}{(2\pi r)^{1/2}} \cos\left(\frac{\theta}{2}\right) \begin{pmatrix} 1 + \sin\left(\frac{\theta}{2}\right) \sin\left(\frac{3\theta}{2}\right) \\ \sin\left(\frac{\theta}{2}\right) \cos\left(\frac{3\theta}{2}\right) \\ 1 - \sin\left(\frac{\theta}{2}\right) \sin\left(\frac{3\theta}{2}\right) \end{pmatrix} \tag{A.14}$$

The problem occurring in this expression is that stress can not be taken as a criterion on its own as when approaching the vicinity of the crack stress mathematically goes to infinity which is not physically acceptable. Therefore the criterion chosen here is the following relation with K:

$$K_1 \geq K_{Ic} \tag{A.15}$$

It should be noticed that K_{Ic} is theoretically unique for a particular material and therefore is a fundamental material property for material selection and design. However, in the case of adhesive bonding, it has been shown (Yan et al. 2001a, Daghyani et al. 1995) that fracture toughness varies with adherend material and adhesive thickness.

In the case where the crack is close to a bimaterial interface, the problem becomes more difficult because one must take into account both tensile and shear stress around the crack vicinity:

$$\begin{pmatrix} \tau_{12} \\ \sigma_{22} \end{pmatrix} = \frac{f\left(K_{Ii}, K_{IIi}\right)}{(2\pi r)^{1/2}} \begin{pmatrix} \sin\left(\zeta \ln r\right) \\ \cos\left(\zeta \ln r\right) \end{pmatrix} \tag{A.16}$$

Where ζ is a bimaterial constant that depends on shear modulus and Poisson's ratio of both adherend and adhesive materials.

It is important to notice that the above expression exhibits an oscillatory behaviour that is not physically possible. However these oscillations are only observed mathematically in a limited region very close to the tip and it has been found that for the near and far field, the stress is reasonably predicted as shown by (Rice & Sih 1965) and (England 1965). The region mentioned above has been derived to be of the order of $2a \times 1.2610^{-4}$.

There exists a relationship between the stress intensity factor approach and the energy balance approach which is as follows:

$$G = \frac{(1-\nu^2)K^2}{E_a} \tag{A.17}$$

This is used to convert the stress intensity factor K calculated after the finite element analysis into the energy release rate G, which is compared to the results from the analytical solutions presented above. In the expression, E_a and ν are the Young's modulus and the Poisson ratio of the adhesive respectively.

Appendix B

Example of DCB calculation

This appendix presents how the fracture toughness of the DCB joint is obtained via a spreadsheet and intermediate graph, this follows the protocol written by (Moore et al. 2001). The spreadsheet is based on the equations A.9 to A.12 and the associated intermediate calculations for each specimen.

Table B.1 presents the input data recorded during the test: vertical displacement, corresponding load and length of the crack. Table B.2 presents the actual results used for the study: fracture toughness calculated for different crack length with the different analytical formulations and the finite element solution (column 2 to 7). The column 1 corresponds to the vertical displacement corrected taking into account the compliance of the machine. Table B.3 presents the intermediate calculations used to calculate the fracture toughness from equations A.9 to A.12. Eventually, Table B.4 summarises the regression analysis carried out to obtain Δ and n from Figures B.1 and B.2 respectively.

Tables

DATA INPUT BOX 4: TEST DATA

Text	Text	a [mm]	Load [N]	d [mm]
insert	NL			
insert	Visual	29	2280	1.3
precrack	Visual	31	1120	0.83
	Propagation	33	1460	1.03
	Propagation	35	1830	1.24
	Propagation	41	2190	1.67
	Propagation	44	2110	1.9
	Propagation	48	2070	2.02
	Propagation	52	1920	2.36
	Propagation	53	1810	2.56
	Propagation	59	1720	2.72
	Propagation	63	1680	2.87
	Propagation	69	1600	3.26
	Propagation	73	1530	3.55
	Propagation	77	1450	3.87
	Propagation	79	1370	4.23
	Propagation	82	1330	4.4
	Propagation	87	1290	4.62
	Propagation	92	1210	5.16
	Propagation	95	1180	5.34
	Propagation	98	1170	5.5
	Propagation	101	1130	5.79
	Propagation	104	1100	6.07
	Propagation	107	1050	6.35
	Propagation	110	1020	6.65
	Propagation	113	1010	6.91
	Propagation	115	960	7.26

Table B.1: Example of input data for tested DCB specimen with Al 6082 and Al 6082

CALCULATED VALUES

dCOR [mm]	G SBT [J/m2] Eqn. [A.9]	G CBT [J/m2] Eqn. [A.10]	G ECM [J/m2] Eqn. [A.11]	G KCALC (J/m2)	G J-int lin (J/m2)	G J-int nonlin (J/m2)
1.05	673.42	2737.57	3545.40			
0.70	184.37	873.56	1098.89			
0.87	352.96	1350.61	1654.88	569.65	561.05	468.13
1.04	620.71	1952.69	2336.13	973.21	955.90	771.75
1.43	1206.76	2915.56	3284.51	1773.19	1741.65	1353.56
1.66	1285.19	3133.32	3442.81	1840.01	1807.29	1402.11
1.79	1466.07	3118.28	3327.66	2033.13	1996.97	1539.09
2.15	1475.58	3284.35	3416.97	1989.67	1954.29	1509.09
2.36	1361.33	3357.60	3472.83	1824.04	1791.61	1393.04
2.53	1518.22	3171.26	3178.48	1966.66	1931.70	1494.77
2.68	1648.58	3134.32	3085.13	2095.86	2058.61	1586.76
3.08	1789.95	3205.74	3081.53	2216.52	2177.13	1674.41
3.38	1829.98	3221.87	3054.32	2232.21	2192.54	1686.15
3.71	1826.94	3216.73	3011.22	2202.22	2163.09	1665.80
4.08	1716.00	3275.93	3048.64	2052.44	2015.98	1558.09
4.25	1741.42	3221.79	2973.35	2065.24	2028.55	1567.61
4.48	1842.59	3140.68	2861.73	2155.49	2117.20	1632.64
5.02	1811.56	3163.36	2849.39	2092.08	2054.92	1587.17
5.21	1836.36	3116.33	2789.17	2107.23	2069.81	1598.70
5.37	1920.55	3106.67	2763.81	2187.73	2148.88	1656.44
5.66	1902.26	3088.45	2731.96	2154.29	2116.04	1632.54
5.95	1910.73	3082.30	2711.82	2156.21	2117.93	1523.33
6.23	1842.39	3012.33	2636.70	2063.79	2027.16	1458.03
6.54	1837.04	2999.46	2612.67	2044.90	2008.60	1444.68
6.80	1900.37	3020.60	2618.91	2106.80	2069.41	1488.41
7.15	1777.95	2977.32	2573.73	1968.54	1933.61	1390.73

Table B.2: Example of calculated values for tested DCB specimen with Al 6082 and Al 6082

CALCULATED INTERMEDIATE VALUES

Text	a [mm]	F [-]	N [-]	F/N [-]	C [mm/N]	(C/N)^1/3	Log [C/N]	Log (a)	m [1/mm]	d/a
Visual	29.00	1.00	1.00	1.00	0.00	0.08	-3.34	1.46	1.44	0.04
Visual	31.00	1.00	1.00	1.00	0.00	0.09	-3.20	1.49	1.63	0.02
Propagation	33.00	1.00	1.00	1.00	0.00	0.08	-3.23	1.52	1.84	0.03
Propagation	35.00	1.00	1.00	1.00	0.00	0.08	-3.25	1.54	2.06	0.03
Propagation	41.00	1.00	1.00	1.00	0.00	0.09	-3.19	1.61	2.79	0.03
Propagation	44.00	1.00	1.00	1.00	0.00	0.09	-3.10	1.64	3.20	0.04
Propagation	48.00	1.00	1.00	1.00	0.00	0.10	-3.06	1.68	3.80	0.04
Propagation	52.00	1.00	1.00	1.00	0.00	0.10	-2.95	1.72	4.44	0.04
Propagation	53.00	1.00	1.00	1.00	0.00	0.11	-2.89	1.72	4.61	0.04
Propagation	59.00	1.00	1.00	1.00	0.00	0.11	-2.83	1.77	5.69	0.04
Propagation	63.00	1.00	1.00	1.00	0.00	0.12	-2.80	1.80	6.48	0.04
Propagation	69.00	1.00	1.00	1.00	0.00	0.12	-2.72	1.84	7.76	0.04
Propagation	73.00	1.00	1.00	1.00	0.00	0.13	-2.66	1.86	8.67	0.05
Propagation	77.00	1.00	1.00	1.00	0.00	0.14	-2.59	1.89	9.64	0.05
Propagation	79.00	1.00	1.00	1.00	0.00	0.14	-2.53	1.90	10.14	0.05
Propagation	82.00	1.00	1.00	1.00	0.00	0.15	-2.50	1.91	10.92	0.05
Propagation	87.00	1.00	1.00	1.00	0.00	0.15	-2.46	1.94	12.28	0.05
Propagation	92.00	1.00	1.00	1.00	0.00	0.16	-2.38	1.96	13.73	0.05
Propagation	95.00	1.00	1.00	1.00	0.00	0.16	-2.36	1.98	14.63	0.05
Propagation	98.00	1.00	1.00	1.00	0.00	0.17	-2.34	1.99	15.56	0.05
Propagation	101.00	1.00	1.00	1.00	0.01	0.17	-2.30	2.00	16.53	0.06
Propagation	104.00	1.00	1.00	1.00	0.01	0.18	-2.27	2.02	17.52	0.06
Propagation	107.00	1.00	1.00	1.00	0.01	0.18	-2.23	2.03	18.54	0.06
Propagation	110.00	1.00	1.00	1.00	0.01	0.19	-2.19	2.04	19.59	0.06
Propagation	113.00	1.00	1.00	1.00	0.01	0.19	-2.17	2.05	20.67	0.06
Propagation	115.00	1.00	1.00	1.00	0.01	0.20	-2.13	2.06	21.40	0.06

Table B.3: Example of intermediate data to calculate fracture energy release rate of tested DCB specimen with Al 6082 and Al 6082

REGRESSION ANALYSES

Method	**CBT**		**ECM**	
	slope	Y-axis	slope	Y-axis
Value	0.001385	0.032166	2.157685	-6.628851
Correction	Δ=	**23.22**	**n=**	**2.16**
Corr. coeff.	r^2=	0.995551	r^2=	0.986656

Table B.4: Example of intermediate data to calculate fracture energy release rate of tested DCB specimen with Al 6082 and Al 6082

Figures

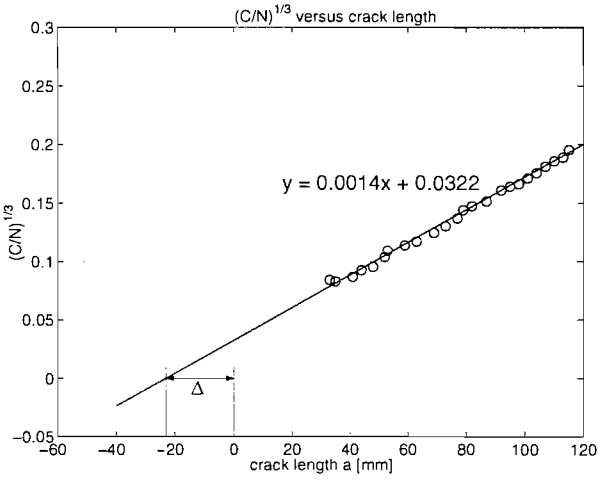

Figure B.1: Graph allowing the deduction of the correcting factor Δ for a specimen with Al 6082 / Al 6082 adherends

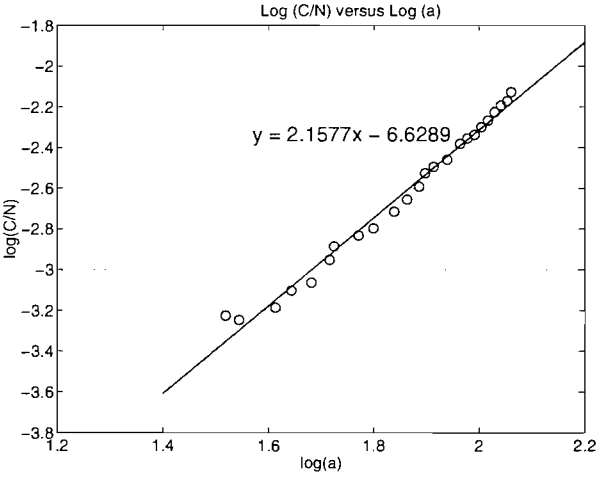

Figure B.2: Graph allowing the deduction of the slope of the plot log(C) versus log(a) for a specimen with Al 6082 / Al 6082 adherends

Appendix C

Flexural tests

C.1 Fabrication

The specimens tested in bending, the two end faces were butted together and held in position. Strips of MDF (Medium Density Fiber) wood were nailed to the surface in order to align to the two halves of the joint before bonding. To avoid the weld lines interfering with the joint alignment, areas were cut away and the whole assemble was raised above the work surface. The joint was clamped in place until a full cure of the adhesive had been achieved. The butt straps were bonded over the joint and clamped in position during curing. In order to set the correct adhesive thickness, a 3mm aluminium spacer was temporarily pushed into the joints during the aligning process. This was removed, with the gap produced being back-filled once the joint had been clamped in position.

C.2 Experimental flexural behaviour

Each specimen was loaded on an Instron 100 kN universal-testing machine up to failure. A constant rate of loading of 0.015mm/sec (1 mm/min) was applied. The tests were performed at room temperature. During the experiments applied load, mid span deflexion and vertical displacement of the crosshead were recorded Figure C.2.

For joint A, Figure C.3 (a) presents the flexural behaviour of the joint and Table C.1 summarises the ultimate load and corresponding maximum bending moment carried by the joints. Figure C.3 shows that between 0 and 20 kN (and ignoring the initial non-linearity due to the take-up of play at the beginning of the test), the

joint behaves in the linear domain followed by a plastic region between 20 and 25 kN. Very steep drop of the load carrying capacity shows that catastrophic failure occurs. However, the load is sustained at a lower level because the joint did not fail completely. The curves and the average results show good consistency between the specimens tested as the bending stiffness is 7.4 kN/mm with a standard deviation of 0.2 kN/mm.

In terms of locus of failure it was observed that in most cases cohesive failure occurred in the adhesive, as it can be seen from Figure C.4. However, as for the butt strap specimens (Chapter 5), some adhesive failure was observed at the steel interface. Two causes can be considered: the first one is because too much primer was applied and the second one is because the interlocking between steel and the primer-adhesive system is not as good as the one between aluminium and primer-adhesive system. This confirms the sensitivity of the combination between surface preparation and/or coating and the adherend materials highlighted by many authors (Brockmann 1986, Kinloch 1990). (Cantrill et al. 2004) outlined that a more specific surface preparation such as shot blasting would give a better adhesion and hence a more satisfactory mode of failure when steel is used.

For joint B, Figure C.3 (b) shows the typical flexural behaviour of the joint. The curves are characterised by a relatively long take up of play between 0 and 3 kN, followed by a linear portion up to 15 kN. A non linear domain is then observed up to the ultimate load, quickly followed by a drop of the load showing failure of the specimen. The curves and the average results also show good consistency between the specimens tested as the bending stiffness is 3.5 kN/mm with a standard deviation of 0.2 kN/mm. The average flexural strength and stiffness are summarised in Table C.1.

Failure was observed to occur along the vertical adhesive bond and the bond between the bottom strap and the box section. Figure C.5. This is a similar mode of failure to the steel to aluminium connection. After having loaded the specimen further in bending, locus of failure could be observed, Figure C.5. The joint presented cohesive failure along the interface between the 2 box sections (vertical interface on the picture). Cohesive failure was also observed along the bottom strap, but very close to the box adherend.

Experimentally, it was shown that the steel-to-aluminum joint had a higher flexural

stiffness (7.5 kN/mm) than the unit-to-unit joint (3.8 kN/mm): it is twice stiffer. This can be explain by the design of the joints: the steel to aluminium connection has a smaller bonded area than the aluminium to aluminium connection which in turn is softer. Also, the steel adherend is intrinsically stiffer than the aluminium alloys, the L shape accentuating this property of the joint in bending.

Tables

	Ultimate load [kN]	Bending Moment [kN.m]	Bending Stiffness [kN/mm]
Deck to superstructure	23.2 ± 1.8	3.2 ± 0.3	7.4 ± 0.2
Unit to unit	20.4 ± 1.3	2.8 ± 0.2	3.5 ± 0.2

Table C.1: Average ultimate flexural strength of structural joints

Figures

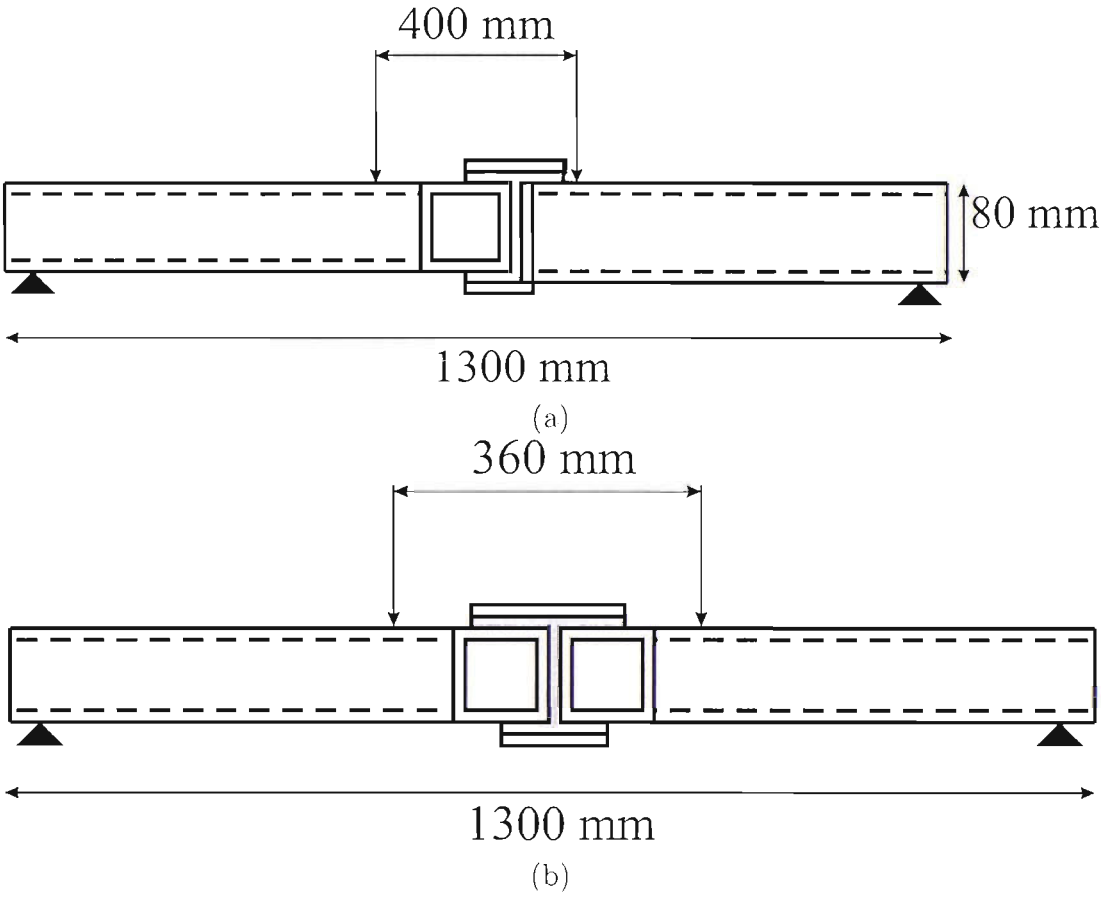

Figure C.1: Structural joints in 4-point bending configuration: (a) Steel to aluminium connections. (b) Aluminium to aluminium connection.

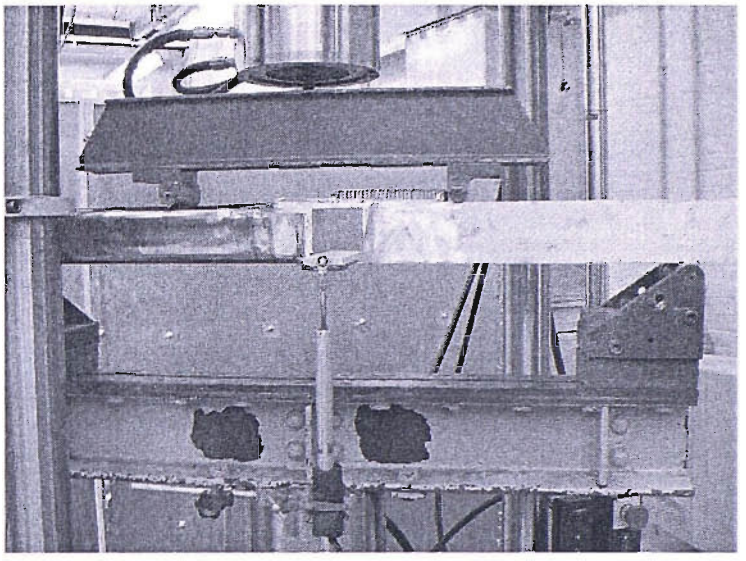

Figure C.2: Setup of 4-point bending test for steel to aluminium connection.

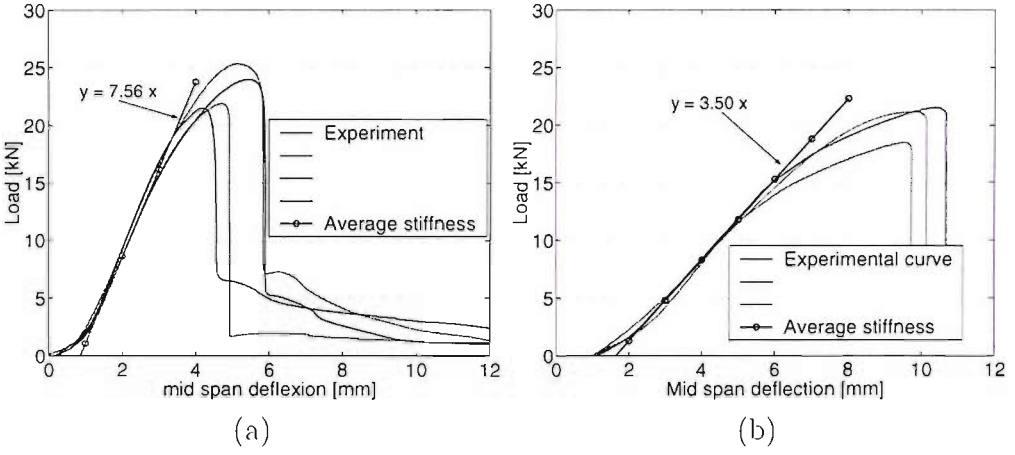

(a) (b)

Figure C.3: Load-deflection behaviour of structural joints in a four point bending configuration: (a) Steel to aluminium connections, (b) Aluminium to aluminium connection.

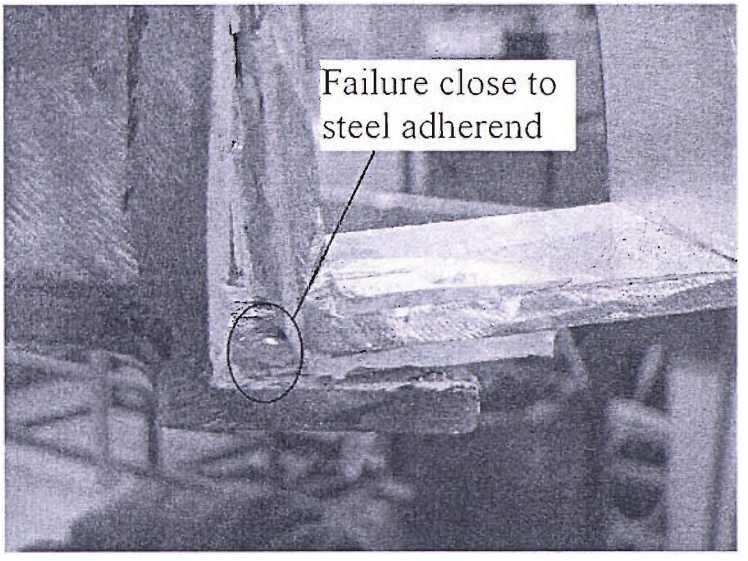

Figure C.4: Locus of failure of steel to aluminium connections tested in bending.

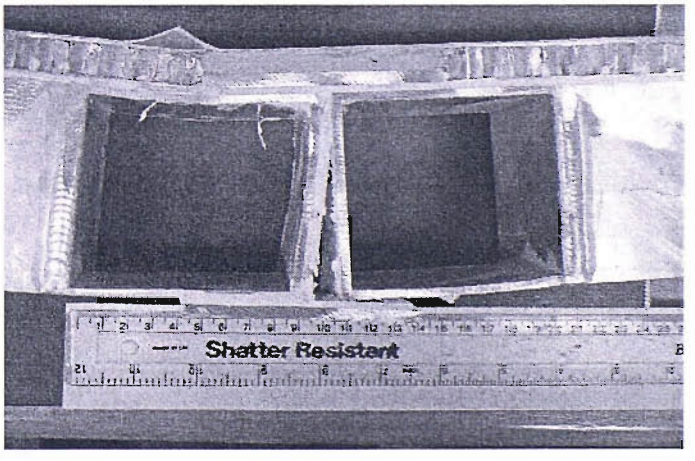

Figure C.5: Failure of aluminium connection in bending.

Appendix D

Failure criterion

Regarding the adhesive and the adherends used in the case considered, it was likely that joints will failed in the adhesive rather than in the adherend. Therefore, an adhesive failure criteria has to be defined to predict failure in the adhesive. Several methods can be used to predict failure:

- Von Mises criterion $\sigma_{failure} = \sqrt{3{\tau_{ultimate}}^2 + {\sigma_{ultimate}}^2}$,
- Raghava criterion,
- Empirical criteria.

Brede *et al* (cited by (Weitzenböck et al. 2004a)) have developed an empirical failure criterion based on experimental data and numerical modelling which is described in the following. An experimental programme on a simple joint design (butt strap joint) provide an average ultimate shear strength value and an average load to failure. From this set of data, the average load at failure is applied to a finite element model of the simple joint. Shear and peel stresses or maximum principal and equivalent stress (when complex joints are considered) are averaged along a line corresponding to the adhesive thickness t_a at a distance $t_a/10$ from the adherend. Figure 5.16. Because of numerical uncertainty at the free surface, the last three nodes before the edge of the joint should not be taken into account. It should be noticed that a similar level of mesh refinement between the generic and the complex joint should be achieved in order to obtain relevant results.

The failure will then occur in the complex joint FE model when any of the averaged calculated values recorded in the simple joint adhesive bond at failure is reached along a line at a distance $t_a/10$ from one of the adherends. This method ensures a conservative criterion and reduces numerical singularity increasing the stress around any corner or free surface.

References

Adams, R. D., Comyn, J. & Wake, W. C. (1997), *Structural Adhesive Joints in Engineering*, Chapman and Hall.

Adams, R. D. & Harris, J. A. (1987), 'The influence of local geometry on the strength of adhesive joints', *International Journal of Adhesion and Adhesives* **7**, 69.

Adams, R. D. & Peppiatt, N. A. (1974), 'Stress analysis of adhesive-bonded lap joints', *Journal of Strain Analysis* **9**, 185–196.

Allan, R. C., Bird, J. & Clarke, J. D. (1986), The use of adhesives in the repair of cracks in ships' structures, *in* 'Structural Adhesives in Engineering', pp. 169–178.

Allman, D. J. (1977), 'A theory for elastic stresses in adhesive bonded lap joint', *Quarterly Journal of Mechanics and Applied Mathematics* **30**, 415–436.

Anderson, T. L. (1995), *Fracture Mechanics: Fundamentals and Applications*, CRC Press.

Ansys (2002), 'Ansys 6.1 online user manual'.

Armstrong, K. B. (1997), 'Long term durability in water of alluminium alloy adhesive joints bonded with epoxy adhesives', *International Journal of Adhesion and Adhesives* **17**, 89–105.

ASTM (1998), 'Standard test method for adhesive-bonded surface durability of aluminum (wedge test) astm d 3762-98'.

Atkins, A. G. & Mai, Y. W. (1985), *Elastic and plastic fracture*, Ellis Horwood Ltd. ISBN 0-85312-562-7.

Beevers, A. (1999), 'Durability testing and life prediction of adhesive joints', *International Journal of Materials and Product Technology* **14**, 373–384.

Bell, A. & Kinloch, A. J. (1997), 'The effect of the substrate material on the value of the adhesive fracture energy, g_c', *Journal of Materials Science Letters* **16**, 1450–1453.

Bezine, G., Roy, A. & Vinet, A. (1996), 'Stress in bonded adherends for single lap joints', *Journal of Ship Production* **12**, 167–171.

Bigwood, D. A. & Crocombe, A. D. (1989), 'Elastic analysis and engineering design formulae for bonded joints', *International Journal of Adhesion and Adhesive* **9**, 229–242.

Bigwood, D. A. & Crocombe, A. D. (1990), 'Non-linear adhesive bonded joint design analyses', *International Journal of Adhesion and Adhesive* **10**, 31–41.

Blackman, B. R. K., Dear, J. P., Kinloch, A. J. & Osiyemi, S. (1991), 'The calculation of adhesive fracture energies from double-cantilever beam test specimens', *Journal of Materials Science Letters* **10**, 253.

Blackman, B. R. K., Kinloch, A. J. & Paraschi, M. (2001), 'The effect of the substrate material on the value of the adhesive fracture energy, g_c: further considerations', *Journal of Materials Science Letters* **20**, 265–267.

Blackman, B. R. K., Kinloch, A. J., Paraschi, M. & Teo, W. S. (2003), 'Measuring the mode i adhesive fracture energy, g_{Ic}, of structural adhesive joints: the results of an international round-robin', *International Journal of Adhesion and Adhesive* **23**, 293–305.

Boeman, R. G., Erdman, D., Klett, L. & Lomax, R. (1999), A practical test method for mode i fracture toughness of adhesive joints with dissimilar substrates, *in* 'Advanced Composites Conference', SAMPE-ACCE-DOE. P99-104246.

Bondship (2003), 'Bonding of lightweight materials for cost-effective production of high-speed crafts and passenger ships'. GROWTH project number G3RD-CT-2000-00101, http://research.dnv.com/bondship.

Bowditch, M. R. (1996), 'The durability of adhesive joints in the presence of water', *International Journal of Adhesion and Adhesives* **16**, 73–79.

Boyd, S. W. (2005), Strength and durability of co-cured steel-to-composite joints for application in the marine industry, PhD thesis, University of Southampton. To be submitted.

Brede, M. (2002), Final report on analytical and fe modelling of joints and verification of easy-to-use design rules, Technical Report 1-11-W-2002-01-0, Bondship consortium.

Brockmann, W. G. (1986), The importance of surface pretreatment prior to bonding, *in* 'Structural Adhesives in Engineering', pp. 61–70.

BSI (1993), 'Adhesive – guide to the selection of standard laboratory ageing conditions for testing bonded joints'.

BSI (2002*a*), 'Determination of mode i fracture energy g_{Ic} of structural adhesives using the double cantilever beam and tapered double cantilever beam specimens'.

BSI (2002*b*), 'Methods of test for adhesives – determination of bond strength in longitudinal shear for rigid adherends'.

Cantrill, J., Kapadia, A. & Pugh, D. (2004), 'Lessons learnt from designing and producing adhesively bonded prototyping structurse in a shipyard', *Proc Instn Mech Engrs, Part M: Journal of Engineering for the Maritime Environment* **218**, 267–272.

Carpenter, W. C. (1991), 'A comparison of numerous lap joint theories for adhesively bonded joints', *Journal of Adhesion* **35**, 55–73.

Chalmers, D. W. (1993), *Design of ships' structures*, Ministry of Defense. ISBN 0 11 772717 2.

Chapman, J. C. (1961), 'The behaviour of long deckhouses', *Transaction of the Royal Institution of Naval Architects* **103**, 281–292.

Chen, B., Dillard, D. A., Dillard, J. G. & Clarke, R. L. (2002), 'Crack path selection in adhesively bonded joints: the roles of external loads and specimens geometry', *International Journal of Fracture* **114**, 167–190.

Clarke, J. L., ed. (1996), *EUROCOMP Design Code and Handbook*, E & F.N. Spon, London.

Colak, A. (2001), 'Parametric study of factors affecting the pull out strength of steel rods bonded into precast concrete panels', *Internaional Journal of Adhesion and Adhesives* **21**, 487–493.

Cooper, P. (1979), 'Critical examination of stress in elastic single-lap joint', *NASA technical paper 1507*.

Cornell, R. W. (1953), 'The determination of stress in cemented lap joints', *Transaction ASME Journal of Applied Mechanics* **20**, 17–27.

Crocombe, A. D. (1989), 'Global yielding as a failure criterion for bonded joints', *Int. J. Adhesion and Adhesive* **9**, 145–153.

Crocombe, A. D. (1997), 'Durability concept and tools for the cohesive environmental degradation of bonded structrures', *International Journal of Adhesion and Adhesives* **17**, 229–238.

Daghyani, H. R., Ye, L. & Mai, Y. W. (1995), 'Mode i fracture behaviour of adhesive joints. part i. relationship between fracture energy and bond thickness', *Journal of Adhesion* **53**, 149–162.

Delale, F., Erdogan, F. & Aydinoglu, M. N. (1981), 'Stress in adhesively bonded joints: a closed form solution', *Journal of Composite Materials* **15**, 249–271.

Di, S., Kelly, D., Chowdhury, M., Goss, P. & Berkovits, A. (1997), Developement of a generic ship model for the study of fatigue in welded aluminium catamaran, *in* 'FAST 97'.

DNV (2001), 'Rules for classification of high speed, light craft and naval surface craft'.

Earl, J. S. (2001), The influence of hygrothermal ageing on polymeric sandwich materials and structures, PhD thesis, University of Southampton.

England, A. H. (1965), 'A crack between dissimilar media', *Journal of Applied Mechanics, Trans ASME* **32**, 400–402.

Erdogan, F. (1963), 'Stress distribution in a nonhomogenuous elastic plane with cracks', *Journal of Applied Mechanics. Trans ASME* **30**, 232–236.

Evans, J. H. (1983), *Ship structural design concepts - Second cycle*, Cornell Maritime Press, Centreville, Maryland. ISBN 0-87033-303-8; page 172.

Fernlund, G., Papini, M., McCammond, D. & Spelt, J. K. (1994), 'Fracture load predictions for adhesive joints', *Composite Science and Technology* **51**, 587–600.

Fernlund, G. & Spelt, J. K. (1991), 'Failure load prediction of structural adhesive joints', *International Journal of Adhesion and Adhesives* **11**, 213–227.

Goland, M. & Reissner, E. (1944), 'The stress in cemented joints', *Transaction ASME Journal of Applied Mechanics* **11**, 17–27.

Grabovac, I. (2003), 'Bonded composite solution to ship reinforcement', *Composites Part : Applied science and manufacturing* **34**, 847–854.

Grabovac, I., Bartholomeusz, R. A. & Baker, A. A. (1993), 'Composite reinforcement of a ship superstructure - project overview', *Composites* **24**, 501–509.

Griffith, A. A. (1920), 'The phenomena of rupture and flow in solids', *Phil. Trans. Roy. Soc.* **A221**, 163.

Hamoush, S. A. & Ahmad, S. H. (1989), 'Fracture energy release rate of adhesive joints', *International Journal of Adhesion and Adhesives* **9**, 171–178.

Harris, J. A. & Adams, R. D. (1984), 'Strength prediction of bonded single lap joints by non-linear finite element methods', *International Journal of Adhesion and Adhesives* **4**, 65–78.

Hart-Smith, L. J. (1973), Adhesive bonded single lap joint, Technical Report 112236, NASA.

Hart-Smith, L. J. (1999), 'A peel type durability test coupon to assess interfaces in bonded, co-bonded and co-cured composite structures', *International Journal of Adhesion and Adhesives* **19**, 181–191.

Hashemi, S., Kinloch, A. J. & Williams, J. G. (1989), 'Corrections needed in double cantilever beam tests for assessing interlaminar failure of fiber-composites', *Journal of Materials Science Letters* **8**, 125–129.

Hashemi, S., Kinloch, A. J. & Williams, J. G. (1990), 'Interleminar fracture of polymer composites', *Proceedings of the Royal Society* **A 427**, 173–199.

Hashim, S. A. (1999), 'Adhesive bonding of thick steel adherends for marine structures', *Marine Structures* **12**, 405–423.

Hashim, S. A. & Knox, E. M. (1999), 'Structural performance of thick adherend steel-composite adhesive joints', *Proceedings IMechE Part L* **213**, 47–58.

Hashim, S. A. & Knox, E. M. (2004a), 'Aspects of joint design and evaluation in thick adherend applications', *Journal of Adhesion* **80**, 569–583.

Hashim, S. A., Winkle, I. E. & Cowling, M. J. (1990), 'A structural role for adhesive in shipbuilding ?', *The Naval Architect* pp. 203–220.

Holton, T., Spinks, G. M. & Isle, N. A. (1992), Structural adhesive performance in marine environments, *in* 'International Symposium on Polymer Materials: Preparation, Characterization and Properties - Polymer '91', Vol. 28, pp. 9–17.

Irwin, G. R. (1957), 'Analysis of stress and strain near the end of a crack traversing a plate', *Trans ASME, Journal of Applied Mechanics* **24**, 361–364.

Jarry, E., Shenoi, R. A., Kapadia, A. & Miao, S. (2004), Design and fabrication of an adhesively bonded aluminium ship superstructure, *in* 'PRADS 2004, 9^{th} Symposium on Practical Design of Ships and Other Floating Structures', pp. 982–988.

Jones, M. T., Pitcher, P. D., Pool, P. & Stone, M. H. (1986), Effect of surface pretreatment and alloy type on the durability of adhesive bonded titanium alloy joints, *in* 'Structural adhesive in engineering', pp. 93–104.

Joshi, S. B., Gray, T. F., Banks, W. M., Haymar, D., Gilmore, R., Yates, L. W. & Pethrick, R. A. (1997), 'Environmental ageing of adhesively-bonded joints. ii. mechanical study', *Journal of Adhesion* **62**, 317–335.

Judd, G., Dodkins, A. & Maddison, A. (1996), Adhesively bonded aluminium superstructures, *in* 'International Conference on Lightweight Materials in Naval Architecture', University of Southampton.

Kecsmar, J. & Shenoi, R. A. (2004), 'Some notes on the influence of manufacturing on the fatigue life of welded aluminium marine structures', *Journal of Ship Production* **20**, 164–175.

Kinloch, A. J. (1990), *Adhesion and Adhesives: Science and Technology*, Chapman and Hall.

Kinloch, A. J. & Shaw, S. J. (1981), 'The fracture resistance of a toughened epoxy adhesive', *Journal of Adhesion* **12**, 59–77.

Knox, E. M. & Cowling, M. J. (2000*a*), 'Durability aspects of adhesively bonded thick adherend lap shear joints', *International Journal of Adhesion and Adhesives* **20**, 323–331.

Knox, E. M. & Cowling, M. J. (2000*b*), 'A rapid durability test method for adhesives', *International Journal of Adhesion and Adhesives* **20**, 201–208.

Lee, D. G., Kwon, J. W. & Cho, D. H. (1998), 'Hygrothermal effects on the strength of adhesively bonded joints', *Journal of Adhesion Science and Technology* **12**, 1253–1275.

Li, G. & Lee-Sullivan, P. (2001), 'Finite element and experimental studies on single balanced lap joints in tension', *Internartional Journal of Adhesion & Adhesives* **21**, 211–220.

Li, G., Lee-Sullivan, P. & Thring, R. W. (1999), 'Non-linear finite element analysis of stress distributions across the adhesive thickness in composite single lap joints', *Composite Structures* **46**, 395–403.

Loscombe, P. R. (1990), Key aspects of structural design of small SWATH ships, PhD thesis, University of Southampton.

Mitra, A. K. & Ghosh, B. (1995), 'Interfacial stresses and deformations of an adhesive bonded double strap butt joint under tension', *Computers and Structures* **55**, 687–694.

Moore, D. R., Pavant, A. & Williams, J. G. (2001), *Fracture mechanics testing methods for polymers, adhesive and composites*, ESIS publication 28.

Narasimhan, S., Shenoi, R. A. & Jeong, H. K. (2004), 'Three dimensional in adhesively bonded lap joints with non-identical adherends', *Journal of materials: design and application, Proceedings of IMechE* **218 Part L**, 283–298.

Ojalvo, I. U. & Eidinoff, H. L. (1978), 'Bond thickness efects upon stresses in single-lap adhesive joints', *American Institute of Aeronautics and Astronautics Journal* **16**, 204–211.

Ouezdou, M. B. & Chudnovsky, A. (1988), 'Stress and energy analysis of toughenss measurement for adhesive bonds', *Engineering Fracture Mechanics* **29**, 253–261.

Phillips, H. J., Shenoi, R. A. & Moss, C. E. (1999), 'Damage mechanics of top hat stiffeners used in frp ship construction', *Marine Structures* **12**, 1 – 19.

Pocius, A. V. & Dillard, D. A. (2002), *Adhesion Science and Engineering - I: The Mechanics of Adhesion*, Elsevier. ISBN 0 444-515140-7 volume 1.

Polmear, I. J. (1995), *Light Alloys: Metallurgy of the Light Metals*, Butterworth Heinemann.

Pradhan, S. C., Iyengar, N. G. R. & Kishore, N. N. (1995), 'Finite element analysis of crack growth in adhesively bonded joints', *International Journal of Adhesion and Adhesives* **15**, 33–41.

Raghava, R., Cadell, R. M. & Yeh, G. S. Y. (1973), 'The macroscopic yield behaviour of polymers', *Journal of Material Science* **8**, 225–232.

Reddy, J. N. & Roy, S. (1988), 'Non-linear analysis of adhesively bonded joints', *International Journal of Non-linear mechanics* **23**, 97–112.

Renton, W. J. & Vinson, J. R. (1977), 'Analysis of adhesively bonded joints between panels of composite materials', *Journal of Applied Mechanics, Trans ASME* **45**, 101–106.

Rice, J. R. (1968), 'A path independent integral and the approximate analysis of strain concentration by notches and cracks', *Journal of Applied Mechanics, Trans ASME* **35**, 379–386.

Rice, J. R. & Sih, G. C. (1965), 'Plane problems of cracks in dissimilar media', *Journal of Applied Mechanics, Trans ASME* **32**, 418–423.

Ripling, E. J., Mostovoy, S. & Corten, H. T. (1970), 'Fracture mechanics: a tool for evaluating structural adhesives', *Journal of Adhesion* **3**, 107–123.

Ripling, E. J., Mostovoy, S. & Patrick, R. L. (1963), 'The application of fracture mechanics to adhesives joints', *A.S.T.M. S.T.P. 360*.

Roland, F., Manzone, L., Kujala, P., Brede, M. & Weitzenböck, J. (2004), 'Advanced joining techniques in european shipbuilding', *Journal of Ship Production* **20**, 200–210.

Semerdjiev, S. (1970), *Metal-to-metal adhesive bonding*, Business Books Ltd, London. ISBN: 0220799504.

Shenoi, R. A., Read, P. J. C. L. & Hawkins, G. L. (1995), 'Fatigue failure mechanisms in fibre reinforced plastic laminated tee joints', *International Journal of Fatigue* **17**, 415–426.

Trantina, G. G. (1972), 'Fracture mechanics approach to adhesive joints', *Journal of Composite Materials* **6**, 192–207.

Tsai, M. Y. & Morton, J. (1994), 'An evaluation of analytical and numerical solutions to the single-lap joint', *International Journal of Solid Structures* **31**, 2537–2563.

Tsai, M. Y., Morton, J. & Matthews, F. (1995), 'Experimental and numerical studies of a laminated composite single-lap adhesive joint', *Journal of Composite Materials* **29**, 1254–1275.

Veazie, D. R., Robinson, K. R. & Shivakumar, K. (2004), 'Effects of the marine environment on the interfacial fracture toughness of pvc core sandwich composites', *Composites Part B*. To be published.

Venables, J. D. (1982), Adhesion and durability of metal/polymer bonds, *in* K. L. Mittal, ed., 'Adhesive joints, Formation, Characteristics and Testing'.

Volkersen, O. (1938), 'Die nietkraftverteilung in zugbeanspruchten nietverbindungen mit konstanten laschenquerschnitten', *Luftfarhtvorschung* **15**, 41–47.

Volkersen, O. (1965), 'Recherche sur la theorie des assemblages', *Constructions Mecaniques* **4**, 3–13.

Wang, S. S., Mandell, J. F. & McGarry, F. J. (1978), 'An analysis of the crack tip stress field in dcb adhesive fracture specimens', *International Journal of Fracture* **14**, 39–58.

Wang, X., Mieth, U. & Capeletti, A. M. (2004), 'Numerical methods for design of bonded joints for ships', *Proc Instn Mech Engrs Part M: Journal of Engineering for the Maritime Environment* **218**, 273–277.

Weitzenböck, J., McGeorge, D. & Osnes, H. (2004a), Bondship guidelines: recommended practices, Technical Report 2004–0193, DNV.

Williams, J. G. (1989), 'End corrections for orthotropic dcb specimens', *Composite Science and Technology* **35**, 330–347.

Wilson, I., Sheasby, P. G. & Maddison, A. (1997), Significance of environment for performance of structural adhesive bonding, *in* 'Proceedings of the 1997 International Congress and Exposition', Vol. 1251, pp. 1–9.

Winkle, I. E., Cowling, M. J., Hashim, S. A. & Smith, E. (1991), 'What can adhesive offer to shipbuilding ?', *Journal of Ship Production* **7**, 137–152.

Wooley, G. R. & Carver, D. R. (1971), 'Stress concentration factors for bonded lap joints', *Journal of Aircraft* **8**, 817–820.

Yan, C., Mai, Y. W. & Ye, L. (2001b), 'Effect of bond thickness on fracture behaviour in adhesive joints', *Journal of Adhesion* **75**, 27–44.

Yan, C., Mai, Y. W., Yuan, Q., Ye, L. & Sun, J. (2001a), 'Effects of substrate materials on fracture toughness mesurement in adhesive joints', *International Journal of Mechanical Science* **43**, 2091–2102.

Zanni-Deffarges, M. P. & Shanahan, M. E. R. (1995), 'Diffusion of water into an epoxy adhesive: comparison between bulk behaviour and adhesive joint', *International Journal of Adhesion and Adhesives* **15**, 137–142.